University of Alberta

Rapid Mixing with HEV Static Mixers: the Effects on Aluminum Hydroxide Precipitation and Coagulation with Alum

by

Corrina C. Kennedy ©

A thesis submitted to the Faculty of Graduate Studies and Research in partial fulfillment of the requirements for the degree of Master of Science

In

Chemical Engineering

Department of Chemical and Materials Engineering

Edmonton, Alberta

Spring 2004

Library and Archives Canada
Published Heritage Branch
395 Wellington Street
Ottawa ON K1A 0N4
Canada

Bibliothèque et Archives Canada
Direction du Patrimoine de l'édition
395, rue Wellington
Ottawa ON K1A 0N4
Canada

Your file Votre référence
ISBN: 0-612-96499-X
Our file Notre référence
ISBN: 0-612-96499-X

The author has granted a non-exclusive license allowing the Library and Archives Canada to reproduce, loan, distribute or sell copies of this thesis in microform, paper or electronic formats.

L'auteur a accordé une licence non exclusive permettant à la Bibliothèque et Archives Canada de reproduire, prêter, distribuer ou vendre des copies de cette thèse sous la forme de microfiche/film, de reproduction sur papier ou sur format électronique.

The author retains ownership of the copyright in this thesis. Neither the thesis nor substantial extracts from it may be printed or otherwise reproduced without the author's permission.

L'auteur conserve la propriété du droit d'auteur qui protège cette thèse. Ni la thèse ni des extraits substantiels de celle-ci ne doivent être imprimés ou aturement reproduits sans son autorisation.

In compliance with the Canadian Privacy Act some supporting forms may have been removed from this thesis.

While these forms may be included in the document page count, their removal does not represent any loss of content from the thesis.

Conformément à la loi canadienne sur la protection de la vie privée, quelques formulaires secondaires ont été enlevés de cette thèse.

Bien que ces formulaires aient inclus dans la pagination, il n'y aura aucun contenu manquant.

Canada

Abstract

The application of an HEV static mixer in the "Alum Rapid Mix" stage for the water treatment industry was evaluated by measuring and comparing the effects of its mixing intensity and dispersion characteristics to a continuous stirred tank and a pipe in turbulent flow.

Experimental results indicate that the rate of change of pH, which occurs as North Saskatchewan River water is mixed with liquid alum, determines the morphology of the aluminum hydroxide precipitate: a result of the degree of supersaturation created by a combination of the dilution effect on pH and the pH sensitive thermodynamic solubility interaction of the alum/water mixture. The literature review revealed that a low degree of supersaturation forms precipitates 100 times larger than a high degree. Mixing conditions designed to produce the larger precipitates, will have flocculation rates over 10 times faster. Production of the larger precipitate is obtainable with an HEV static mixer.

Dedication

I would like to dedicate this thesis to my parents. A special thanks to my Father for the drawings he completed for my thesis.

Acknowledgement

I would like to acknowledge Dr. Cliff Shook and Don Lamour's indirect contribution to this thesis. Dr. Cliff Shook encouraged me to obtain my graduate degree. Don Larmour encouraged me to continue looking for the unexpected. It was my work experience with Don on crystallization and that one misbehaved lamella that helped me put the pieces of this puzzle together. I would also like to thank the staff at Epcor for their technical support, assistance and use of equipment, and my supervisor, Dr. Suzanne Kresta, for teaching me how to tell the story.

Table of Contents

Chapter 1 Literature Review 1

1.1 Introduction 2

1.2 The Sedimentation Process 4

1.2.1 Colloidal Particles 5

1.3 Chemistry of Alum in Aqueous Solution 8

1.3.1 Solubility 9

1.3.2 Supersaturation with Alum 15

1.3.3 How Alum Affects the Solution pH 19

1.3.4 When Alum Precipitates 21

1.4 Aluminum Hydroxide Precipitation 22

1.4.1 Morphology of Aluminum Hydroxide Precipitate 24

1.4.1.1 The Two Habits of Amorphous Aluminum Hydroxide Precipitate 25

1.4.2 Affected Properties and Mechanisms of Aluminum Hydroxide Precipitation for Each Industry 28

Ceramics 28

Flame Retardant Industry (Ultra-fine Powders by homogeneous Precipitation Method) 33

Alumina Catalyst by Precipitation Method 33

Extractive Metallurgy-The Bayer Cycle 33

Mineral Formation 36

Water Treatment 36

1.4.3 Summary of Observed Influential Conditions on Aluminum Hydroxide Precipitation. 37

Rate of precipitation 37

Degree of Supersaturation 38

Solution pH at the Time of Precipitation or Critical pH for Precipitation 38

Concentration of Hydroxide Ion 39

Mixing 40

1.5 Coagulation and Flocculation 41

1.5.1 Collision Rate Equations 41

Brownian 42

Differential Settling 42
Fluid Shear 42
The Effect of Precipitate Size on the Total Collision Rate 47
1.6 Colloidal Stability and Removal in Water Treatment **50**
1.6.1 Stabilization Mechanisms of Colloidal Particles *50*
1.6.2 How Alum Destabilizes Colloids *55*
1.6.2.1 Charge Neutralization 55
1.6.2.2 Sweep 55
1.6.3 How Polymer Destabilzes Colloids *56*
1.6.4 Determining Whether the Mechanism of Coagulation with Alum is Sweep or Charge Neutralization *56*
1.7 Mixing **60**
1.7.1 Concepts *60*
Dispersion 60
Scales of Mixing: Macro versus Micromixing 61
Radial and Axial Dispersion in a Pipe 61
Backmixing 61
Dilution 62
Tracer Test (Residence time distribution) 62
1.7.1.2 The Effects of Dispersion on Local Concentrations 67
1.7.1.3 Mixing Intensity Due to Turbulence 69
1.7.2 Equipment *71*
1.7.2.1 Static Mixers 71
Pressure Drop 72
Characteristic Shear Rate, G 73
Blend time 73
Dispersion 75
1.7.2.2 Turbulent Mixing in a Pipe 75
Pressure Drop 75
Characteristic Shear Rate, G 76
Blend time 76
Dispersion 77
1.7.2.3 Continuous Stirred Tank (CST) 78
Power 78
Characteristic Shear rate, G 78
Blend time 79

Dispersion 80
1.7.2.4 Jar 80
Characteristic Shear rate, G 82
Impeller Power 82
Blend time 83
Dispersion 83
1.7.2.5 Inline Mechanical Mixer 83
1.8 Rapid Mixing and Coagulation **83**
1.9 Summary **86**
1.10 References **89**

Chapter 2 Experimental Methods **95**

2.1 Introduction **96**
2.2 Analytical Methods **98**
2.2.1 Turbidity *99*
2.2.1.1 Aluminum Concentration 101
2.3 Jar Test **102**
2.4 Initial Alum Mixing Conditions **108**
2.4.1 Pilot Plant *109*
2.4.1.1 Train one 112
2.4.1.2 Train two 113
2.4.1.3 Continuous Stirred Tank 113
2.4.1.4 Pipes 116
2.4.1.5 Static Mixers 116
2.4.1.6 Inline Mechanical Mixer 116
2.4.2 Mixing Conditions *117*
2.4.3 Pumps *118*
2.5 Experimental Procedures **122**
2.5.1 Jar *122*
2.5.2 Pilot Plant Train *123*
2.5.3 Isolation Test Line *124*
2.6 Experimental Design **127**
2.7 Determining the Mechanism of Coagulation **134**

2.8 References 136

Chapter 3 Results and Discussion 138

3.1 Introduction 139
3.2 Blocking of Experimental Results 140
3.3 The Relationship between Turbidity and Aluminum Concentration. 142
3.4 The Effects of Alum Dosage 144
3.5 Initial Mixing at all Injection Locations 146
3.6 Effectiveness of Inline Mechanical Mixer 148
3.7 Determining the Mechanism of Coagulation with the Jar Test 148
3.8 Continuous Stirred Tank Results 148
3.8.1 Pipe line Injection with and without Static Mixers 152
3.9 How Total Gt Affects Turbidity Removal 154
Effect on Sample Scatter 154
The Effect of Pipe Diameter on Minumum Gt 155
The Effect of Alum Dosage on Minimum Gt 156
3.10 Dispersion 158
3.10.1 CST 159
3.10.2 Jar 160
3.10.3 Pipe and Static Mixer 161
3.10.4 Effect of G t on Final Aluminum Concentration 164
3.11 Comparison to Plant 165
3.12 Conclusions 167
Implications 168
Recommendations for Future research 169
3.13 References 171

Appendix A 172

Table of Tables

Table 1-1	Natural Particle Dimensions and Settling Times (based on a clay particle with SG=2.65)	5
Table 1-2	Calculation results for settling velocity of a particle in a multi-particle system. (ν=9e-7m^2/s, ρ_s=2650 kg/m^3, C=0.001).	8
Table 2-1	Summary of standard jar test procedures for Epcor and project jar test procedures	103
Table 2-2	Summary of pipe diameters, lengths and bends for each train.	110
Table 2-3	Properties and Dimensions of the CST	115
Table 2-4	Summary of mixing conditions (0 °C and ν = 9 e-7 m^2/s).	117
Table 2-5	Mixing Conditions for Pilot Plant Train experiments	124
Table 2-6	Differences between Jar, Pilot Plant Train and IsolationTest Line experiments. Total Gt is the total Gt summed from the Gt from the initial alum mix and additional alum mix steps.	125
Table 2-7	Flow rate and Reynolds numbers for continuous flow experiments in the IsolationTest line and Pilot Plant Train experiments.	126
Table 2-8	Control experiment used for this project	128
Table 2-9	Paired extremes of experimental variables. (PP – Pilot Plant Train, ITL – Isolation Test Line, JT- Jar Test)	131
Table 3-1	Block summary of raw water turbidity, experimental procedures and alum injection methods (PP train= pilot plant train). All tests were done on Edmonton's winter water at a temperature of 3.0±2 ° C.	141
Table 3-2	Dispersion calculation results for pipe line injection	163
Table 3-3	Dispersion calculation results for the CST and Jar	163

Table of Figures

Figure 1-1 Sedimentation in a cylinder, the rising and settling velocities of a multiparticle system (from Shook, 1993). 7

Figure 1-2 The effect of pH on the solubility of Aluminum hydroxide (data from Misra, 1986) 10

Figure 1-3 Speciation and solubility diagram of aqueous aluminum a) by O'Melia *et al.*, 1972 (from and cited by Faust and Aly, 1983) (The hatch box illustrates the region where amorphous aluminum hydroxide precipitate exists) b) from Martin, 1991 c) from Rubin, 1976. 11

Figure 1-4 Dependence of aluminum solubility on alkalizing reagent used. Measurement of dissolved aluminum with pH changes created by the alkalizing reagent (data taken from Fursenko *et al*, 1975). 13

Figure 1-5 Changes in aluminum sulfate solubility with aging time (reproduced without permission from Rubin,1974) 14

Figure 1-6 Illustration of the rate of relief of supersaturation with high and low degrees of supersaturation. 18

Figure 1-7 Effects of alum dosage on pH of Edmonton's Winter River Water. Experimental data taken from jar tests (Reproduced with permission from Epcor, Lingling Chu, 2001) 20

Figure 1-8 Example of precipitation determination. 22

Figure 1-9 Classification of aluminum hydroxide precipitate 24

Figure 1-10 Scanning electron microscope picture from a study of weathering products of K-feldspar a)group of larger spherical amorphous aluminum hydroxide precipitate b) single larger spherical amorphous aluminum hydroxide precipitate c) smaller fibrous amorphous aluminum hydroxide precipitate (from Kawano and Tomita, 1996) 25

Figure 1-11 Scanning electron microscope pictures from a ceramics industry study (from Nagai *et al.*,1991) a) Larger spherical particles, which form under conditions of slow precipitation (Scale of 3 microns) b) Smaller non-spherical particles, which form under conditions of fast precipitation (Scale of 0.2 microns) 27

Figure 1-12 Proposed growth routes for aluminum hydroxide particles (from Nagai *et al.*, 1991) 29

Figure 1-13 Pathway of agglomeration/growth mechanism for aluminum hydroxide formation (proposed by Nagai et al., 1993) 30

Figure 1-14 Effects of precipitation rate on aluminum hydroxide precipitate agglomerate formation. The precipitation rate is directly related to rate of urea hydrolysis (data taken from Nagai *et al.*, 1993). 31

Figure 1-15 Effects of mixing on the coagulation of aluminum hydroxide during precipitation in a dilute aluminum sulfate solution. Photo 1 is with mixing, photo 2 is without mixing (from Nagai *et al.*, 1991) 32

Figure 1-16 Mechanism for aluminum precipitation under the caustic and highly concentrated conditions found in the Bayer Process (reproduced without permission from Gerson, 2001). 35

Figure 1-17 The total collision rate function for larger aluminum hydroxide precipitates. (d_2=1 micron, SG=2.65 , G=1500 s^{-1}) 49

Figure 1-18 The total collision rate function for smaller aluminum hydroxide precipitates. (d_2=0.01 micron, SG=2.65, G=1500 s^{-1}) 49

Figure 1-19 The Nernst Potential and the Zeta Potential of the inner fixed (Stern) and outer double diffuse layer of ions surrounding a particles. 52

Figure 1-20 Illustration of two mechanisms by which Alum destabilizes colloids in solution a) adsorption/charge neutralization b) sweep 53

Figure 1-21 The bridging model of adsorption and interparticle binding achieved with polymers (Faust and Aly, 1983) 54

Figure 1-22 The design and operation diagram for alum coagulation for general water. (from Amirtharajah and Mills, 1982) 57

Figure 1-23 Optimum rapid mix time (Alum dosage = 10 mg/L, G=1,000 s^{-1}) (Data taken from Letterman et al, 1973) 58
Figure 1-24 The dependence of optimum Gt on Alum dosage and initial G (data taken from Letterman, 1973). 59
Figure 1-25 Settled water turbidity curves at 15 mg/L of alum and pH of 7.7-8.0 (data taken from Amirtharajah and Mills, 1982) 59
Figure 1-26- Illustration of Tracer detection for a pipe. The fraction of injected tracer detected by a) tracer sensor at 1 minute from injection point b) tracer sensor at 3 minutes from injection point. 64
Figure 1-27 Illustration of the tracer detection for an ideal stirred tank in batch and continuous modes a) a batch stirred tank with a residence time of 3 minutes b) ideal continuous stirred tank with a residence time of 3 minutes. 66
Figure 1-28 The extent of micro and macro mixing in reactor models with continuously stirred tank and turbulent pipe flow (plug flow) reactors (from Nauman and Buffman, 1983 cited from Amirtharajah *et al.*, 1991) 67
Figure 1-29 Dissipation of Energy from Power Input 70
Figure 1-30 HEV static mixer (from Chemineer website, 2003) 71
Figure 1-31 Flow pattern of the double vortex off of each tab in the HEV static mixer (from chemineer website, 2003) 72
Figure 1-32 Mixing in HEV static mixer after 3 pipe diameters – for HEV with 2 sets of tabs (HEV2) if Re>10,000, the coefficient of variation is <0.006. 74
Figure 1-33 Plume profile in an HEV static mixer with chemical injection inline with the top tab of an HEV static mixer (tabs not drawn to scale) (drawn by Louis Kennedy, 2003). 75
Figure 1-34 Profile of injected alum plume in a turbulent pipe (drawn by Louis Kennedy, 2003). 76
Figure 1-35 The Jar test apparatus (from the Phipps & Bird website) 81

Figure 1-36 The Jar test correlation between impeller speed and G (from the Phipps & Bird website) 82
Figure 2-1 Effects of polymer mix intensity, when mixing 35 mg/L of alum for 10 minutes in untreated water of 4 NTU. 105
Figure 2-2 Effect of polymer mixing time on jar test results at 200 RPM 105
Figure 2-3 Dependency of turbidity on alum dosage when alum is injected with a diaphragm pump into a 4 inch pipe at an Re=5,800 (Data taken from block 4). 106
Figure 2-4 Effect Alum dosages of 8-33 mg/L with changes in total Gt before polymer addition (the sum Gt from rapid and slow alum mixing steps) (25 RPM upon alum addition = no initial rapid mix, 300 RPM upon alum addition= with initial rapid mix. Data taken from block 8) 107
Figure 2-5 The three parts of each pilot plant train. 109
Figure 2-6 Schematic of trains one and two (train one is on the bottom). (drawn by Louis Kennedy, 2003) 111
Figure 2-7 A schematic of the sample points in train one. 112
Figure 2-8 Diagram of CST in Pilot Plant. Dimensions are in millimeters (drawn by Louis Kennedy, 2003) 114
Figure 2-9 Alum plume with chemical injection into the center of a pipe. (drawn by Louis Kennedy, 2003) 116
Figure 2-10 Continuous injection into center of pipe (drawn by Louis Kennedy) 118
Figure 2-11 Intermittent Injection into center of 4 inch pipe with 1 stroke per second. Only shaded areas contain injected fluid (drawn by Louis Kennedy). 118
Figure 2-12 Pump calibration curves for the gear pump for line pressures used for "Test Line" experiments. 119
Figure 2-13 Actual frequency curve for the diaphragm pump. 120
Figure 2-14 Diaphragm pump calibration at a stroke length setting of 30. 120

Figure 2-15 Diaphragm pump flowrate calibration at stroke length setting of 15. 121

Figure 2-16 Flowrate calibration for the Peristaltic Pump. 121

Figure 2-17 Effects of the inline mechanical mixer on turbidity removal. (Total Gt for alum mixing= 37.5±0.5 data taken from block one) 132

Figure 2-18 Changes in sample variation with alum dosage for alum injection into a 4 inch pipe and at the impeller of a CST, the 4 inch pipe sample standard deviation is between 0.03-0.1 while the CST is between 0.1-1.1 (data taken from block 4) 133

Figure 3-1 Daily average raw water turbidity in each block. 142

Figure 3-2 Relationship between final turbidity and final aluminum concentration for CST and pipeline injection. (Data taken from block six.) 143

Figure 3-3 Effect of alum dosage on final pH. Test results from alum injection directly into the jar. (Total Gt of alum mixing=189 000, Block 8) 145

Figure 3-4 Effect of alum dosage on turbidity removal (Total Gt from initial and additional alum mixing=37.5±0.5 10^4, data taken from block 4 in Table A-4) 146

Figure 3-5 Comparision of calculated and measured alum concentration of pilot plant train samples. (Data taken from Table A-6 block 6, sample points 1 and 2 for pipeline injection and sample point 3 for the CST. Total Gt from alum mixing = 37.4±5 10^4). The plot reveals that alum injection at the wall of the 2 inch pipe results in samples with much higher alum dosages than calculated at sample point one: thus not fully mixed at 100 pipe diameters from the injection point. 147

Figure 3-6 Comparision of turbidity removal with alum injection into a CST and a 4 inch pipe at high raw water turbidity (Total Gt from alum mixing = 37.4±5 10^4, Alum dosage = 30-50 mg/L) a) Block 6 Raw Water NTU = 3.1-3.3 b) Block 5 Raw Water NTU = 3.1- 4.0 (Data taken from Table A-6 and A-5) 150

Figure 3-7 Comparision of turbidity removal with alum injection into a CST and a 4 inch pipe at lower raw water turbidity (Total Gt from alum mixing = 37.4±5 10^4, Alum dosage = 30-50 mg/L) (data from Block 5 in Table A-5, Raw water NTU = 3.1- 4.0) 151

Figure 3-8 a) Regardless of the initial G, good turbidity removal is achieved with pipeline injection and poor results are seen with CST injection (Gt 37.4±5 10^4, data taken from block 6) b) differences between pipeline injection methods are seen if Gt is plotted instead of initial G (data taken from block 6). 153

Figure 3-9 Minimum final turbidity and sample scatter decrease as Gt increases for all pipeline injection methods. 154

Figure 3-10 Effect of pipe diameter on final turbidity a) without static mixers b) with static mixers (Gt= total Gt from alum mixing) 155

Figure 3-11 Effect of alum dosage on the minimum Gt in pipeline injection. a) Alum dosage =20 mg/L, data taken from block 7 b) Alum dosage = 7-15 mg/L, data taken from block 8. 157

Figure 3-12 Effect of a 2 inch Pipe and 1 inch static mixer on minimum Gt. (Alum dosage = 30-50 mg/L data from block 6) 158

Figure 3-13 Fraction of vessel containing alum for the period of time shorter than the blend time for the CST. 160

Figure 3-14 Fraction of vessel containing alum for the period of time shorter than the blend time for the jar. 161

Figure 3-15 Alum plume liquid alum concentration one second after alum injection. Higher liquid alum concentration upon precipitation results in better turbidity removal. (data taken from block 7 and 8 with alum dosages for Jar = 8mg/L, for pipeline injection=7-30 mg/L and for CST=20 mg/L, all Gt>20,000) 162

Figure 3-16 The effect of Gt on final aluminum concentrations at low alum dosages (Alum dosage = 7 & 15 mg/L, data taken from block 8) 164

Figure 3-17 Comparision of Plant results to pipeline injection and jar tests (G x t =20±5 10^3, data from blocks 7 and 8) 166

Nomenclature

A	cross sectional area of pipe (m^3)
A & B	two soluble species
a	activity ($moles/m^3$)
C	for tanks - off bottom impeller clearance (m)
C	for settling equations - particle concentration volume fraction
C	concentration of solute (mol/m^3)
C^*	equilibrium concentration of solute (mol/m^3)
C_D	drag coefficient
D	impeller diameter (m)
d	particle diameter (m)
d_p	particle diameter (m)
D_P	pipe diameter (m)
F	friction losses, J (kgm^2/s^2)
f	Darcy/Fanning friction factor
f'	Moody friction factor
F_D	drag force (N)
F_{ng}	net gravitational force (N)
g	acceleration due to gravity (m/s^2)
G	characteristic shear rate or the inverse of the Kolmogorov time scale. Historically referred to as the absolute or mean velocity gradient (s^{-1})
H	height of liquid level, (m)
h	vessel height, (m)
l	for tank – Inlet pipe to CST off bottom of tank clearance, (m)
I	for turbidimeter - Intensity of electromagnetic radiation at x ($photons/m^2s$)

I_o	incident intensity of electromagnetic radiation at x=0 (before sample) (photons/m^2s)
m	slope of boundary of chemical plume in pipe. Slope of plume boundary from injection point to 50 pipe diameters from injection point
MW_{Al}	molecular weight of Aluminum (g/mole)
MW_{alum}	molecular weight of alum (g/mole)
N_k	particle collision rate (cm^3/s)
N	impeller rotational speed, revolutions per second (rps)
n_i	particle concentration of subscripted particle – volume fraction
N_p	power number for impeller, dimensionless
O	off bottom pipe clearance (m)
P	pressure (kPa)
Q	volumetric flowrate of water, (m^3/s)
r_1	radius of particle 1 (m)
r_2	radius of particle 2 (m)
r	radius of pipe (m)
Re	Reynold's Number, dimensionless
Re_p	Reynold's Number for a particle, dimensionless
Re_s	Reynold's Number for interfacial drag in multi-particle system
Re_t	tank Reynolds number
r_N	rate of nucleation (s^{-1})
$r_p(z)$	radius of alum plum at distance z from the injection point (m)
RPM	revolutions per minute
rps	revolutions per second
s	sample standard deviation
S^i	supersaturation
S	surface area (cm^2)

SG	specific gravity
T	tank width if a square tank or Tank diameter if cylindrical (m)
t	time (s)
T_k	absolute temperature (K)
U_∞	terminal velocity of a single particle in a large body of fluid (m/s)
u_b	bulk fluid velocity (m/s)
u_f	fluid velocity (m/s)
U_r	the relative velocity between the particle and the fluid (m/s)
u_s	particle settling velocity in multiparticle system (m/s)
V	volume (m^3)
V_{swept}	impeller swept volume (m^3)
W	width of vessel (m)
w_r	radial component of relative velocity (m/s)
x	(for turbidity) distance incident beam travels through sample media, (m)
x	distance along pipe from injection point (m)
Y	concentration (mg/L of water)
z	for settling - distance in settling direction (m)
β	collision rate factor or collision frequency function (cm^3/s)
ε	turbulent kinetic energy dissipation rate per unit mass (m^2/s^3)
γ	activity coefficient
μ	dynamic viscosity (kg/ms)
θ_b	blend time (s)
ρ	density (kg/m^3)
ρ_f	density of fluid (kg/m^3)
ρ_s	density of solid (kg/m^3)
υ	kinematic viscosity (m^2/s)

υ_f	kinematic viscosity of the fluid (m^2/s)
σ	standard deviation
η	Kolmogorov length scale of the smallest eddies (m)
τ	turbidity (NTU)
τ_K	Kolmogorov time scale of the smallest eddies (s)
τ_s	shear stress (N/m^2)

Chapter 1

Literature Review

1.1 Introduction

Particulate matter in natural waters must be removed to obtain pure drinking water. The particulate matter covers a wide range of sizes and compositions: sand (1mm), silt (0.01mm), bacteria (1 μm) and colloids (particles smaller than 1μm), which include inorganic substances such as clays, and organic substances such as fulvic and humic acids. Historically and presently, the removal of unwanted particulate matter is accomplished with sedimentation followed by filtration. The sedimentation process is often assisted with coagulation and flocculation of the naturally occurring particulate matter with alum. The terms coagulation, flocculation and precipitate have more than one meaning. Coagulation often includes both the agglomeration and flocculation of particles, but for this work coagulation will refer solely to agglomeration, the process by which particles are joined. The term flocculation will be limited to the creation of loose fibrous structures called flocs. Often flocs are referred to as precipitate, but in this thesis, the term precipitate will be reserved for the initial aluminum hydroxide precipitates that form from alum.

This thesis will focus on the effects of the mixing conditions during addition of the coagulant, alum. Alum's aqueous products may coagulate with natural colloidal particles or they may agglomerate with each other before coagulating with natural particles and forming flocs. The flocs formed are larger than naturally occurring particles, thus settle faster and dramatically reduce the settling time required in the sedimentation process. The initial coagulation with the natural particles, initial precipitate morphology (structure and size) and particle collision rates all play an important role: all three are influenced by the mixing conditions of alum.

Alum is the general name given to all hydrous forms of aluminum sulfate. The hydrated form of alum used in this project had a pH of 3. Its composition was 48 % by weight $Al_2(SO_4)\bullet 14H_2O$ in water. Upon addition to water, alum decomposes into its respective ions, which then undergo a series of reactions with hydroxide ions to form a number of aluminous complexes. The hydrolysis

reactions and the ultimate precipitation are both important. Aluminum is amphoteric, meaning either aluminous cations or anions may form. In addition to the numerous possible ionic complexes, aluminum may also precipitate as $Al(OH)_3$, aluminum hydroxide. The ionic composition and precipitate formation in solution are both determined by solution pH. Not only does the local pH determine whether a precipitate will form: the rate of change of pH will determine the precipitate morphology, as will be introduced in Section 1.3.2. It will be proposed that mixing controls the rate of change of pH and thus the precipitate size and structure by changing the local concentrations that exist during precipitation.

A sequence of ions form as the hydrolysis reactions between the aluminum ion and hydroxide ions proceed. The positive ions which initially form may be adsorbed onto the surface of negatively charged colloids and the number adsorbed may be directly proportional to the number of collisions between the ions and colloids. Since the number of collisions is determined by the intensity of mixing, ionic adsorption is also affected by mixing conditions. Therefore, both the extent of ionic adsorption and the precipitate size will be influenced by the initial mixing conditions. The significance of mixing and the optimum mixing conditions of each will be addressed in this chapter.

The goal of this project is to determine whether an HEV static mixer can be effectively used for the initial mixing of alum and water. An HEV static mixer creates fast radial mixing with minimal axial mixing and the mixing intensity in a static mixer may be high if the flowrate, thus pressure drop, is large. Mixing intensity and dispersion influence the rate of particle collisions and the precipitation pathways of aluminum hydroxide, respectively. The literature review will summarize the effects of solubility (1.3.1), supersaturation (1.3.2) and pH (1.3.3). The existence and formation of the two distinct morphologies of amorphous alum precipitate will be presented in Section 1.4 and the effect of precipitate size on particle collisions will be discussed in Section 1.5. Dispersion created by different mixing methods and its effect on local concentration will be

presented in Section 1.7.1. Section 1.7.2 will cover the fundamental equations for each mixing method.

1.2 The Sedimentation Process

The sedimentation process at Epor Water Services' E.L. Smith water treatment plant is a continuous process divided into six stages: alum injection, alum mixing, polymer injection, polymer mixing, flocculation, and settling. The alum and polymer mixing stages are further divided, into an initial rapid mix period followed by a slow mix period. The alum and polymer are used to promote the formation of larger flocs, which coagulate with naturally occurring particles and settle dramatically faster than the naturally occurring particles.

Alum is often mixed with water by the impeller of an inline mechanical mixer or a stirred tank. The point of injection and the operation of the mixing equipment determine the rate of dispersion, mixing intensity and retention times: all of which may be varied to optimize the performance of alum. The definition and details of dispersion will be covered in Section 1.7.1. Depending upon whether the mechanism of coagulation is sweep or charge neutralization, the precipitate size or the number of ionic/colloidal collisions, respectively, will be responsible for the alum's performance. If the optimum mixing conditions are not matched with the dominant mechanism of coagulation, undesired consequences, such as the formation of an initial precipitate 100 times smaller than optimum, results. A smaller precipitate requires longer floc formation times, thus reducing the effectiveness of the coagulant. Mixing conditions that create smaller precipitates also increase the number of collisions between the negatively charged colloids and the aqueous aluminous ions, which is desirable for the adsorption/charge neutralization mechanism. If the dominating mechanism of coagulation is thought to be adsorption/charge neutralization but is actually sweep, mixing conditions believed to be optimum may actually be detrimental.

1.2.1 Colloidal Particles

Colloids are defined by their size range, which is somewhat arbitrary and can change from source to source. According to Hiemenz (1997), any particle, which has a linear dimension between 0.001 and 1 micron is classified as a colloid. The properties of particles 1 micron and smaller present in natural water are summarized in Table 1-1. Bacteria are of the size range of 1 micron. Particles less than one micron in diameter include inorganic compounds such as clay minerals and organic compounds such as humic and fulvic substances.

The settling rate of colloids is much slower than that of larger particles, as shown in Table 1-1. Colloidal particles can remain suspended in solution for hours, days or even years. The larger surface area per mass that arises as the particles get smaller increases the drag force per unit mass. Since the drag forces are dependent upon surface area and the forces due to gravity are dependent upon mass, the drag forces eventually equal the forces due to gravity and the particles remain in suspension.

Table 1-1 Natural Particle Dimensions and Settling Times (based on a clay particle with SG=2.65)

Type of Particle	Diameter (micron)	Surface Area (per gram)	Settling Time (per 1 m) *
Gravel	10 000	3.14 cm^2	1 sec
Coarse Sand	1 000	31.4 cm^2	10 sec
Fine Sand	100	314 cm^2	2 min
Silt	10	0.31 m^2	2 hours
Bacteria	1	3.1 m^2	8 days
Colloid	0.01	3.2 m^2	2 yrs
Colloid	0.001	2832 m^2	21 yrs

The terminal velocity of a single particle in a large body of fluid can be calculated by the summation of the drag forces and the net gravitational force, which includes the buoyancy force of the fluid.

The equation for net gravitational force is:

$$F_{ng} = \left(\frac{\pi d^3}{6}\right)(\rho_s - \rho_f)g \qquad (1.1)$$

The equation for drag force on a sphere is:

$$F_D = \frac{C_D \rho_f U_\infty^2 (\pi d^2 / 4)}{2} \qquad (1.2)$$

The summation of Equation 1.1 and 1.2 gives the equation for the terminal velocity of the particle in Equation 1.3 :

$$U_\infty = \sqrt{\left(\frac{4gd(\rho_s - \rho_f)}{3C_D \rho_f}\right)} \qquad (1.3)$$

If the Reynolds number for a particle is less than 0.1, a solution for C_D can found by applying Stokes's law. Stokes calculated the drag coefficient in the Stokes Law region to be:

$$C_D = \frac{24}{\mathrm{Re}_p} \qquad (1.4)$$

The Reynold's number of a particle is defined by:

$$\mathrm{Re}_p = \frac{U_r d_p}{\upsilon_f} \qquad (1.5)$$

Where:

U_r = the relative velocity between the particle and the fluid

d_p= the diameter of the particle

υ_f= kinematic viscosity of the fluid

For a multi-particle system, the inter-particle forces should also be taken into account. The settling velocity of a multi-particle system can be calculated with the hindered settling equation (Equation 1-6), which was first obtained experimentally by Richardson and Zaki (Richardson & Zaki, 1954). If the particle concentration is smaller than 1 percent by volume, the effects of inter-particle drag forces per unit volume become negligible and the settling velocity is essentially equal to the terminal velocity of a single particle in a large body of fluid.

$$-u_s = U_\infty (1-C)^{4.7} \qquad (1.6)$$

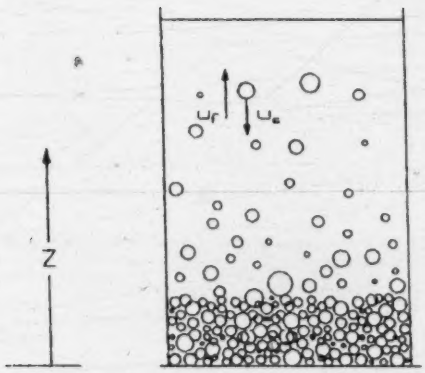

Figure 1-1 Sedimentation in a cylinder, the rising and settling velocities of a multiparticle system (reprinted with permission from Shook, 1993).

The settling and terminal velocity calculations in Table 1-1 and Table 1-2 used a specific gravity of 2.65, which may be representative of clay, since clay has a specific gravity of 1.4 to 2.65. The calculation results, summarized in Table

1-2, show that smaller particles have slower settling times. Table 1-2 also shows that for a low particle concentration, the settling velocity in the jar is essentially equal to the terminal velocity of a single particle in a large body of fluid.

Table 1-2 Calculation results for settling velocity of a particle in a multi-particle system. (ν=9e-7m^2/s, ρ_s=2650 kg/m^3, C=0.001).

Particle Diameter (microns)	C_D	Terminal Velocity U_∞ (m/s)	Settling Velocity U_s (m/s)	Distance settled in 10 min (cm)	Time To Settle 6 cm
10	2.2E+04	1.0E-04	9.9E-05	6.0	10 minutes
1	2.2E+07	1.0E-06	9.9E-07	0.1	28 hours
0.1	2.2E+10	1.0E-08	9.9E-09	6.0E-04	116 days
0.01	2.2E+13	1.0E-10	9.9E-11	6.0E-06	many years

1.3 Chemistry of Alum in Aqueous Solution

In order to optimize the mixing conditions for alum addition, the water chemistry and the formation of precipitates from alum must be understood. Alum is the common name for hydrated forms of aluminum sulphate. The hydrated form of alum used in this project was liquid Alum, 48 % by weight $Al_2(SO_4)\bullet 14H_2O$ in water. The pH of the liquid alum used in this work was 3. The water chemistry of alum is complex and its various ionic and solid products each contribute differently to coagulation. The positively charged hydrolysis products of alum adsorb to negatively charged colloids and the aluminum hydroxide precipitate agglomerate and coagulate with colloids. The water chemistry of alum may be summarized in three steps: dissociation, hydrolysis and precipitation. Upon addition to water, aluminum sulfate dissociates into its respective ions, the positive aluminum ion and the negative sulfate ion. The aluminum ion undergoes a series of hydrolysis reactions with OH^- to form

monomeric and polymeric cations of aluminum such as $Al(OH)_2^+$, and $Al(OH)^{2+}$, which may eventually precipitate as aluminum hydroxide, $Al(OH)_3$. The reactions to form the monomeric ions are as follows:

$$Al^{3+} + OH^- \leftrightarrow Al(OH)^{2+}$$
$$Al(OH)^{2+} + OH^- \leftrightarrow Al(OH)_2^+$$
$$Al(OH)_2^+ + OH^- \leftrightarrow Al(OH)_3(s)$$
$$Al(OH)_3(s) + OH^- \leftrightarrow Al(OH)_4^-$$

In this work, the polymeric ions will not be addressed, for reasons stated in Section 1.3.1.

Aluminum is amphoteric, so depending upon the pH, it may also form the anion, aluminate ($Al(OH)_4^-$). The solution conditions required for each ionic and precipitate form of aluminum will be discussed in Section 1.3. The conditions where aluminum precipitates as aluminum hydroxide, $Al(OH)_3$: the precipitate required for sweep coagulation and floc formation will be addressed in Section 1.3.1 and 1.3.4. Sweep coagulation will be introduced in Section 1.6.

1.3.1 Solubility

The solubility of alum's precipitate, aluminum hydroxide, in water is shown in Figure 1-2. This curve illustrates the pH conditions and aluminum hydroxide concentrations required for precipitation. In regions of both high and low pH the aluminum hydroxide is fully soluble in water. In a mid pH range between 4-9, alum is only sparingly soluble and precipitation occurs even at low concentrations of aluminum hydroxide.

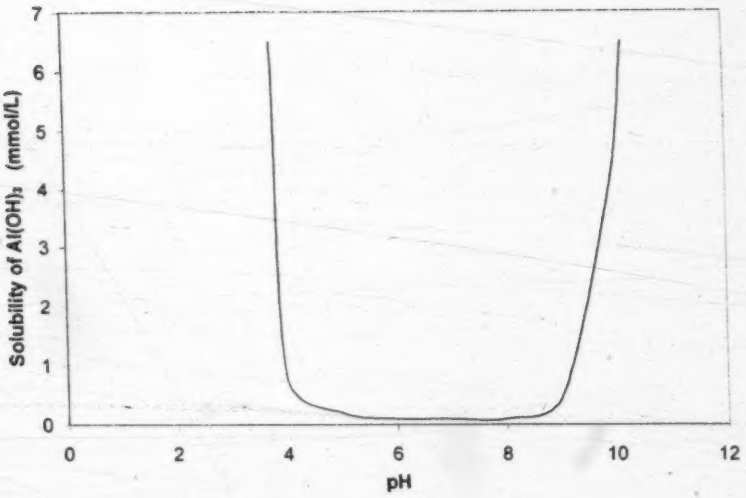

Figure 1-2 The effect of pH on the solubility of Aluminum hydroxide (data from Misra, 1986)

Misra's (1986) solubility diagram (Figure 1-2) only shows the quantity of solid aluminum hydroxide that dissolves in aqueous solution with increasing pH, not the various soluble ionic complexes of aluminum hydroxide formed at high, mid and low pH. The details of the solubility and aluminum species formed as aluminum hydroxide or alum is mixed with water are in Figure 1-3. Figure 1-3a is the solubility diagram commonly used in the water treatment industry. The hatched region indicates the region where aluminum hydroxide precipitates, and the boxed region indicates the region where the precipitate remains amorphous. Martin's (1991) diagram in Figure 1-3b is the most recent and provides the most detail in the mid pH region of low solubility. Other solubility diagrams, such as Rubin's (1976), Figure 1-3c, do not show the speciation of aluminum in the mid pH range at low solubility. Martin's curves were calculated using the equilibrium constants for the hydrolysis equilibria reactions, assuming an ionic strength of 0.16 and a temperature of 25°C.

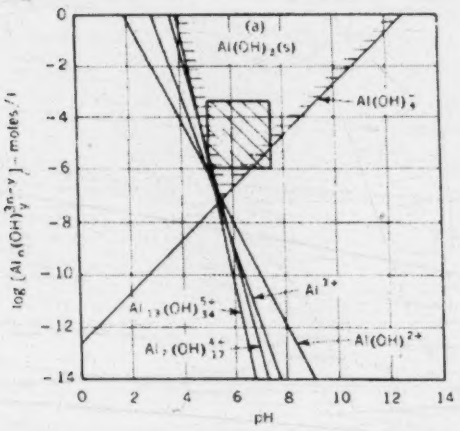

a)

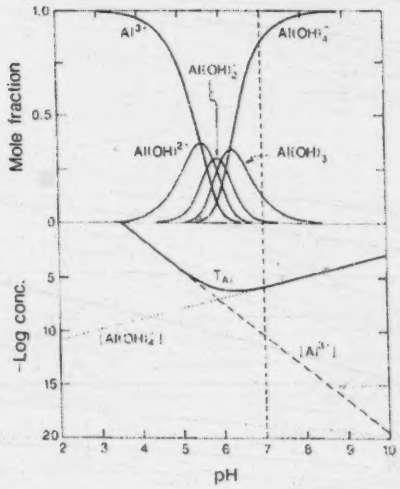

b)

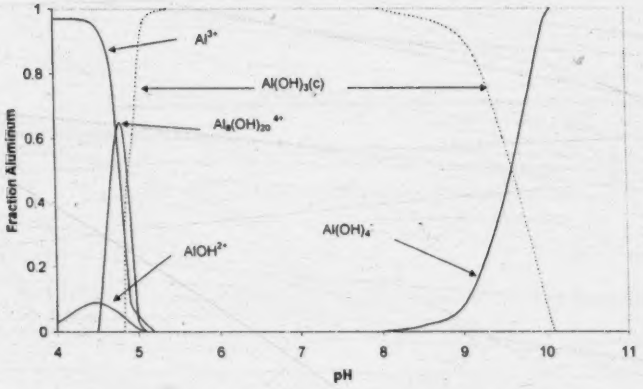

c)

Figure 1-3 Speciation and solubility diagram of aqueous aluminum a) O'Melia *et al.*, 1972 (O'Melia, C. R. In: Physicochemical Processes for Water Quality Control, W.J. Weber Jr., 1972 John Wiley & Sons. Reprinted by permission of John Wiley & Sons, Inc.) (The hatch box illustrates the region where amorphous aluminum hydroxide precipitate exists) b) Martin, 1991 (Reprinted from Journal of Inorganic Biochemistry, Vol 44, Martin *et al.*, *Fe^{3+} and Al^{3+} Hydrolysis Equilibria, Cooperativity in Al^{3+} Hydrolysis Reactions*, pp 141-147, 1991, with permission from Elsevier) c) Rubin, 1976 (data from Rubin, 1976)

In addition to the formation of these monomeric species of aluminum shown in Figure 1-3b, polymeric complexes of aluminum may also occur. Polymeric species are significant if the pH is greater than 12 (Gerson, 2001), but the existence of polymeric species at a lower pH is still debated. According to Martin (1991) in Figure 1-3b, in aqueous solutions with a pH less than 10, four possible monomeric species of aluminum form in solution, $Al(OH)^{2+}$, $Al(OH)_2^{+}$, $Al(OH)_3$ and $Al(OH)_4^{-}$. But according to O'melia the polymeric aluminum ion, $Al_8(OH)_{20}^{4+}$ also forms at a pH below 5.5. The range of pH of raw water in this study is 8-8.2, while the pH of alum is 3. As liquid alum is diluted, the pH will change and the equilibrium between the ionic species will shift. In this work, the pH will always remain below 8.3; therefore, it was assumed that the effect of the polymeric species, if they in fact exist, is negligible.

Aluminum solubility curves from other sources show variations from Figure 1-3, due to type of alkalizing reagent and aging time. Fersenko's (1975)) study, whose data is plotted in Figure 1-4, showed that the solubility curve of aluminum changes with the alkalizing reagent used. An alkalizing reagent is the chemical used to increase the pH of the solution. The two alkalizing agents used by Fersenko were NaOH and NH_4OH: a strong and weak base respectively. NaOH fully dissociates in water, while the k_b of NH_4OH is only 1.8×10^{-5} (Latimer, 1964). The activity coefficients of the ionic species and their effect on the thermodynamic equilibrium created by the addition of base will differ between a strong base and weak base. How each activity affects the thermodynamic equilibrium of the hydrolysis products of aluminum is outside the scope of this project, but it is important to note that alkalinity may also have a similar affect, since the alkalinity of water also acts in the same way as an alkalizing reagent. Alkalinity is the acid-neutralizing capability of water and like the alkalizing reagents used in Figure 1-4, the alkalinity of the water works to increase pH. Since the possibility exists that results in Figure 1-4 may apply to the water treatment industry, its results will be explained further. The strong base used in

Figure 1-4, NaOH, fully dissociates in water, while the weak base, NH_4OH does not, as shown below.

$$[NH_4OH] \leftrightarrow NH_4^+ + OH^-$$

So there exists a competition between aluminum and ammonium for hydroxide ions, which is dependant upon the activity of each species. This difference may explain the observed changes in aluminum solubility shown Figure1-4. However, these differences may instead be due the difference in ionic concentration required to achieve a given pH, or maybe because of some other unmeasured phenomenon. The key point that should be taken from the data in Figure 1-4 is that the solubility of aluminum may potentially be affected by the alkalinity of the water; therefore, general solubility diagrams may not apply to all water conditions. If the competition for hydroxide ions does affect aluminum solubility, the results in Figure 1-4 that show higher aluminum solubility results when NaOH is used as an alkalizing reagent suggest that the solubility of aluminum increases as the competition for OH^- ions decreases.

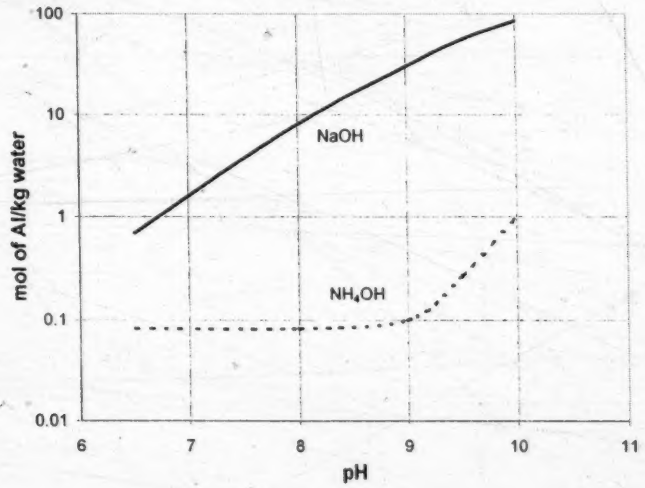

Figure 1-4 Dependence of aluminum solubility on alkalizing reagent used. Measurement of dissolved aluminum with pH changes created by the alkalizing reagent (data taken from Fursenko *et al*, 1975).

Aging time also changes the solubility of aluminum in the high pH region, as illustrated in Rubin's diagram in Figure 1-5. In the region of lower pH, the solubility of aluminum remains constant with time but in the higher pH range, the aging time significantly affects the solubility of aluminum sulfate. Therefore, it appears that solubility at the lower pH range is more stable than the solubility at a higher pH. Even though differences exist between solubility diagrams from various sources, all diagrams indicate that there is large decrease in aluminum solubility at a pH of 4 and large increase at a pH of 7.

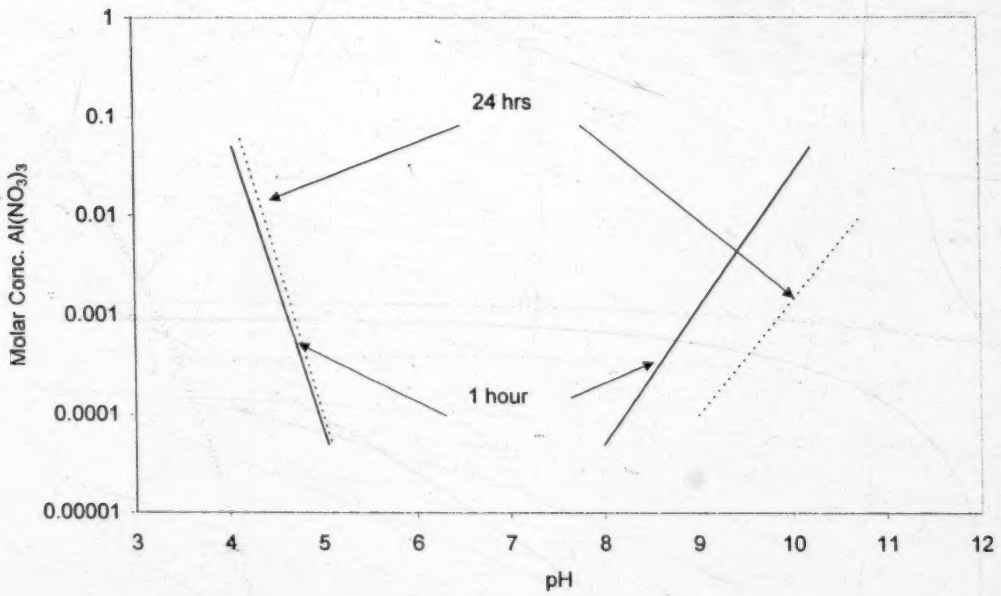

Figure 1-5 Changes in aluminum sulfate solubility with aging time (data from Rubin, 1976)

The change in solubility with pH, shown in Figure 1-2 and Figure 1-3, is important. This drastic change in solubility provides a source of supersaturation: the driving force for precipitation. In addition to drastic changes in the overall solubility, the top portion of Figure 1-3b illustrates extreme changes in solubility

with increasing pH for each individual soluble species of aluminum. Changes in total and individual species solubility are important since the pH of water and alum are extremely different. The pH of liquid alum and natural water used in this work is 3 and 8 respectively. When alum and water are mixed, the sudden decrease in solubility will cause the solution to become supersaturated. As alum is injected into water, there are sudden changes in the equilibrium solubility as local regions of high pH and local regions of low pH form. Mixing condition will determine the local pH and thus the local degree of supersaturation, as the alum solution is dispersed in the water. If a region of low pH is suddenly mixed into a region of high pH, the solubility of aluminum will suddenly drop and a high degree of supersaturation will result. Mixing conditions determine the local degrees of supersaturation in the mixture. Mixing condition with lots of dispersion can induce regions of high supersaturation. Mixing Conditions with no back mixing and slow radial mixing may gradually increase the pH of the injected alum plume, maintaining a low degree of supersaturation throughout aluminum hydroxide precipitation.

1.3.2 Supersaturation with Alum

All four solubility diagrams: Misra (Figure 1-2), O'melia ((Figure 1-3a), Rubin (Figure 1-3c) and Martin (Figure 1-3b) reveal that a drastic change in solubility occurs at both a low and high pH, thus providing a potential source of supersaturation as the pH of an alum/water solution is changed. In order to explain this potential source of supersaturation, saturation and supersaturation will be defined and then the potential source of supersaturation from a change in pH will be discussed.

An alum/water solution is saturated if the solid and liquid phases are in thermodynamic equilibrium. A change in the thermodynamic equilibrium of the solution may be induced by varying properties such as the temperature or pH. In the case of an alum/water solution, the thermodynamic equilibrium is sensitive to pH. In Figure 1-2, the aluminum hydroxide dissolves in water, so aluminum hydroxide will be considered the solute. If the pH of a saturated alum/water

solution is altered, the equilibrium concentration will be shifted according to the solubility diagrams in Figure 1-2 and Figure 1-3. For an increase in pH from 3 to 8, the equilibrium concentration of dissolved aluminum hydroxide will be dramatically lowered. Since the solute concentration at 3 is much higher than the final equilibrium solute concentration at a pH of 8, there will exist a large concentration difference between the actual and equilibrium solute concentrations. A difference between actual and equilibrium solute concentration provides a driving force for precipitation, quantified by supersaturation, which will be now be discussed.

The most common expressions for supersaturation are defined by the concentration driving force, where C is the actual concentration and C* is the equilibrium concentration. A common equation used to define supersaturation is given in Equation 1.7(Mullin, 2001). However, the true thermodynamic measurement of supersaturation actually uses the difference in chemical potential rather than concentration, as shown in Equation 1.8 (Mullin, 2001). For an ideal solution the activity coefficients (γ) are unity and the activity (a), as defined in Equation 1.9, becomes equal to the concentration and equation 1.8 becomes equation 1.7. For the purpose of this work, the ideal case will be assumed and supersaturation will be defined by a concentration driving force.

$$S = \frac{C}{C^*} \qquad (1.7)$$

$$\frac{\Delta\mu}{RT} = \ln\left(\frac{a}{a^*}\right) = \ln S \qquad (1.8)$$

$$a = \gamma C \qquad (1.9)$$

Where:

R =gas constant

μ = chemical potential

γ = activity coefficient

C = solute concentration

a = activity

S = supersaturation

* = equilibrium values

The degree of supersaturation will determine the rate of nucleation and growth. Nucleation is the formation of discrete nuclei and growth is the deposition of precipitate onto existing nuclei. If a solution is unsaturated, it is stable and precipitation is impossible. If the solution is slightly supersaturated, the solution is said to be metastable and spontaneous precipitation is unlikely: but if a precipitate it added to this solution, growth onto this precipitate would occur. If supersaturation is high enough, the solution is unstable and precipitation may be spontaneous through the formation of nuclei. In order for precipitation to be spontaneous and thus form nuclei, the critical Gibbs free energy must be exceeded. This critical free Gibbs energy is dependant upon temperature, the degree of supersaturation and interfacial tension (Mullin, 2001). The relationship between the degree of supersaturation and rate of relief of supersaturation is illustrated in Figure 1-6. As stated earlier, a high degree of supersaturation results in spontaneous nucleation, thus these conditions have a

higher nucleation rate. The higher the nucleation rate, the greater the number of nuclei and thus a high proportion of smaller precipitate form. The opposite occurs for a low degree of supersaturation: the nucleation rate is slower and more supersaturation is relieved by growth, thus the overall precipitate size will be larger.

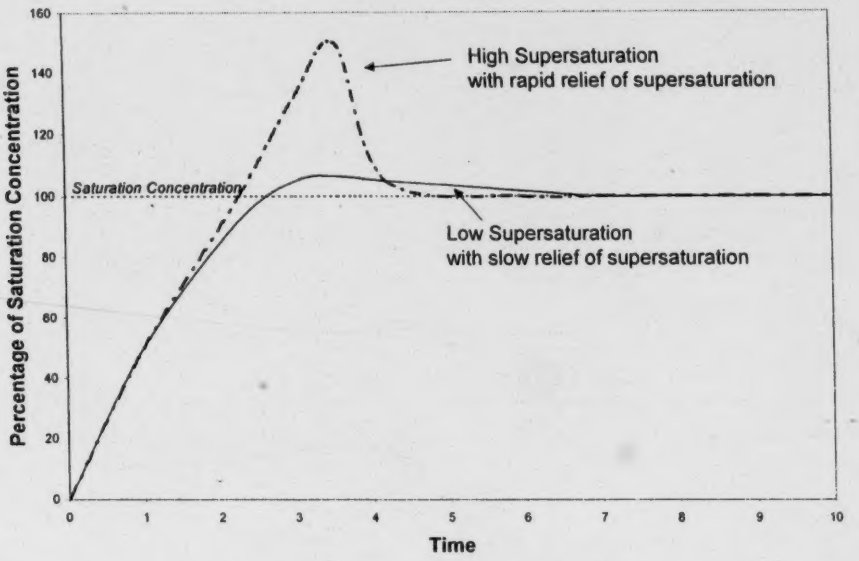

Figure 1-6 Illustration of the rate of relief of supersaturation with high and low degrees of supersaturation.

The purpose of this work is not to quantify the degree of supersaturation or define the thermodynamics of the alum/water system, rather to point out mixing conditions where conditions of low and high degree of supersaturation may be created. By measuring changes in local concentration created by various mixing conditions, conditions likely to create regions of low and high supersaturation may be identified. Most often in water treatment the mixing of alum and water is thought of as mixing alum into water. To more easily identify mixing conditions most likely to create a low degree of supersaturation, the logic should be reversed. If water is mixed into an aqueous alum solution of 48% alum with a pH of 3, the hatched region in Figure 1-3a shows that the pH of the alum

solution must be increased before precipitation can occur. The pH of the water is higher than the aqueous alum solution used in this work. For the case of Edmonton's North Saskatchewan River water in the winter, the pH is between 8 and 8.2. As the water is dispersed into the aqueous alum solution, the alum solution will be diluted and its pH will increase. The rate of water addition and the volume of water added, will determine the local rate of change of pH in the aqueous alum solution. The rate of change of pH is important. Referring back to Figure 1-2, it can be seen that as the pH of the alum solution increases from 3 the solubility of its precipitate aluminum hydroxide sharply decreases around a pH of 4. A more gradual change in solubility occurs between a pH of 4 and 5.5 and from 5.5 to 8 the solubility remains constant at a low value. According to Figure 1-2 and 1-3, a sudden change in pH from 3 to 8 will result in a large concentration driving force, as the actual concentration of dissolved aluminum at a pH of 3 is much higher than the equilibrium concentration of dissolved aluminum at the new pH of 8. Differences between actual and equilibrium concentrations may be reduced if the pH is gradually increased from 4 to 5.5, as indicated by the more gradual slope from a pH of 4 to 5.5 in Figure 1-2. A gradual rise in pH from 4 to 5.5 will create local conditions with a low degree of supersaturation. Different mixing methods will change the rate at which the alum solution is diluted with of water, thus the rate of change of pH in the alum solution. This in turn affects the concentration driving force and the degree of supersaturation. The concept of supersaturation will be used throughout this work and its the driving force will continue to be defined by concentration driving forces rather than chemical potential.

1.3.3 How Alum Affects the Solution pH

The above sections revealed that the composition of aluminum species formed in solution depends upon the pH of the solution. To complicate matters further, the addition of alum alters the pH of the original solution. It is the solution's final pH and concentration (Figure 1-3), which determine the

equilibrium solubility; however the concentration of alum affects the solution's final pH as illustrated in Figure 1-7.

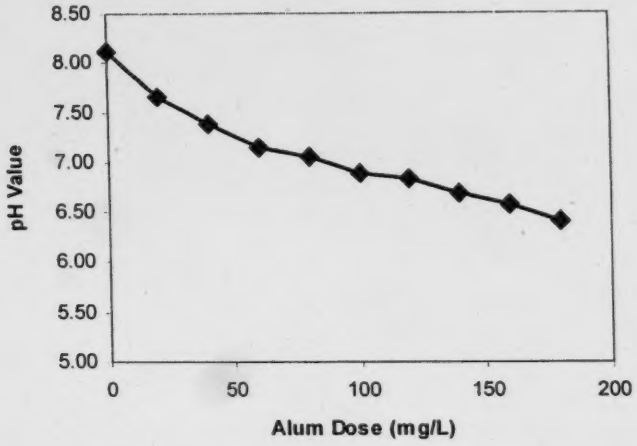

Figure 1-7 Effects of alum dosage on pH of Edmonton's Winter River Water. Experimental data taken from jar tests (data reproduced with permission from Epcor, Lingling Chu, 2001)

The final pH of an alum/water mixture can be estimated with models that take into account pH, alkalinity, ionic strength and the inorganic carbonate content or pH data can be obtained from experiments. A plot of experimental data in Figure 1-7, illustrates the relationship between alum dosage and the final pH for Edmonton's NSR raw water in the winter. These experiments reveal that the overall effect of adding alum is a lowering of the pH.

When alum is added to water it dissociates into the aluminum ion and the sulfate ion. The aluminum ion undergoes a series of hydrolysis reaction shown in Section 1.3. These hydrolysis reactions release hydrogen ions from water. An example is shown below.

$$Al^{3+} + H_2O \leftrightarrow H^+ + Al(OH)^{2+}$$

The excess H^+ produced during the hydrolysis reactions is partially consumed by the carbonate ions in solution during the carbonic acid equilibrium reactions. This acid neutralizing capability of water is referred to as its alkalinity. The

carbonic acid equilibrium that reduces the acidity created from the dissociation of water due to alum is as follows.

$$CO_2 + H_2O \leftrightarrow H_2CO_3 \leftrightarrow H^+ + HCO_3^-$$
$$HCO_3 \leftrightarrow H^+ + CO_3^{2-}$$

The overall acid neutralizing reaction of alum and the alkalinity in the water as calcium bicarbonate (Faust & Aly, 1983) is:

$$Al_2(SO_4)_3 \bullet 14H_2O + 3Ca(HCO_3)_2 = 2Al(OH)_{3(S)} + 3CaSO_4 + 6CO_{2(g)} + 14H_2O$$

There is often not enough alkalinity in the water to completely neutralize all of the acidifying effects of alum. This is always true for Edmonton's NSR water in the winter. As illustrated in Figure 1-7, the addition of alum results in a decrease in the pH of the water.

1.3.4 When Alum Precipitates

If the alum dosage and the final pH of the solution are known, the precipitation event can be predicted. First the final pH can be determined by using Figure 1-7 and then precipitation can be predicted utilizing O'Melia's solubility diagram (Figure 1-3a). For ease of reference, the y-axis on O'Melia's diagram has been converted from mol/L to mg/L of alum in Figure 1-8. If 8 mg/L of alum is added to Edmonton's natural untreated water the final pH will be 7.9 (Figure 1-7). According to Figure 1-8, for a pH of 7.9, alum is fully soluble if the dosage is below 5 mg/L, but precipitates if the dosage is increased above 6 mg/L; therefore, at an alum dosage of 8 mg/L, aluminum hydroxide will precipitate from solution.

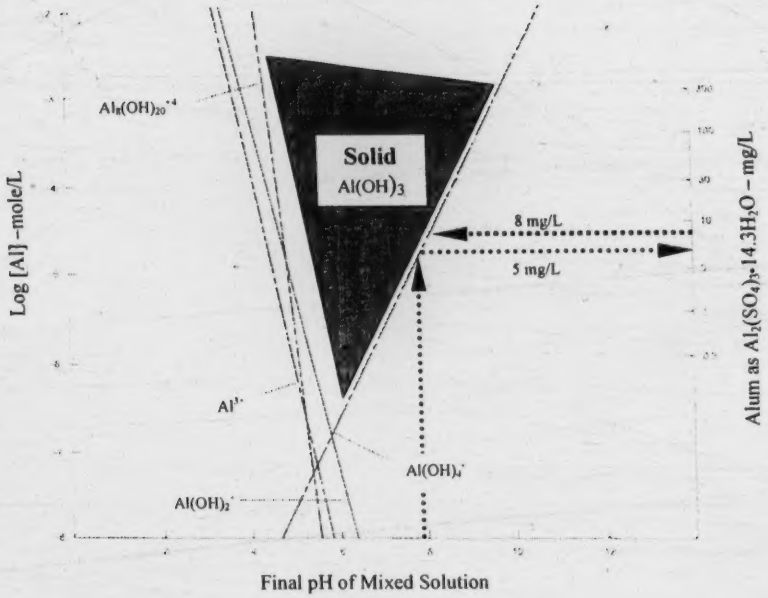

Figure 1-8 Example of precipitation determination.

1.4 Aluminum Hydroxide Precipitation

The local conditions during precipitation of alum as aluminum hydroxide determine the morphology of the aluminum hydroxide precipitate. Some conditions result in amorphous precipitate with a diameter on the order of 0.01 microns, while other conditions produce initial precipitates with a diameter that is of the order of 1 micron: 100 times larger than the smaller precipitate. Conditions that produce the larger precipitate are desirable, since a larger precipitate will require shorter flocculation times. This section will discuss the various precipitation rates and habits (shape and size) that result from various mixing conditions. Studies of the rate and habit of aluminum hydroxide formation are limited in water treatment: fortunately, aluminum hydroxide has a variety of uses outside the water treatment industry, so studies from other industries will provide many of the insights required for this study.

Aluminum hydroxide has a number of purposes: it is suitable as a flame retardant, a smoke suppressant, reinforcing filler of organic polymers, adsorbent for column chromatography and is a starting material for the catalyst and ceramics industries. Many of these industries are interested in the production of monodisperse or ultrafine powders with isotropic morphology, and therefore have explored the effects of the conditions during aluminum hydroxide precipitation on the precipitate. Of all the studies reviewed, the ceramic industry studies by Nagai *et al. (1991 & 1993) and* its continuation studies by members of the same group in Unuma *et al.* (1998) are most similar to the conditions found in water treatment. Like water treatment, their conditions deal with dilute aluminous solutions at a low pH. The highest pH tested was 5.8, while the final solution pH during the treatment of Edmonton's NSR water in the winter is generally between 7 and 8.

The variables used to control precipitate formation are remarkably similar between industries. The five common variables, which will be referred back to throughout this thesis are:

- rate of precipitation
- degree of supersaturation
- local solution pH at the time of precipitation (the local pH during precipitation in the region of the solution where precipitation occurs)
- concentration of the hydroxide ion
- mixing

The definition of the degree of supersaturation and how it influences the rate of precipitation was discussed in Section 1.3.2. The existence of two different morphologies of aluminum hydroxide precipitate and the conditions required for their formation will be addressed in this section (1.4).

1.4.1 Morphology of Aluminum Hydroxide Precipitate

There exist numerous forms of aluminum hydroxide ranging from amorphous to gelatinous to various crystalline structures, each of which can have more than one habit (size and structure). The conditions of precipitation and aging determine which crystalline, amorphous or gelatinous form the aluminum hydroxide takes. Aluminum hydroxide is different from most precipitates, in that it must pass through an amorphous phase before it becomes crystalline. Figure 1-9 illustrates the numerous forms of aluminum hydroxide and their pathways. If the solution pH is under 7 and at a low temperature, the precipitate is always initially amorphous. Amorphous precipitates are x-ray diffraction indifferent (Misra, 1986). With aging and under the right conditions, the precipitate transforms into gelatinous pseudo-boehmite (AlO(OH)) and then trihydroxide crystalline forms. There exist three polymorphs of crystalline aluminum hydroxide: Norstrandite, Gibbsite and Bayerite. The crystal habit for each can vary. For example, Bayerite is a well developed crystal with diverse shapes, such as cones, wedges, rods and hour glass figures (Alwitt, 1976). Under the conditions found in water treatment, aluminum hydroxide is initially amorphous in form and remains amorphous, since the pH does not exceed 8.

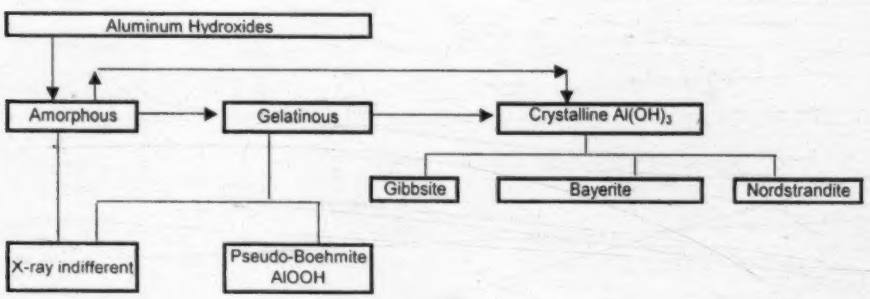

Figure 1-9 Classification of aluminum hydroxide precipitate

1.4.1.1 The Two Habits of Amorphous Aluminum Hydroxide Precipitate

Aluminum hydroxide precipitate is highly hydrophillic, so it easily forms gels, which are of great industrial significance to industries such as the alumina catalyst industry (Misra, 1986). The amorphous precipitate may be dispersed in solution or grouped as a gel. It and has been seen to occur as two distinctly different habits with distinct size ranges and shapes. The smaller of the two is of a non-spherical form, less that 0.02 microns in diameter, and the second is a larger spherical habit less than 1 micron in diameter (Kawano and Tomita, 1996).

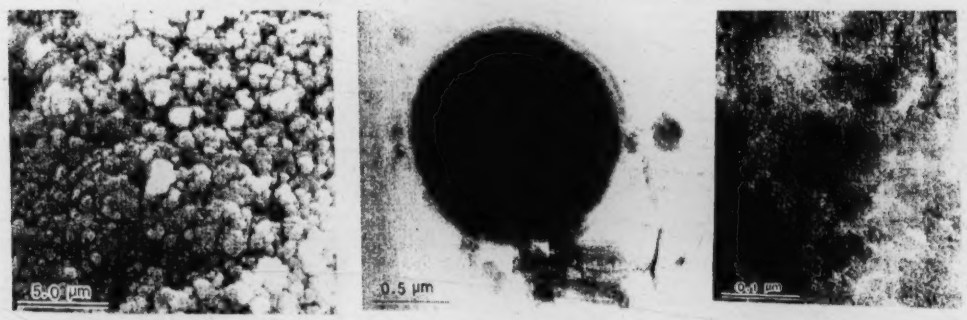

a) Scale = 5.0 microns b) Scale = 0.5 microns c) Scale = 0.1 micron

Figure 1-10 Scanning electron microscope picture from a study of weathering products of K-feldspar a) group of larger spherical amorphous aluminum hydroxide precipitate b) single larger spherical amorphous aluminum hydroxide precipitate c) smaller fibrous amorphous aluminum hydroxide precipitate (Kawano and Tomita, *Amorphous Aluminum Hydroxide Formed at the Earliest Weathering Stages of K-Feldspar*, Clays and Clay Minerals, 1996. Courtesy of Clays and Clay Minerals)

The two different habits of amorphous aluminum hydroxide have been photographed by different industries using scanning electron microscopy. Figure 1-10 shows the results of study of the naturally occurring weathering products on K-feldspar as it transforms into Gibbsite. The aluminum hydroxide samples were collected during the earliest stages of weathering, crushed then ultrasonically cleaned. The experimental conditions for this study were uncontrolled, so they were unable to identify the cause of the two different habits, only that two amorphous habits of aluminum hydroxide exist. A more controlled experiment for the ceramics industry by Nagai *et al.* (1991) is shown in Figure 1-11. They also photographed two habits of amorphous aluminum hydroxide and proposed causes for the formation of each.

Nagai *et al.(1991)* induced a slow rate of precipitation with malonic acid and a fast rate of precipitation with acetic acid. The slow rate produced large spherical particles (Figure 1-11 a) and the fast rate produced smaller irregular particles (Figure 1-11b). Nagai *et al.*(1991) also tested 6 other acid additives. All additives inducing a fast rate of precipitation resulted in ultrafine particles and those inducing a slow rate of precipitation resulted in larger spherical particles.

a) b)

Figure 1-11 Scanning electron microscope pictures from a ceramics industry study a) Larger spherical particles, which form under conditions of slow precipitation (Scale of 3 microns) b) Smaller non-spherical particles, which form under conditions of fast precipitation (Scale of 0.2 microns) (Nagai *et al.*, 1991, *Synthesis of Aluminum Hydroxide by Homogeneous Precipitation Method 1 - Effect of Additives on the Morphology of Aluminum Hydroxide*, British Ceramic Transaction Journal. Courtesy of Maney Publishing, administrator of IoM Communications Ltd, a wholly owned subsidiary of the Institute of Materials, Minerals and Mining.)

It is interesting to note the similarities of these two studies. Both the size range and structure of the particles photographed are similar. The size range of amorphous aluminum hydroxide particles observed by Nagai *et al.* (1991) was less than 0.05 to 3 microns, while Kawano and Tomita (1996) observed particles less than 0.02 to 1 micron in size. This finding is extremely relevant to water treatment. A precipitate 100 times smaller will require dramatically longer flocculation times, since the dominating collision mechanism will be the slower Brownian motion rather than the faster fluid shear.

1.4.2 Affected Properties and Mechanisms of Aluminum Hydroxide Precipitation for Each Industry

In addition to size, other properties are influenced by the conditions of aluminum hydroxide precipitation. Many industries have conducted studies on what effects the conditions during aluminum hydroxide precipitation have on their products. Some industries rely on trial and error to find the optimum precipitation conditions, while others have attempted to understand the mechanisms that influence the properties of their products. The key findings are summarized for each industry.

Ceramics

The preparation of metal oxide powders for the ceramics industry often involves the precipitation of metal hydroxide from a metal-salt solution, followed by a thermal treatment to decompose it to its metal oxide. The properties of the oxide powder are affected by both procedures (Nagai *et al.*, 1991).

Studies by Kato & Nagai *et al. (1991 &* 1993) attempted to understand the mechanisms of precipitation. They proposed that the rate of precipitation controls the habit of the initial amorphous phase of aluminum hydroxide. If the rate of precipitation is rapid, ultrafine aluminum hydroxide form and conversely, if the rate of precipitation is slow, larger spherical particles or gels of spherical particles form. The rate of precipitation can be controlled by how much the solution exceeds its critical supersaturation or pH; thus determining the habit of the amorphous aluminum hydroxide precipitates (Nagai *et al.*, 1991). The relationship between precipitate morphology and rate of precipitation is illustrated in (Figure 1-12). It should be noted that the rate of precipitation and the degree of supersaturation are interrelated, as previously discussed in Section 1.3.2.

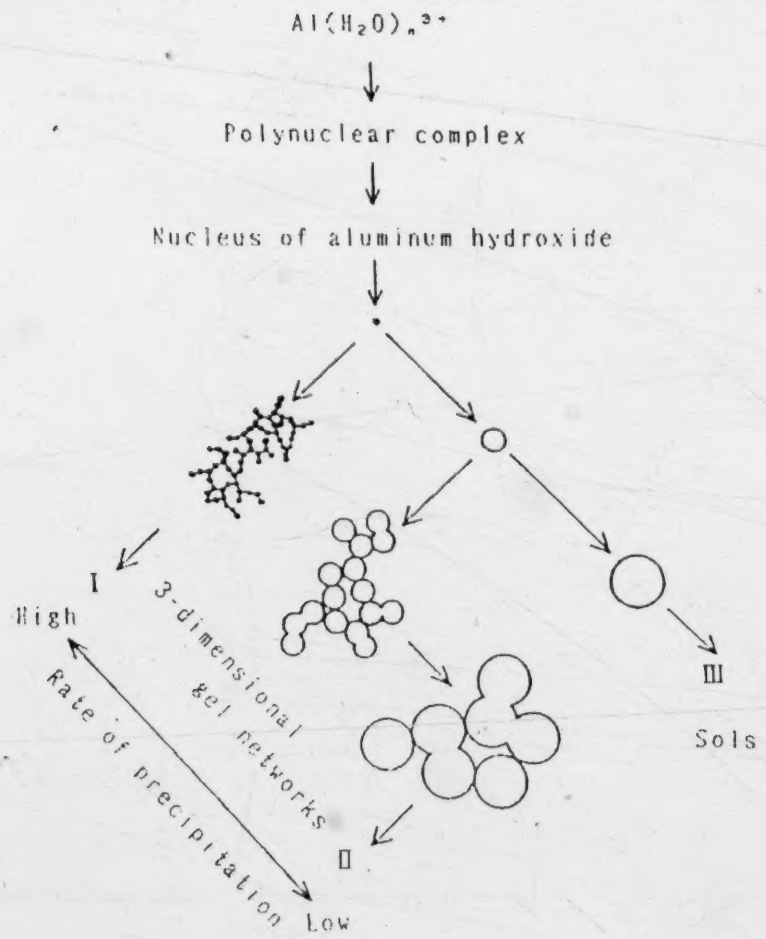

Figure 1-12 Proposed growth routes for aluminum hydroxide particles (Nagai *et al.*, 1991, *Synthesis of Aluminum Hydroxide by Homogeneous Precipitation Method 1 - Effect of Additives on the Morphology of Aluminum Hydroxide*, British Ceramic Transaction Journal. Courtesy of Maney Publishing, administrator of IoM Communications Ltd, a wholly owned subsidiary of the Institute of Materials, Minerals and Mining.)

Nagai *et al.* (1991) investigated precipitation in dilute aluminous solutions of aluminum nitrate and aluminum sulfate. The conditions were similar to water treatment since the concentration of aluminum sulfate solution was the equivalent of 30 mg/L of alum and the critical pH studied ranged between 2-6. Nagai *et al. (1991)* discovered a consistent relationship between the critical pH for precipitation and rate of precipitation with the precipitate morphology. They observed that if the critical pH for precipitation was greater than 4.5, the rate of precipitation was fast and small precipitate formed. If the critical pH for precipitation was less than 4.5, the rate of precipitation was slower and larger precipitate resulted.

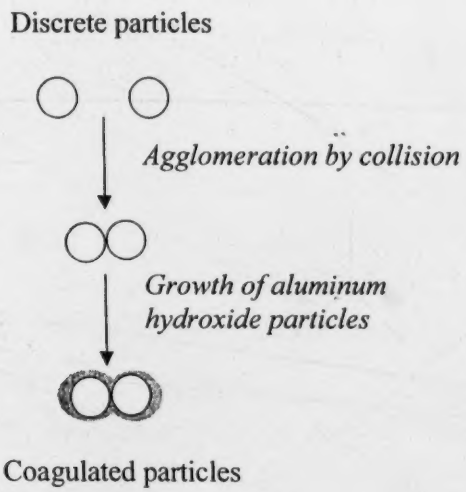

Figure 1-13 Pathway of agglomeration/growth mechanism for aluminum hydroxide formation (concept proposed by Nagai et al., 1993)

Nagai *et al (1993)*, continued their 1991 research and found that the rate of precipitation also affects the extent of agglomeration during precipitation. They proposed a mechanism for agglomeration during precipitation, which is illustrated in Figure 1-13. Nagai *et al.* (1993) reported that a number of factors

influenced the process of growth and agglomeration illustrated in Figure 1-13. The factors affecting the agglomeration step were mixing of the solution, the concentration of particles and the electrochemical state of the surface. The growth step was affected by the precipitation rate.

The degree of agglomeration during precipitation is linearly related to precipitation rate as indirectly shown in Figure 1-14, since the urea hydrolysis reactions that take place when urea is added to an aluminous solution cause aluminum hydroxide to precipitate from solution; the rate of urea hydrolysis directly corresponds to the rate of aluminum hydroxide precipitation. The plot in Figure 1-14, showing a higher percentage of agglomerate formation at lower urea hydrolysis rates, indicates that more agglomerates form as the aluminum hydroxide precipitation rates decrease.

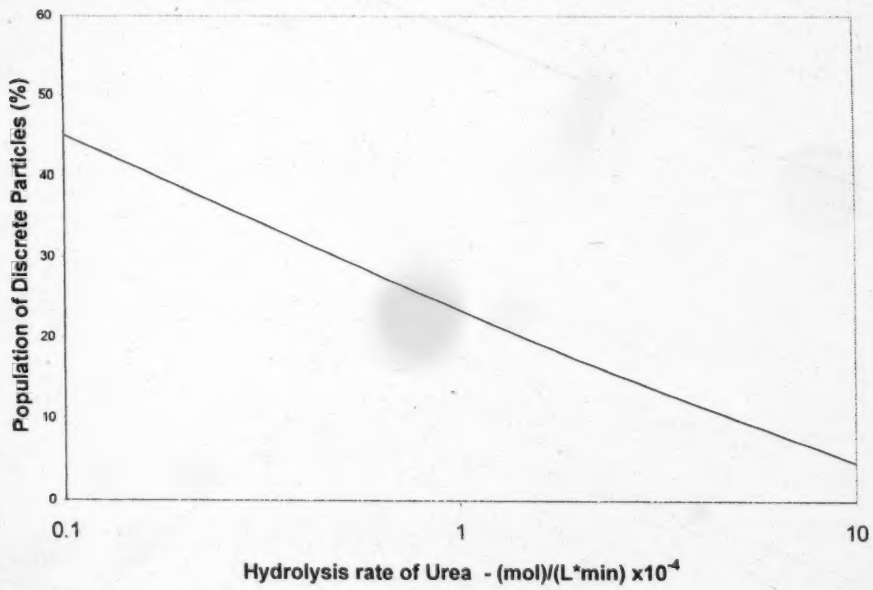

Figure 1-14 Effects of precipitation rate on aluminum hydroxide precipitate agglomerate formation. The precipitation rate is directly related to rate of urea hydrolysis (data taken from Nagai *et al.*, 1993).

Nagai *et al.* (1991, 1993) also revealed that the degree of particle agglomeration during precipitation increased remarkably when the solution was mixed during precipitation, shown in Figure 1-15.

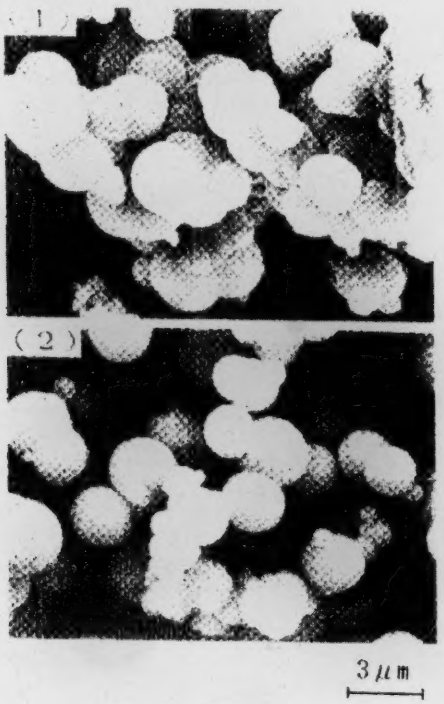

Figure 1-15 Effects of mixing on the coagulation of aluminum hydroxide during precipitation in a dilute aluminum sulfate solution. Photo 1 is with mixing, photo 2 is without mixing (Nagai *et al.*, 1991, *Synthesis of Aluminum Hydroxide by Homogeneous Precipitation Method 1 - Effect of Additives on the Morphology of Aluminum Hydroxide*, British Ceramic Transaction Journal. Courtesy of Maney Publishing, administrator of IoM Communications Ltd, a wholly owned subsidiary of the Institute of Materials, Minerals and Mining.)

In summary, the three significant discoveries made by Nagai *et al.(1991 &* 1993): the effect of the critical pH for precipitation, the rate of precipitation and of mixing on precipitate habit, all are relevant to the water treatment industry. The rate of precipitation can vary between the mixing conditions found in water

treatment. The rate of precipitation, which is determined by the degree of supersaturation, was discussed in section 1.3.2. The variations due to different mixing conditions will be addressed later in Section 1.7.1.

Flame Retardant Industry (Ultra-fine Powders by homogeneous Precipitation Method)

Ultra-fine aluminum hydroxide powders are used in the flame retardant and smoke suppressant industry. This industry is interested in producing ultra fine aluminum hydroxide, since it has a better flame retardancy and a higher filling percentage (Chen *et al.*, 2003). Numerous methods of preparing ultrafine Aluminum hydroxide have been developed. One method is the reactive precipitation method: a process where nanoparticles are formed by providing a high degree of supersaturation and uniform spatial concentration (Chen *et al.*, 2003).

Alumina Catalyst by Precipitation Method

Solid oxide catalysts or their carriers are frequently prepared by precipitation of metal salts from aqueous solution followed by a thermal treatment to form solid oxides such as alumina. During precipitation, pH and the nature of ions in solution are used to control the phase composition and properties of the catalyst active sites (Trawczynski, 1996).

Extractive Metallurgy-The Bayer Cycle

The processing of bauxite ore is done utilizing the Bayer Cycle which produces Gibbsite, from caustic aluminate ($Al(OH)_4^-$) liquors with an initial pH greater than 14. The slowest step in the Bayer process is the precipitation of aluminum hydroxide (Gerson, 2001), so improvements in the rate of would be economically significant. Although this process was invented over 100 years ago, little was known of the mechanisms of nucleation and eventual crystallization of Gibsite until 1992, when a project was undertaken to examine the fundamental mechanism of Gibsite nucleation (Gerson, 2001). The review revealed that there exists a fundamental difference between the nucleation of

aluminum hydroxide precipitate from concentrated and dilute solutions. The precipitation conditions in the Bayer Cycle are much different that those previously discussed in the ceramics section. The Bayer Cycle involves concentrated aluminate solutions while the ceramics industry deals with dilute cationic solutions.

Under the concentrated conditions seen in the high pH aluminate solutions of the Bayer cycle, the nucleation and growth of crystalline aluminum hydroxide does not follow classical crystal growth mechanistic pathways. The pathway under these conditions is illustrated in Figure 1-16 and is as follows:

a) The formation of ion pairs (monomeric ions) Na^+, $Al(OH)_4^-$
b) Formation of a loose polymeric network (<10 nm) – fibrous (polymeric ions)
c) Clustering of polymers
d) Growth of nuclei – densification of core, while outer layer remains diffuse
e) Once supersaturation is relieved, growth rates drop and a densification of surface layer occurs, followed by crystallization (f).

The rate of densification of the surface layers, which does not occur until step (e), controls agglomeration and the final particle size. If the supersaturation is high, densification of the outer particle layer is slow and the diffuse outer layer exists longer, thereby preventing the particles from approaching close enough to allow for Van der Waals forces to promote agglomeration. Since slow densification discourages agglomeration, the particle agglomerates formed under these conditions tend to be small resulting in a large percentage of fine crystalline particles. It is also generally accepted that the rate of formation of Al-OH-Al bridges is a rate determining step in the precipitation of aluminum hydroxide.

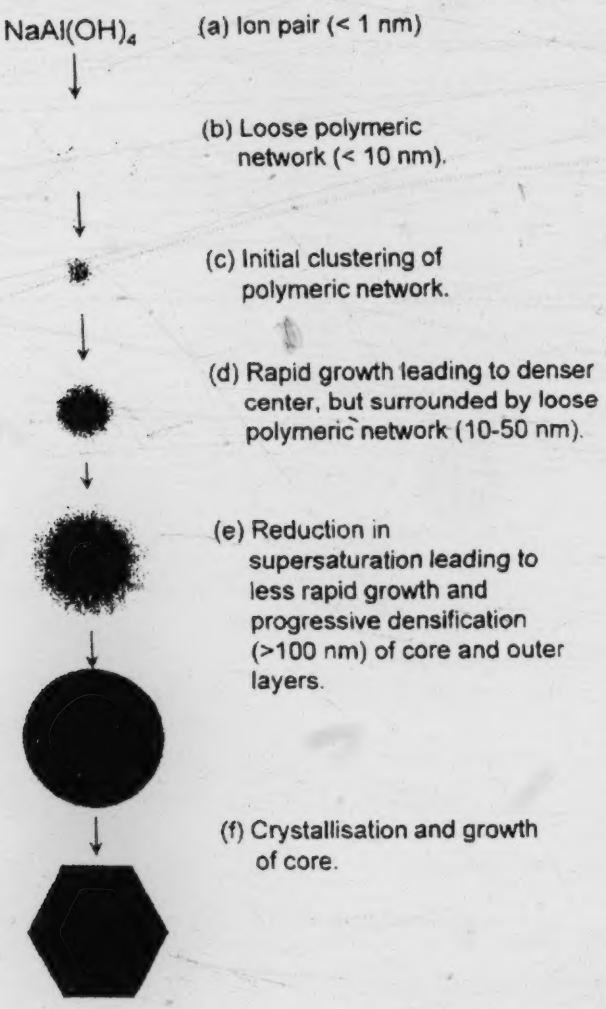
NaAl(OH)4
(a) Ion pair (< 1 nm)
(b) Loose polymeric network (< 10 nm).
(c) Initial clustering of polymeric network.
(d) Rapid growth leading to denser center, but surrounded by loose polymeric network (10-50 nm).
(e) Reduction in supersaturation leading to less rapid growth and progressive densification (>100 nm) of core and outer layers.
(f) Crystallisation and growth of core.

Figure 1-16 Mechanism for aluminum precipitation under the caustic and highly concentrated conditions found in the Bayer Process (Reprinted from Crystal Growth and Characterization of Materials, Vol 43, Gerson, A., *The Role of Fuzzy Interfaces in the Nucleation, Growth and Agglomeration of Aluminum Hydroxide in Concentrated Caustic Solutions*, pp 187-220, 2001, with permission from Elsevier).

Mineral Formation

Before aluminum hydroxide forms a stable crystalline mineral, it first forms a metastable amorphous phase. This was observed in a study of the earliest of stages during the weathering of K-Feldspar before the stable crystalline phase of Gibbsite formed (Kawano and Tomita, 1996). Kawano and Tomita (1996) took samples from the earliest stages of weathering, crushed and then ultrasonically cleaned them. Violante and Huang (1993) made a similar observation. They stated that aluminum hydroxide precipitates into an amorphous form before is goes through a dissolution-reprecipitation reaction to form crystalline precipitates. They found that the rate of precipitation influences the final crystalline structure of aluminum hydroxide. Conditions with rapid crystallization yield Bayerite and slow crystallization yield Gibbsite (Violante and Huang, 1993).

Water Treatment

The purpose of aluminum hydroxide precipitation from alum is to provide a material for colloid collection, floc formation and ultimately timely turbidity removal. Precipitation of aluminum hydroxide in water treatment occurs from dilute aluminous solutions rather than from concentrated caustic solution; therefore, the mechanisms proposed by the ceramics industry are most relevant to water treatment.

Knowledge of the habit of aluminum hydroxide precipitates initially formed in water treatment is presently limited. Aluminum hydroxide precipitate is always amorphous if the pH is below 7 and the pH during water treatment is generally between 6-8, so it can be assumed that the aluminum precipitate formed in water treatment is amorphous. Under the conditions where the solution pH approaches 8, it may be possible to form pseudo-boehmite (AlOOH) instead of the $Al(OH)_3$, but there have been no reports of this in the literature.

It is generally accepted in the water treatment industry that the precipitate is amorphous and forms in 1-7 seconds (Amirtharajah *et al.*, 1991). A literature

review revealed no literature studying the mechanisms of precipitation specifically for water treatment.

1.4.3 Summary of Observed Influential Conditions on Aluminum Hydroxide Precipitation.

The effects of the solution conditions during precipitation have been studied by numerous industries. The five variables used by each industry to control precipitation are the rate of precipitation, the degree of supersaturation, the local solution pH at the time of precipitation (the local pH at the time of precipitation is analogous to the local pH during precipitation), the concentration of the hydroxide ion and mixing, all of which may be affected by mixing conditions found in water treatment. In water treatment, close attention should be paid to how dispersion and dilution causes changes in local concentration and pH, thus solubility. The initial pH and alkalinity of raw water will determine the final pH. Dispersion will determine the quantity and rate of water mixed (dilution) with the alum and thus all five variables stated above: This section will summarize the effects of the five variables on precipitation and how each variable may be controlled.

Rate of precipitation

The rate of precipitation has been shown to be an influential variable in both the ceramics powder technology and the alumina catalyst industry. The rate of precipitation of aluminum hydroxide influences the mean particle size, particle size distribution, and agglomeration of the precipitates. Recent studies in powder technology for the ceramics industry show that the mean size of the precipitates can be controlled in a range of 0.3 to 1.9 microns by adjusting the urease concentration (Unuma *et al.*, 1998). Since the rate of precipitation correlates with the concentration of urease, it can be concluded that the rate of precipitation controls the size and distribution of aluminum hydroxide powders. It has also been shown that more agglomerated precipitates will form if the rate of precipitation is low (Nagai *et al.*, 1993), as illustrated in Figure 1-14.

In water treatment, the rate of precipitation of alum may be controlled by the rate at which water mixes with liquid alum. Infinitely fast dilution, giving a fast rate of precipitation, can be achieved with a continuous stirred tank (CST). A slow rate of dilution of alum with water results in a slow rate of precipitation and can be achieve using an empty pipe in turbulent flow. Dilution will be addressed in Section 1.7.1.1 and 1.7.1.2. The relationship between dilution and mixing methods will be discussed in Section 1.7.2.

Degree of Supersaturation

Conventional precipitation theory says that the degree of supersaturation will determine the rate of precipitation, so the degree of supersaturation may be interpreted to be analogous to the rate of precipitation, but for now the two will be discussed separately.

Studies of the production of ultra-fine aluminum hydroxide particles have shown that a high degree of supersaturation produces nanoparticles (Chen & Zheng, 1996). This finding may be applied to water treatment, since the degree of local supersaturation varies between alum injection methods. In water treatment the degree of supersaturation is controlled by changes in local pH, which is determined by the rate, quantity and properties of the water mixed with the alum. The larger the quantity or faster the rate of mixing water into alum, the higher the degree of supersaturation. Supersaturation was introduced in Section 1.3.2, and an introduction of the differences in supersaturation between mixing methods will be addressed in Section 1.7.1.2.

Solution pH at the Time of Precipitation or Critical pH for Precipitation

Numerous industries have noted the effects of the pH at the time of precipitation on the final habit of crystalline and amorphous aluminum hydroxide. The habit, surface properties and properties of active sites of alumina, a product of aluminum hydroxide, are influenced by the pH of precipitation of aluminum hydroxide (Jiratova *et al.*, 1991). The pH and the nature of ions in solution during aluminum hydroxide precipitation control the phase composition and the strength and distribution of alumina active sites (Trawczynski, 1996). The surface area of

the precipitate is larger if the solution pH at the time of precipitation is higher (Jiratova *et al.*, 1991). The alumina catalyst's surface reactivity is also affected by the solution pH and morphology of its precursor, aluminum hydroxide (Lefevre & Fedoroff, 2002).

The work by Nagai *et al.* (1991) was most similar to conditions found in water treatment, of all the studies examining the effects of critical pH on aluminum hydroxide precipitate morphology. Nagai *et al.* (1991) discovered that if the pH at the time of precipitation was below 4.5, precipitation was slow and larger precipitate formed. In water treatment, the local pH at the time of aluminum hydroxide precipitation can be kept below 4.5 by controlling the rate at which liquid alum is mixed into the water. The effects of changes in local pH as alum is added to water were addressed in Section 1.3. The different local pH conditions created by different mixing methods in water treatment will be addressed in Section 1.7.1.2

Concentration of Hydroxide Ion

The concentration of hydroxide ions and the availability of hydroxide ions have an effect on the solubility of aluminum as noted in the Section 1.3.1. It was shown that the solubility of aluminum changes when a strong versus a weak base is used to change the pH (Figure 1-4). The concentration of hydroxide ions was also found to be important in the Bayer cycle, where it was the concentration of hydroxide ions, rather than the concentration of aluminate ions, which controlled aluminum hydroxide precipitation (Gerson, 2001). In this industry, it is also generally accepted that a rate determining step in the precipitation of aluminum hydroxide is the rate of formation of Al-OH-Al bridges (Gerson, 2001), which would be influenced by the availability of hydroxide ions.

In water treatment, the alkalinity of the water and the concentration of alum will determine the final pH and concentration of the hydroxide ions. The activity of the water will influence the ionic competitions for the available hydroxide ions: a concept that is identified but remains outside the scope of this work.

Mixing

Mixing is required for agglomeration during precipitation. The effect of mixing on agglomeration of aluminum hydroxide particles during precipitation has been documented by Nagai *et al.*(1993 &1991). If the rate of precipitation is slow, mixing during precipitation promotes agglomeration of the aluminum hydroxide particles as photographed in Figure 1-15.

Mixing also controls the local degree of supersaturation during aluminum hydroxide precipitation. If water is mixed in to quickly, or in too large of quantities, the supersaturation can rise rapidly, leading to the formation of very small precipitate. In water treatment, different mixing methods will affect the precipitate morphology and agglomeration. Larger precipitates are desired in water treatment as well as a specific final solution pH. If alum is used to control the final solution pH, an appropriate balance between too much and too little mixing must be established to achieve both goals.

1.5 Coagulation and Flocculation

As defined earlier, coagulation is the process by which particles are agglomerated and flocculation is the creation of loose fibrous structures called flocs. A minimum size of floc is required for optimum settling, so the final floc size is important. In coagulation with alum, the precipitates of alum, aluminum hydroxide, collide with each other and agglomerate. The agglomerated precipitates coagulate with naturally occurring particles in the water by engulfing them. These agglomerates of precipitate and natural particulate will further collide and flocculate. Their size increases with the number of collisions and thus the final floc size is dependant upon both its initial size and the total number of collisions. The total number of collisions is the sum of collisions from three collision mechanisms: Brownian motion, fluid shear and differential settling. The dominating collision mechanism is dependant on the size of the colliding particles. If precipitates are extremely small (0.01 micron), Brownian motion dominates and collisions due to differential settling and fluid shear become negligible. However, for very large particles, differential settling becomes the dominant collision mechanism. For the larger aluminum hydroxide precipitate (1 micron), fluid shear is the dominating collision mechanism and the intensity of turbulence, quantified by G, will significantly influence floc formation.

1.5.1 Collision Rate Equations

The Smoluchowski equation (1.18) describes the kinetics of flocculation. The total collision frequency in this equation can be found by adding the collisions due to Brownian motion, fluid shear and differential settling. Brownian motion is the random motion due to the kinetic energy of a particle as it is suspended in solution. Fluid shear is due to the shear forces created by turbulence of the fluid and differential settling is the particle collisions that arise as particles of different sizes settle at different rates.

The Smoluchowski equation is:

$$N_k = \frac{1}{2}\sum_{i+j=k}\beta(i,j)n_i n_j - n_k\sum\beta(i,k)n_i \qquad (1.10)$$

Where β is the collision frequency function (cm^2s^{-1}). The collision frequency function for Brownian motion, fluid shear and differential settling can be estimated from the following equations (as cited in Han and Lawler, 1992), where i and j are particle numbers.

Brownian

$$\beta(i,j) = \frac{2kT}{3\mu}\left(\frac{1}{d_i}+\frac{1}{d_j}\right)(d_i + d_j) \qquad (1.11)$$

Differential Settling

$$\beta(i,j) = \frac{\pi g}{72\mu}(\rho_p - \rho_l)(d_i + d_j)^3|d_i - d_j| \qquad (1.12)$$

Collisions due to differential settling will be zero if for two particles of the same diameter and specific gravity, since they will both settle at the same rate.

Fluid Shear

$$\beta(i,j) = \left(\frac{1}{6}\right)(d_i + d_j)^3 G \qquad (1.13)$$

The fluid shear equation used by Han and Lawler (Equation 1.13) is essentially identical to the universally accepted collision rate due to fluid shear equation derived by Saffman and Turner (1956), for particles larger than the smallest turbulent eddies in turbulent flow.

The Saffman and Turner equation is:

$$\beta_{i,j} = \left(\frac{1}{6.18}\right)\left(d_i + d_j\right)^3\left(\frac{\varepsilon}{\upsilon}\right)^{1/2} \qquad (1.\ 14)$$

Where:

β =collision rate constant (cm^3/s)

d = particle diameter (m)

ε = rate of energy dissipation (m^2/s^3)

υ = kinematic viscosity(m^2/s)

An important parameter in this equation is $(\varepsilon/\upsilon)^{1/2}$, a characteristic of the turbulent motion of the fluid, defined by the rate of turbulent energy dissipation per unit mass (ε) and the kinematic viscosity of the fluid (υ). This parameter only arises in the collision equation due to fluid shear, not in the equations for Brownian motion or differential settling, so turbulent mixing increases the collision rate only when the dominating collision mechanism is fluid shear. The parameter due to fluid shear is commonly expressed as G (Equation 1.15) in the water treatment industry.

$$G = \left(\frac{\varepsilon}{\upsilon}\right)^{1/2} \qquad (1.\ 15)$$

G is the velocity gradient in the smallest eddies, or the inverse of the time required to dissipate the energy in these eddies by viscous forces as defined by equation 1.15. In this work G, will be referred to as the characteristic shear rate instead of the traditionally used term the mean velocity gradient (or mean shear). From the definition of G in Equation 1.15, the Saffman and Turner equation 1.14 can be written as:

$$\beta_{i,j} = \frac{1}{6.18}\left(d_i + d_j\right)^3 G \qquad (1.\ 16)$$

If Equation 1.16 is rearranged, the increase in floc volume given the mixing time and G can be calculated:

$$V = \frac{(d_1 + d_2)^3}{6.18}(Gt) \qquad (1.17)$$

Equation 1.17 reveals that the product of G and time, Gt, is needed to estimate the final floc size due to fluid shear. Since larger floc will settle faster, it should be expected that a higher Gt values would result in better turbidity removal when the dominating collision mechanism is fluid shear.

The Saffman and Turner (1955) equation (Equation 1.18) is a well-defended collision rate equation. A similar equation derived from different assumptions was proposed earlier by Camp and Stein(1943). While Camp and Stein's result is correct, their explanation of the physics is misleading.

Saffman and Turner used Bachelor's similarity theory of turbulence to model drop collisions in turbulent clouds. The similarity theory suggests that for a small scale of motion similar in size to the smallest turbulent eddies, the motion is isotropic. The collision rate due to fluid shear at this scale is:

$$N_k = 1.3 n_1 n_2 (r_1 + r_2)^3 \left(\frac{\varepsilon}{\upsilon}\right)^{1/2} \qquad (1.18)$$

If the radius is converted to diameter and the number densities n_1 and n_2 are accounted for, the equation is the same as Equation 1.14.

Saffman and Turner (1955) made the following well-defended assumptions in their derivation:

- The particles were spherical.
- They assumed that the flow distortion due to the particle was negligible and provided literature data to support this assumption.
- They assumed a collision efficiency of unity and provide literature data to support this.
- They assumed that the drops were of relatively equal size.
- They assume all particles were equally distributed.
- The error arising from assuming the velocity gradient is normally distributed is negligible. This was supported by work done by Townsend (1947).

By using the similarity theory and applying all of these assumptions, they were able to solve for the mean flux of particles into the isotropic sphere of a radius equal to the sum of the radii of the two colliding particles. The equation for the mean flux of fluid into a sphere of radius R is defined by Term 1.19, which integrates the radial components of relative velocity that enter into the sphere of a radius equal to the sum of the radii of the two colliding particles.

$$-\overline{\int_{w_r<0} w_r dS} \qquad (1.19)$$

Where w_r is the radial component of the relative velocity and S is the surface area and integrating for $w_r<0$ is the sum of the radial components of relative velocity whose direction is into the sphere. If the particles are randomly distributed and moving with the fluid the collision rate is described by the following term:

$$-\overline{\int_{w_r<0} w_r dS}(n_1 n_2) \qquad (1.20)$$

In order to evaluate the integral in Equation 1.20, the continuity equation was used to find the solution for the entire sphere.

$$-\overline{\int_{w_r<0} w_r dS} = \frac{1}{2}\int\overline{|w_r|}dS = 2\pi R^2\overline{|w_x|} \qquad (1.21)$$

w_x is the radial relative velocity along the radius parallel to the x-axis.

Since the length scale of the smallest eddy, η, is defined by Kolmogorov as:

$$\eta = \left(\frac{\upsilon^3}{\varepsilon}\right)^{1/4} \qquad (1.\ 22)$$

It can be assumed that R is much smaller than η; therefore, w_x was solved to be:

$$\overline{|w_x|} = R\overline{\left|\frac{\partial u}{\partial x}\right|} \qquad (1.\ 23)$$

Using Taylor's derivation for the mean square of the velocity gradient

$$\overline{\left(\frac{\partial u}{\partial x}\right)^2} = \left(\frac{\varepsilon}{15\upsilon}\right) \qquad (1.\ 24)$$

and assuming that $\delta u/\delta x$ is normally distributed, Equation (1.32) becomes:

$$\overline{\left|\frac{\partial u}{\partial x}\right|} = \left(\frac{2\varepsilon}{15\upsilon}\right)^{1/2} \qquad (1.\ 25)$$

Now substitute the solution for 1.19 into 1.20. The solution for 1.19 is obtained by substituting Equation 1.25 into Equation 1.23 and Equation 1.23 into Equation 1.21 to get Equation 1.26:

$$N = 2.3 n_1 n_2 (r_1 + r_2)^3 \left(\frac{\varepsilon}{\upsilon}\right)^{1/2} \qquad (1.\ 26)$$

Saffman and Turner leave unexplained the removal of the square root of pie to get a constant of 1.3 in Equation 1.18 instead of 2.3 in their final collision equation in Equation 1.26.

Camp and Stein derived a similar equation. The only difference in their final equation was that their constant in Equation 1.18 was 1.33 instead of 1.294. Camp and Stein used a completely different approach and there is some debate that the accuracy of their result is purely coincidental (Cleasby ,1984 & Clark 1985); however, their assumption that energy is conserved as it is transferred into the turbulent fluid is clearly correct.

Camp and Stein (1945) used the fluid shear equation for laminar flow to derive a fluid shear equation for turbulent flow. They assumed that the velocity gradient at a point was equivalent to a mean velocity gradient of the entire turbulent system. They then directly substituted this mean velocity gradient into the velocity gradient term of the shear equation for laminar flow (Equation 1.27). The shear equation for laminar flow is:

$$\tau_s = \mu \frac{du}{dx} \qquad (1.27)$$

There are two mistakes in this direct substitution. The first error was assuming that the viscosity term for laminar flow remains the same for turbulent flow. The molecular viscosity (μ), which is a property of the fluid, becomes negligible in fully turbulent flow and the eddy viscosity becomes dominant. The second error was assuming that the velocity gradient at a point could be directly substituted into the velocity gradient term in the laminar shear equation. Camp (1985) and Cleasby (1984) have discussed these errors in detail. Both claim that it was coincidental that Camp and Stein's equation is similar to the well-defended Saffman and Turner equation, and that the name of the collision parameter should be changed. In this work, G will be referred to as the characteristic shear rate.

The Effect of Precipitate Size on the Total Collision Rate

There exist three processes, each with their corresponding equations, by which particle collisions may occur: Brownian motion, fluid shear and differential settling. Turbulence only plays a role if the dominant collision mechanism is fluid shear. Otherwise, only particle size and fluid properties influence the collision rate. It is generally accepted that the total number of collisions can be found by summing the number of collisions due to all three processes (Han and Lawler, 1992).

The total collision frequency function for each of the aluminum hydroxide precipitate sizes discussed in Section 1.4.1.1 , 0.01 micron and 1 micron, is illustrated in Figure 1-17 and Figure 1-18. For the smaller habit of amorphous

aluminum hydroxide precipitate, Brownian motion is the dominating mechanism of particle collisions and the particle collision rate function remains smaller than 10^{-11} cm^3/s even when G is 1500 s^{-1}, as shown in Figure 1-18. For the larger habit of amorphous aluminum hydroxide precipitate, fluid shear is the dominating mechanism of particle collisions and the collision frequency function is 10^{-9} cm^3/s for G=1500 s^{-1} and $10^{-10} cm^3/s$ for G=50 s^{-1}, as shown in Figure 1-17. As the initial precipitate agglomerates to 10 times its initial size, the collision rate frequency for the larger precipitates quickly exceeds 10^{-7} cm^3/s, while the smaller precipitate continues to be dominated by Brownian motion and the collision rate frequency function remains below 10^{-11} cm^3/s. Therefore, it is reasonable to conclude that the floc formation rate for the larger precipitates will be 10 to 10 000 times faster than the smaller ones. Note that the fluid shear collision rate equation is valid only if the diameter of the colliding particles is smaller than the Kolmogorov length scale, which is of the order of 200 microns (Equation 1.22).

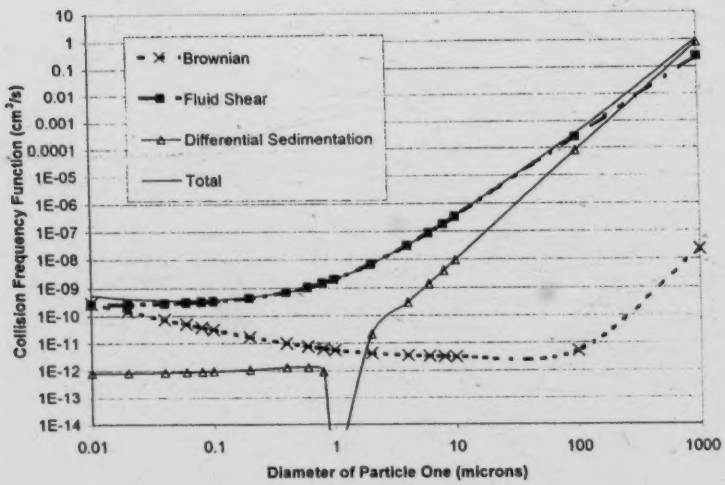

Figure 1-17 The total collision rate function for larger aluminum hydroxide precipitates. (d_2=1 micron, SG=2.65 , G=1500 s^{-1})

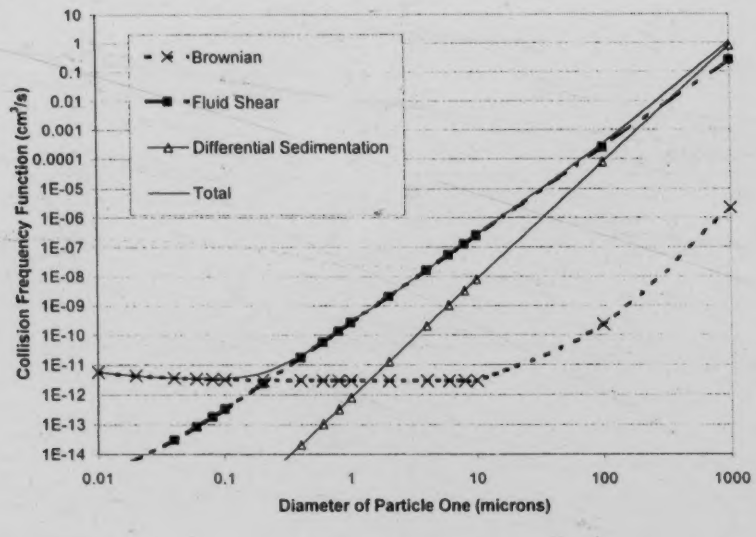

Figure 1-18 The total collision rate function for smaller aluminum hydroxide precipitates. (d_2=0.01 micron, SG=2.65, G=1500 s^{-1})

1.6 Colloidal Stability and Removal in Water Treatment

Forces due to hydration and/or electrostatic charge surrounding each particle prevent agglomeration and promote the sustained suspension of colloids in aqueous solution. These forces are referred to as stabilizing forces. Stabilization of colloids occurs regardless of a naturally occurring particle's affinity to water (ie: hydrophobic or hydrophilic). If the colloid is hydrophilic, it has an affinity to water molecules and the stabilization mechanism is hydration. Because of the particle's affinity to water, an adherent layer of oriented water molecules surrounds the particle. If the colloid is hydrophobic, a layer of oppositely charged ions from the bulk solution, instead of a layer of oriented water molecules, surrounds each colloid. Both the layer of oriented water molecules and the layer of opposite charged ions create a repulsion force between particles that prevents agglomeration. In natural waters, colloids are mostly hydrophobic and because of their negative functional groups are predominantly negatively charged (Faust and Aly, 1983); therefore, they are stabilized by the formation of a layer of positively charged ions from the bulk solution.

1.6.1 Stabilization Mechanisms of Colloidal Particles

Surface stabilization and slow settling times make colloidal removal from solution difficult. Large-scale water treatment depends upon the agglomeration of colloids into larger clusters to reduce settling times. This is accomplished with coagulants and coagulant aids, such as alum and polymer. Coagulants do not react with the colloid, but attach to their surfaces. Alum can either adsorb onto a particle or entrap a particle in an agglomerate of alum's precipitates and colloids. Polymer creates fibrous bridges between particles by adsorbing onto their surfaces.

In water treatment, the removal of electrostatically stabilized colloids may be achieved by four mechanisms: double layer compression, adsorption/charge neutralization, entrapment (sweep), or adsorption/inter-particle binding. Alum works via the adsorption/charge neutralization and entrapment mechanisms.

Polymer promotes removal by adsorbing onto particle surfaces to cause inter-particle binding.

It is important to establish which of these four mechanisms of destabilization a coagulant uses, since the mixing conditions, which optimize one mechanism, could be detrimental to another. If the mechanism is entrapment, mixing conditions producing precipitate 100 times smaller than expected would be detrimental; however, the mixing conditions detrimental to entrapment may increase the number of collisions. This will improve particle removal if the mechanism of destabilization is adsorption/charge neutralization.

The first mechanism, double layer compression, deals with the collapsing of the charged layer, referred to as the "diffuse double layer", surrounding a charged particle. The two surrounding layers that neutralize the charged particle are the Stern layer followed by the "diffuse double layer". The potential gradient across the diffuse double layer is the Zeta Potential and the total potential gradient across both layers is the Nernst Potential, as illustrated in Figure 1-19. The thicker the diffuse layer, the more difficult it becomes for counterions to adsorb to the charged particle, thus hindering coagulation. By compressing the diffuse double layer of ionic charges surrounding the particles in aqueous solution, the Zeta Potential is decreased and adsorption is promoted. One method of compaction of the diffuse double layer simply involves increasing the concentration of electrolytes in solution (Faust and Aly 1983). The concentration of electrolytes in solution will change as the alum dosage changes, thus if double layer compression was an important mechanism in coagulation with alum, Zeta Potential measurements would be valuable.

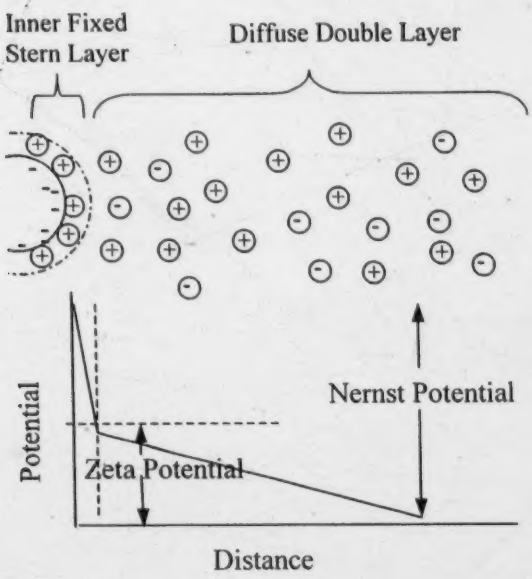

Figure 1-19 The Nernst Potential and the Zeta Potential of the inner fixed (Stern) and outer double diffuse layer of ions surrounding a particles.

The second possible mechanism involves the neutralization of the charged particle with an adsorption mechanism. In Adsorption/Charge Neutralization the particle is neutralized by the adsorption of oppositely charged ions onto the charged particle, as illustrated in Figure 1-20 a.

The third mechanism is a physical entrapment process, often referred to as sweep coagulation, where agglomerates of aluminum hydroxide precipitate physically engulf colloidal particles and then flocculate and settle. This physical mechanism for particle removal is represented in Figure 1-20 b.

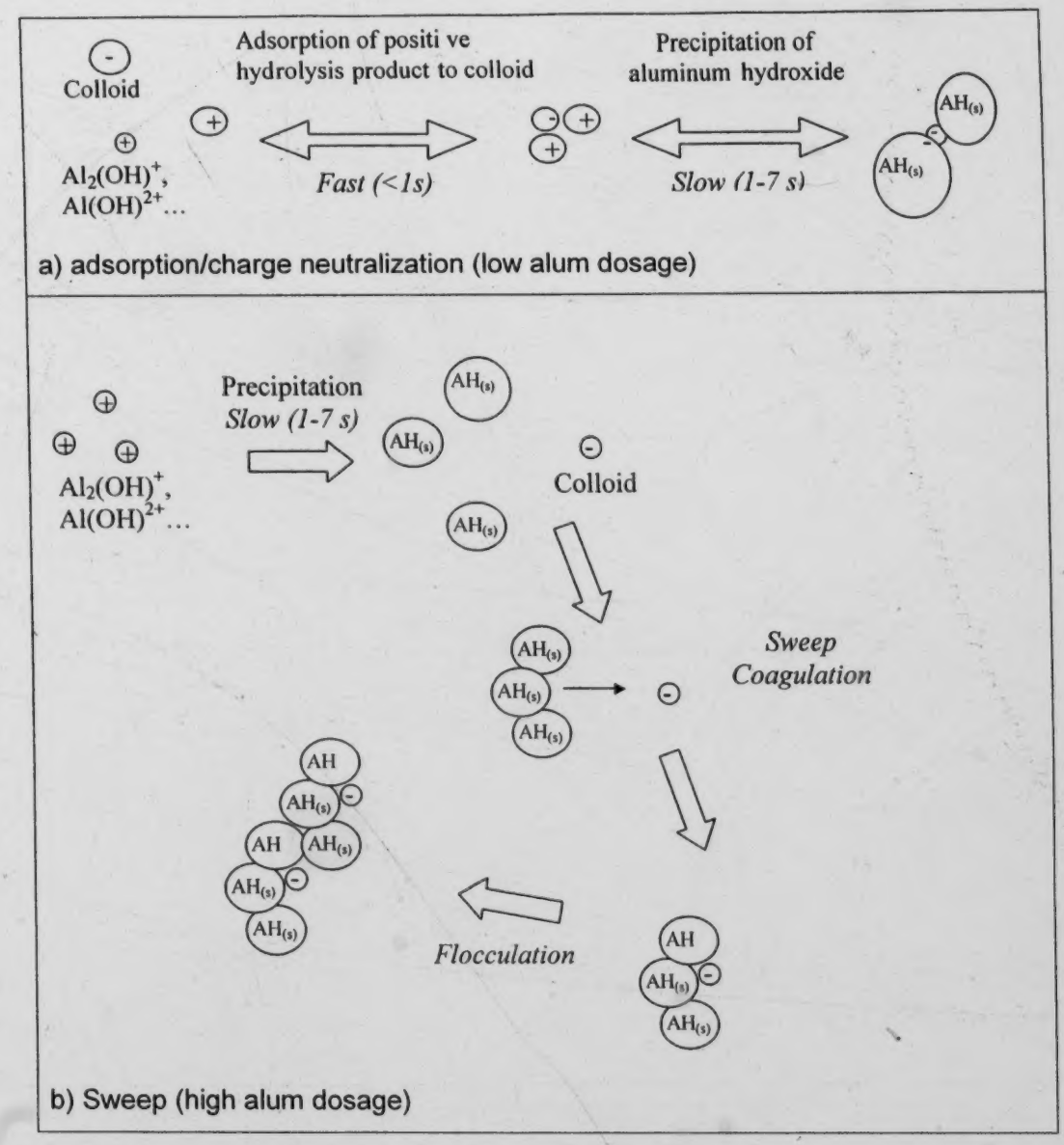

Figure 1-20 Illustration of two mechanisms by which Alum destabilizes colloids in solution a) adsorption/charge neutralization b) sweep

The final mechanism is a bridging model where adsorption and inter-particle binding occur. This mechanism involves the agglomeration of particles by binding them together. This can be achieved with polymers. The polymers

adsorb onto the specific sites of colloidal particles and create fibrous bridges to other particles, binding numerous colloidal particles together. This mechanism is illustrated in Figure 1-21.

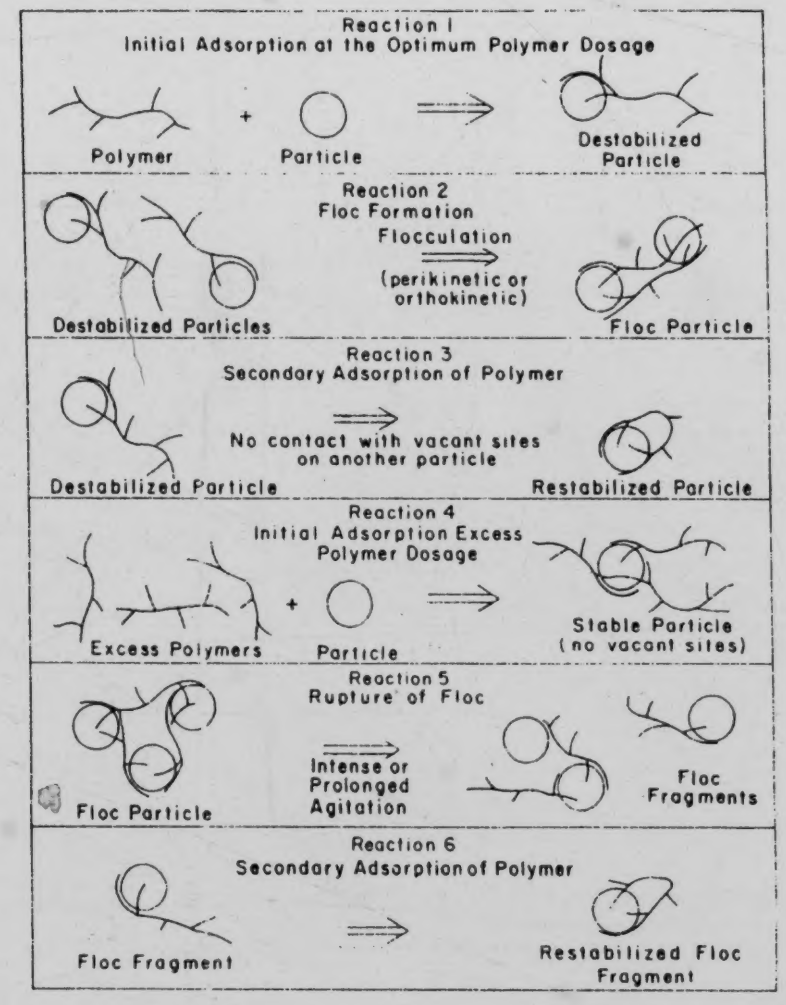

Figure 1-21 The bridging model of adsorption and interparticle binding achieved with polymers (O'Melia, C. R. In: Physicochemical Processes for Water Quality Control, W.J. Weber Jr., 1972, John Wiley & Sons. Reprinted by permission of John Wiley & Sons, Inc.)

1.6.2 How Alum Destabilizes Colloids

There are two widely accepted mechanisms for coagulation with alum in water treatment. These two mechanisms are often referred to as sweep and adsorption/charge neutralization. Sweep involves the colloidal destabilization mechanism of entrapment, while adsorption/charge neutralization involves adsorption-destabilization. The two mechanisms are illustrated in Figure 1-20.

1.6.2.1 Charge Neutralization

Adsorption/Charge Neutralization involves the adsorption of the positive aluminum hydrolysis ionic species to negatively charged colloids before the formation of aluminum hydroxide precipitate (10^{-4} to 1 second) as illustrated in Figure 1-20a. Evidence of this mechanism can be seen with improvements in turbidity removal as the intensity of mixing upon alum addition is increased. The initial intensity of mixing will determine the number of collisions between the colloids and the positively charged hydrolysis products, which exist for only fractions of a second. Therefore, if the mechanism of coagulation is charge-neutralization, an increase in the number of particle collisions in the first second should improve turbidity removal (Amirtharajah *et al.*, 1991). This mechanism is optimized when the mixing conditions have a high initial mixing intensity.

1.6.2.2 Sweep

Sweep coagulation involves collisions between the colloids and agglomerates of the aluminum hydroxide precipitates instead of cationic hydrolysis products. In sweep coagulation, colloidal particles are entrapped by aluminum hydroxide agglomerates during mixing and settling. Therefore, the sweep mechanism is dependent upon the initial precipitate size and the product of G and mixing time (Gt). The initial precipitate size will determine the collision rate, thus rate of formation of the agglomerates, which sweep the colloids in the water (illustrated in Figure 1-20b). A minimum Gt is required to obtain a minimum size of agglomerate required for optimum floc formation and settling.

Sweep coagulation can be broken down into three steps (illustrated in Figure 1-20b):

1. Precipitation of aluminum hydroxide (1-7 seconds)
2. Formation of aluminum hydroxide agglomerate (minutes)
3. Entrapment of the colloidal particles by the aluminum hydroxide agglomerates (minutes)

The size of the aluminum hydroxide agglomerate can be predicted from the collision equation parameter, Gt. Particles collisions only play a role in 2 of the 3 steps; therefore, Gt alone may not fully explain turbidity removal efficiency. Letterman *et al.* (1971) and Vrale and Jordan (1971) have observed the inadequacy of Gt or G in fully predicting turbidity removal. When they compared mixing devices with the same G and mixing times, the residual turbidities still varied. Factors affecting the extent of turbidity removal, in addition to G and time, must exist. Perhaps the effect of mixing on precipitate morphology may further explain differences in turbidity removal.

1.6.3 How Polymer Destabilzes Colloids

The polymer used in this work and by Epcor Water Services promoted coagulation by the inter-particle binding mechanism illustrated in Figure 1-21.

1.6.4 Determining Whether the Mechanism of Coagulation with Alum is Sweep or Charge Neutralization

The mechanism of coagulation with alum can be reasonably predicted or confirmed experimentally. Predictions can be made from the well-established Design and Operation Diagram presented in Amirtharajah and Mills in 1982 (Figure 1-22). Given the final pH and alum dosage, the zone of operation can be determined.

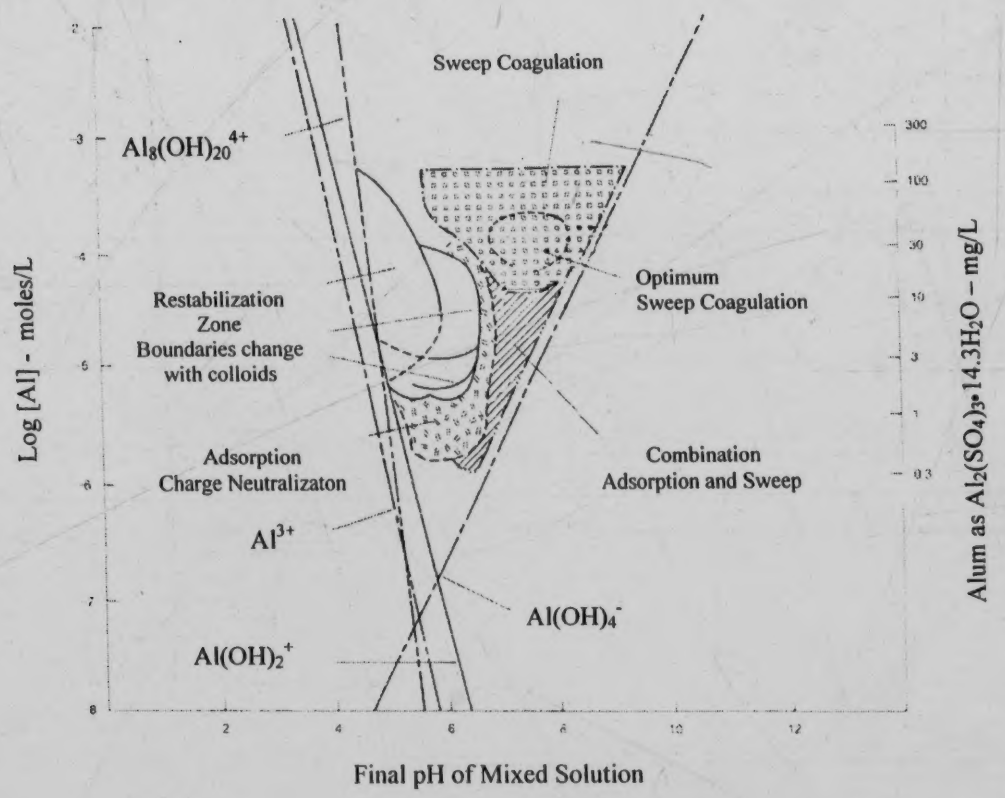

Figure 1-22 The design and operation diagram for alum coagulation in water. (Amirtharajah and Mills, 1982. Reprinted from Mixing in Coagulation and Flocculation, by permission. Copyright 1991, American Water Works Association)

From the Design and Operation diagram in Figure 1-22, it can be seen that if the pH of the mixed solution is 7.5, the mechanism of coagulation will be sweep if the alum dosage is greater than 15 mg/L. If the alum dosage is less than 15 mg/L, experiments must be done to confirm whether the predominant mechanism is sweep or charge neutralization.

Confirmation of the mechanism of coagulation can be made experimentally, by measuring the effect of rapid mixing on turbidity removal. If

turbidity removal does not improve as the intensity of the initial rapid mix period is increased, then the mechanism of coagulation is sweep. It has also been reported that an optimum rapid mix time exists in coagulation by sweep (Letterman, 1973 & Kan *et al.*, 2002), as shown in Figure 1-23. Some experimenters plot rapid mix time versus turbidity removal and use the existence of an optimum point to verify that the mechanism of coagulation is sweep (Kan *et al.*, 2002).

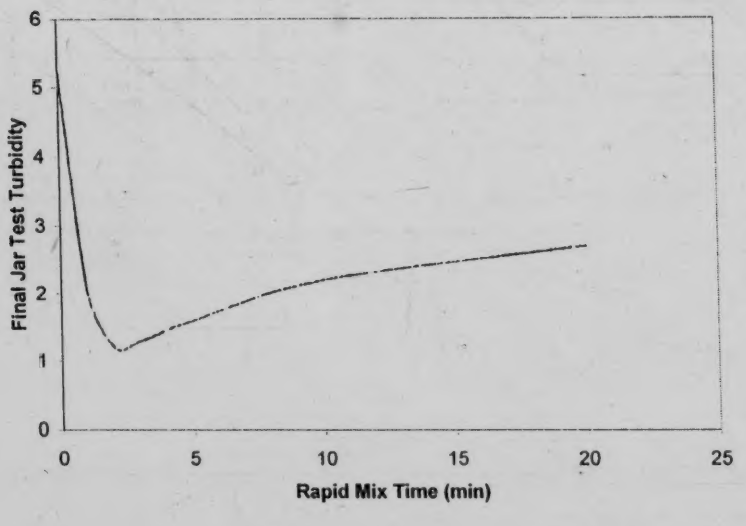

Figure 1-23 Optimum rapid mix time (Alum dosage = 10 mg/L, G=1,000 s^{-1}) (Data taken from Letterman et al, 1973)

The following two plots have a similar shape to Figure 1-23, but illustrate completely different concepts.

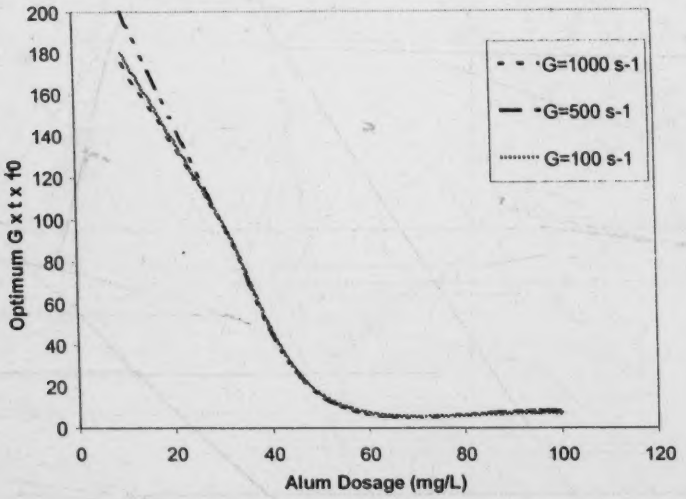

Figure 1-24 The dependence of optimum Gt on Alum dosage and initial G (data taken from Letterman, 1973).

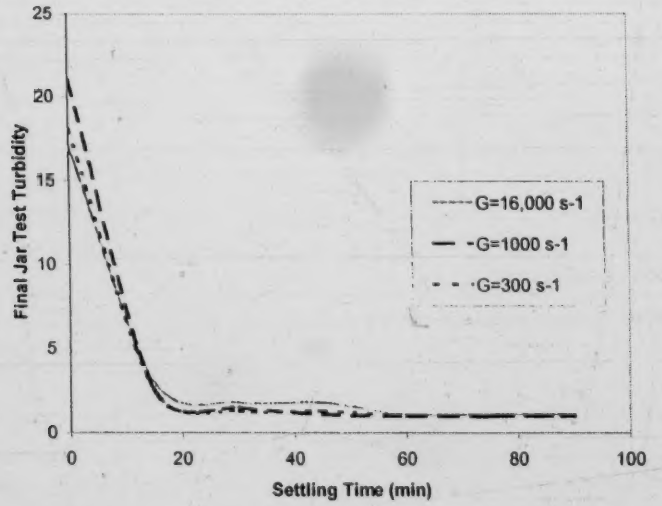

Figure 1-25 Settled water turbidity curves at 15 mg/L of alum and pH of 7.7-8.0. Total Gt is constant at 16 000 (data taken from Amirtharajah and Mills, 1982).

Another method to verify sweep coagulation is to show that only alum dosage and Gt, rather than initial G, influence turbidity removal. Letterman's plot in Figure 1-24 (Letterman, 1973) shows that the optimum Gt requirement increases as the alum dosage decreases, regardless of the initial G. Kan et al (2002) failed to plot Gt versus turbidity. To eliminate the effects of Gt, Amirtharajah and Mills (1982) choose a constant Gt of 16 000 and measured the turbidity removal at settling times from 0 to 90 minutes. Their results are plotted in Figure 1-25. They showed that if the mechanism of coagulation is sweep, turbidity removal is independent of the initial G, as illustrated in Figure 1-25.

1.7 Mixing

The five methods reviewed for this work were pipes in turbulent flow, HEV static mixers, continuous stirred tanks, inline mechanical mixers and standard water treatment jars (batch stirred tanks). The following is a description of the mixing concepts used, followed by the equations used to calculate mixing intensity, dispersion and the time required to fully mix, the blend time.

The mixing intensities and dispersion obtained with each mixing method will be used in this work to determine their effects on the performance of alum.

1.7.1 Concepts

Dispersion

Dispersion is the process of distributing or spreading out of concentration profiles by convection or diffusion. For this work, diffusion will be considered negligible and all dispersion will be assumed to occur by convection that results from turbulent fluid motion. Dispersion of a solute in a solvent may be quantified or described in a number of ways: the extent of macromixing, rate of dispersion, backmixing or rate of dilution. In this work, alum and water are mixed together: alum will be referred to as the solute and water as the solvent.

Scales of Mixing: Macro versus Micromixing

Macromixing and micromixing are the large and small scales of mixing, respectively. Macromixing occurs as one fluid is dispersed by convection into a volume of another fluid resulting in a reduction of the average concentration gradients in that fluid volume. The extent of macromixing will determine the time required to achieve a fully macromixed volume. This mixing time is referred to as the blend time and is influenced by properties of turbulence. Micromixing is also influenced by turbulence. Micromixing is a further reduction in average concentration gradient by convection or diffusion to the point where the scale of uniformity in the fluid is of the same order of magnitude as the individual molecules.

The extent of macromixing varies between a pipe and a CST (continuous stirred tank). In an ideal CST, mixing is instantaneous. In an ideal plug flow pipe, radial mixing is also instantaneous. In a real pipe in turbulent flow, radial dispersion occurs more slowly.

Radial and Axial Dispersion in a Pipe

Dispersion of solute in a pipe may occur radially and axially (longitudinal) as it travels along the direction of flow. In some cases, axial dispersion in a pipe can be assumed negligible. If a pipe is in turbulent flow, the velocity profile is relatively flat and plug flow may be assumed. Therefore, axial dispersion may be considered negligible and the solvent/solute mixture downstream of the injection point will not backmix into newly injected solute. As will be discussed in Section 1.7.2.2, an HEV static mixer has much faster radial dispersion than an empty pipe of the same diameter. Radial mixing will be complete after six pipe diameters for a static mixer but requires fifty pipe diameters for an empty pipe.

Backmixing

Backmixing is a term used to describe a specific case of dispersion. Some mixing conditions mix the solute directly into fresh solvent, while others mix the solute into a solvent that has already had solute added to it. The later of

the two results in the solute being mixed to a solvent/solute mixture and is given the term backmixing. For a stirred tank in a batch test, the solute is injected directly into a volume of solvent, so there is no backmixing. If the stirred tank is in continuous flow however, the solute is injected into a solvent/solute mixture and backmixing dominates. In the water treatment industry, a CST is often referred to as a backmixer.

Dilution

The extent and rate of dilution is another way to quantify dispersion. The dilution rate of a pulse injection into a CST and a stirred tank in batch mode are very different, especially if a reaction takes place and the composition of the injected solute changes form with time. A reaction occurs as liquid alum is added to water: the aqueous form precipitates as aluminum hydroxide. The local concentration of the aqueous form of alum (solute) will be dependant upon the reaction time and the amount of water (solvent) mixed into the alum. During the time preceding precipitation, the dilution of the aqueous form of alum is simply the injected solute (alum) volume divided by the volume of solvent (water) mixed into it. The relative volume of water mixed into the liquid alum before precipitation occurs is orders of magnitude higher for a CST than a batch stirred tank. Since the volume of water mixed into the liquid alum before precipitation occurs is much larger for the CST, the dilution will be extremely higher.

Tracer Test (Residence time distribution)

The tracer test is a one method of measuring dispersion. This test is often used to examine the dispersive properties of a vessel. The results from a tracer test can be summarized in a distribution curve called the residence time distribution curve (RTD). The RTD reports the residence time of each fraction of the injected solute. One type of tracer test involves an instantaneous pulse injection of a known quantity of tracer and its change in concentration is then measured at one point with time.

As discussed earlier, a pipe in turbulent flow has a relatively flat velocity profile and axial dispersion may be considered negligible; therefore, the tracer

will only disperse radially as it travels down the pipe at the same speed as the fluid velocity in the pipe. Once fully radially dispersed, a plug of tracer across the entire cross section of the pipe will continue to flow at the velocity of the fluid in the pipe. When the tracer sensors detect the plug of tracer is dependent upon the velocity in the pipe and how far away the tracer detection point is from the injection point. Figure 1-26 illustrates the detection of the tracer at points 1 and 3 minutes from the injection point.

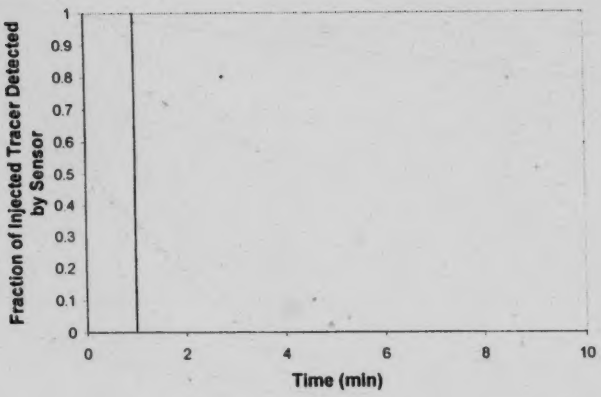

a)

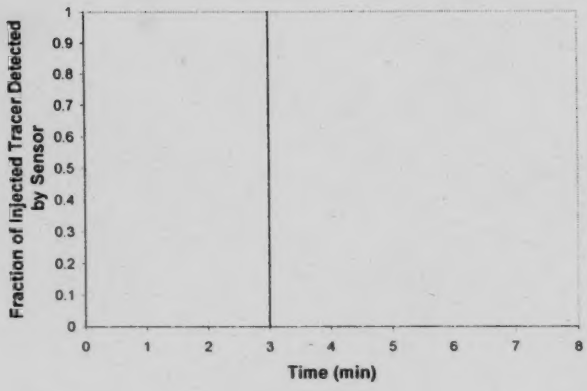

b)

Figure 1-26- Illustration of tracer detection for a pipe. The fraction of injected tracer detected by a) tracer sensor at 1 minute from injection point b) tracer sensor at 3 minutes from injection point.

For stirred tanks in batch mode all injected tracer remains in the stirred tank for the entire length of the batch test as illustrated in Figure 1-27 a. The RTD of a continuous stirred tank is more complex, since some injected tracer leaves the tank immediately after injection and some remains in the tank longer than the residence time of the tank. For an ideal CST with a constant density

system, where ideal means instantaneous mixing, the injected tracer is immediately dispersed throughout the tank, so the tracer concentration detected by a sensor in the tanks is representative of the tracer concentration throughout the tank. The fraction of tracer particles remaining in the tank with time is called the washout function. For an ideal CST the washout function is defined by (Hayes, 2000):

$$W(t) = \exp\left(\frac{-t}{t_m}\right) \qquad (1.28)$$

For a constant density system:

$$t_m = \left(\frac{Q}{V}\right) \qquad (1.29)$$

Where:

W(t)=washout function

t = time

Q = volumetric flowrate

V = volume of the CST

The fraction of injected tracer in a batch and continuous stirred tank with a residence time of 3 minutes is illustrated in Figure 1-27

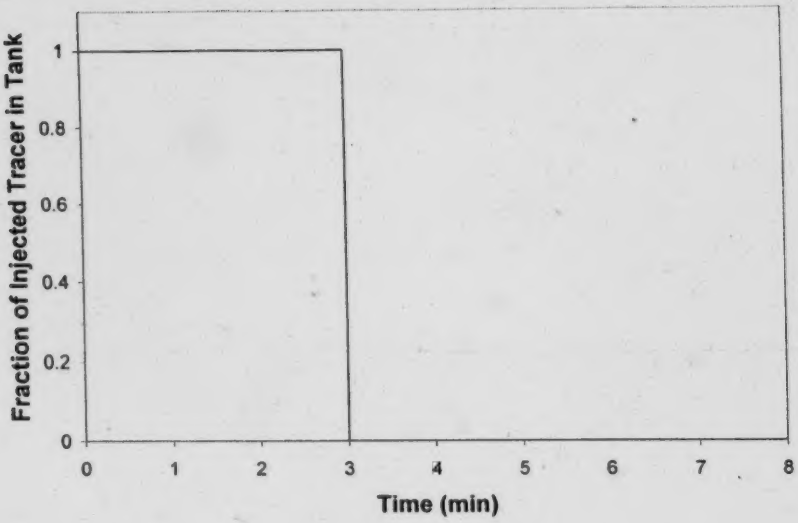

a)

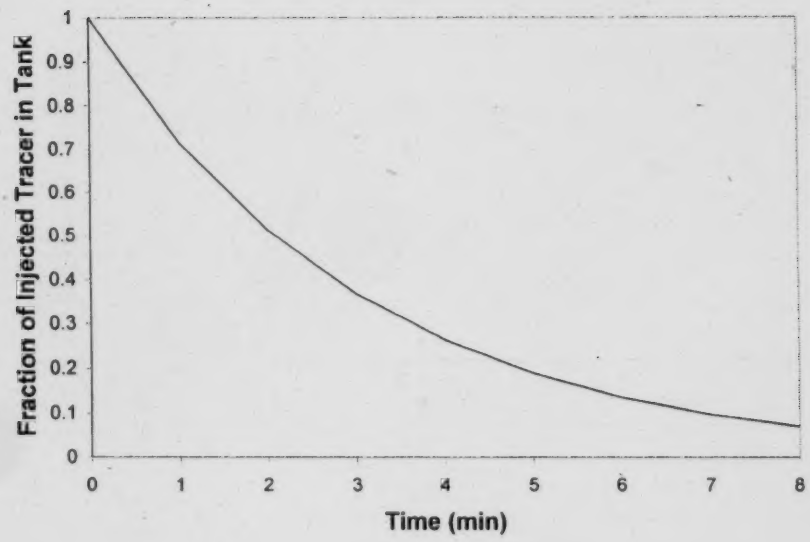

b)

Figure 1-27 Illustration of the tracer detection for an ideal stirred tank in batch and continuous modes a) a batch stirred tank with a residence time of 3 minutes b) ideal continuous stirred tank with a residence time of 3 minutes.

1.7.1.1 The Effects of Dispersion on Local Concentrations

The effect of mixing on local reactant concentrations and thus the reaction rates is recognized in reactor modeling. Figure 1-28 illustrates different reactor models are used for different levels of macro and micromixing. A pipe in plug flow is modeled as a plug flow reactor and a CST as a continuous stirred tank reactor. The purpose of this section is not to go into the details of reactor modeling, but rather to identify the effects of dispersive mixing on local concentrations and thus the reaction rates in a reactor. If the flowrates, reaction rate equations and residence time distributions are known, the change in local reactant concentration with time throughout the reactor vessel may be calculated. Unfortunately, no reaction rate equations for the alum/water system were found during the literature review, so only general concepts can be applied.

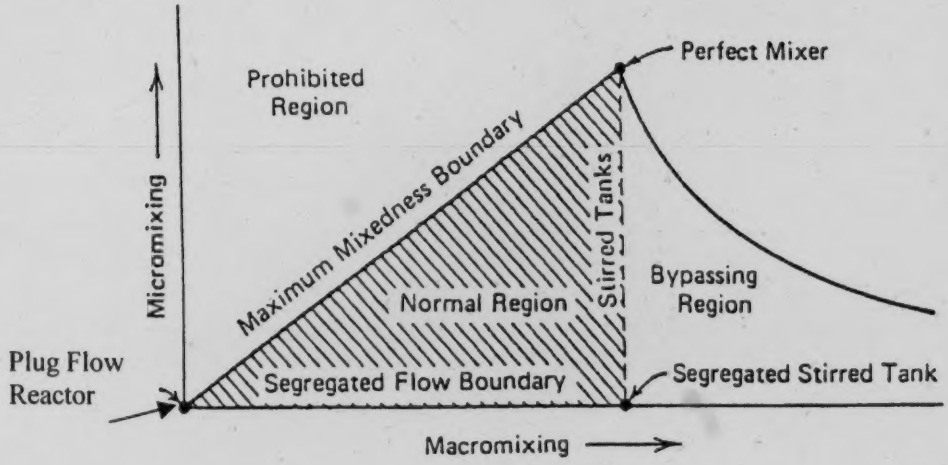

Figure 1-28 The extent of micro and macro mixing in reactor models with continuously stirred tank and turbulent pipe flow (plug flow) reactors (Nauman and Buffman, 1983. Mixing in Continuous Flow Systems, Copyright 1983, John Wiley & Sons, New York. Reprinted by permission of John Wiley & Sons, Inc)

If the reaction kinetics are normal and greater than first order, the overall conversion in a pipe with plug flow will be higher than a CST of the same volume, since a plug flow reactor will have higher local reactant concentrations than a CST. Normal reaction kinetics are when the reaction rate increase as the concentration of the reactants increase. As introduced in Section 1.3, aluminum undergoes a series of hydrolysis reactions before precipitating as aluminum hydroxide, so a higher order overall reaction is likely. Thus, differences in aluminum hydroxide precipitation between a CST and a pipe in plug flow should be expected.

For higher order reactions, a higher local concentration results in a faster reaction rate; therefore, it may initially be expected that the higher liquid alum concentration in the plug flow reactor should result in faster reaction rates and thus faster precipitation. But precipitation from the alum/water system depends upon more than just local concentration. It also depends upon the relationship between equilibrium solubility and pH. Precipitation in the alum/water system involves a complex interaction of reaction kinetics and the pH sensitive thermodynamic solubility. The reaction kinetics for the precipitation of aluminum hydroxide depend upon supersaturation, the difference between actual and equilibrium concentrations, not just the actual concentration. As discussed in Section 1.3.1, the equilibrium concentration is determined by the pH and the rate of change of pH controls the degree of supersaturation and thus the rate of precipitation, as introduced in Section 1.3.2. This effect is highly non-linear. The effects of mixing on [illegible]cipitation mechanisms may be better understood if water is thought to mix into liquid alum, instead of the traditional logic of mixing alum throughout the water. The pH of the liquid alum is low: the pH of the liquid alum used in this work was 3. The pH of water is relatively high, so as water is mixed into liquid alum, the pH of the alum solution will increase. A rapid dilution rate of liquid alum will result in a rapid decrease in the local concentration of alum, which results in a rapid increase in pH and thus a high degree of supersaturation as presented in Section 1.3.2. The degree of supersaturation determines the precipitate size, as was discussed in Section 1.4.3. A gradual dilution of liquid

alum with water during aluminum hydroxide precipitation results in a slow increase in pH and thus a lower degree of supersaturation and slower rate of precipitation. The local concentrations of the reactants will be diluted more quickly in a CST than a plug flow reactor, thus the pH will increase faster and more small precipitate formation should be expected in a CST. The opposite should be expected for mixing in a real pipe; therefore, larger precipitate formation should be expected in this case.

The local reactant concentrations are extremely important, since it was shown in Section 1.3.2 that supersaturation is dependant upon reactant concentration and Section 1.4 showed that that the size and structure of the aluminum hydroxide precipitate is in turn dependant upon supersaturation. By combining the logic in Section 1.3.2 and 1.4, it is concluded that the local reactant concentrations determine the size and structure of the aluminum hydroxide precipitate. Thus, it is reasonable to expect different precipitate morphology between an ideal CST and a pipe with radial dispersion in plug flow.

1.7.1.2 *Mixing Intensity Due to Turbulence*

Energy from a power input may be transferred into a system either directly as heat or as turbulent kinetic energy, which is ultimately also dissipated as heat. If all power entering a turbulent system is assumed to transfer into turbulent kinetic energy the rate of power input is essentially equal to the rate of energy dissipation, since energy is conserved as it is transferred from the large to the smallest eddies. The dissipation of heat by the smallest eddies is illustrated in Figure 1-29. In turbulent theory the rate of turbulent energy dissipation per unit mass (ε) is used to quantify the intensity of turbulence. The power source may be mechanical energy from an impeller, or the pressure drop in a pipe. The size of the smallest turbulent eddies is defined by the Kolmogorov length scale (Equation (1.30)), η, and the time required to dissipate the kinetic energy contained in the smallest eddies is defined by the Kolmogorov time scale, τ_K (Equation (1.31)). The amount of kinetic energy initially transferred to a turbulent system determines the size scale and time scale of the smallest eddies.

$$\eta = \left(\frac{\upsilon^3}{\varepsilon}\right)^{1/4} \qquad (1.30)$$

$$\tau_K = \sqrt{\left(\frac{\upsilon}{\varepsilon}\right)} \qquad (1.31)$$

Any one of the variables ε, η, τ_K or $1/\tau_K$ can be used to define the mixing intensity of a system. Historically G, which is equal to $1/\tau_K$, has been used to define the mixing intensity in the water treatment industry. For a discussion of G and its derivation, refer to Section 1.5.1.

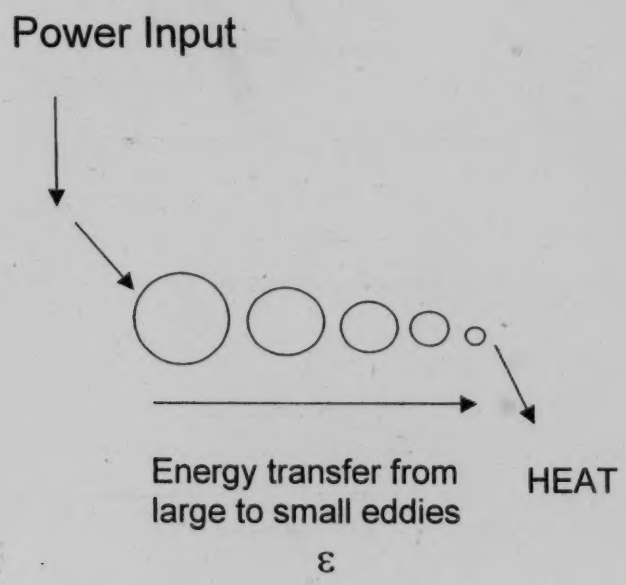

Figure 1-29 Dissipation of Energy from Power Input

1.7.2 Equipment

1.7.2.1 Static Mixers

A static mixer produces mixing conditions of fast radial mixing with minimal axial mixing. A static mixer is a baffled pipe, which is used to continuously induce mixing of the fluid flowing through the pipe. As the flowrate increases, so does the pressure drop across the static mixer and thus the mixing intensity. The power for mixing in the static mixer comes from the pressure drop created as the fluid flows past the baffles.

Static mixers for turbulent flow are based upon the design principles of mixing by large eddies and forced radial convection created by obstacles in the flow (Jaffer *et al.*, 1998). The static mixer used in this study is a high efficiency vortex, HEV, static mixer. It consists of 2 sets of 4 tapered tabs equally spaced around the inner circumference of the pipe. Each tab of the HEV static mixer generates a pair of stream wise counter-rotating vortices that produces vigorous cross-stream mixing and rapid uniformity (Chemineer web site, 2003). The length between tabs of the HEV static mixer is 1.5D (Chemineer website, 2003)

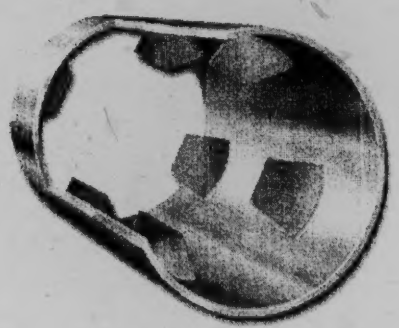

Figure 1-30 HEV static mixer (Courtesty of Chemineer, 2003)

Figure 1-31 Flow pattern of the double vortex off of each tab in the HEV static mixer (Courtesy of Chemineer, 2003)

Pressure Drop

Calculation of the pressure drop across a static mixer is analogous to the calculations used for pressure drop in a pipe. For pressure drop in a pipe Equations 1.32 and 1.33 are used.

$$\Delta P = F\rho \qquad (1.32)$$

$$F = \left(\frac{4fL}{D_p}\right)\frac{u_b^2}{2} \qquad (1.33)$$

Where *f* is the Fanning (Darcy) friction factor. If the Moody friction factor (f') is used, then Equation 1.33 for friction losses becomes equation (1.41) (Perry, 1973):

$$F = \left(\frac{f'L}{D_p}\right)\frac{u_b^2}{2} \qquad (1.34)$$

For an HEV static mixer the Darcy friction factor is 0.7 if the Reynolds number for pipe flow (Equation 1.35) is greater than 10,000 (Fasano & Penny, 1991 as cited in Ch 13 of Paul *et al.*, 2003). The Reynolds number for pipe flow can be calculated by the following equation (Perry, 1973):

$$\mathrm{Re} = \frac{D_p u_b \rho}{\mu} \qquad (1.35)$$

Characteristic Shear Rate, G

If all of the energy input into the fluid from pressure drop is assumed to go into the production of turbulence, the equation for G in a static mixer can be derived. The rate of turbulent energy dissipation per unit mass (ε) is equal to the power input divided by the unit mass (Jaffer *et al*, 1998):

$$\varepsilon = \frac{f'(u_b)^3}{2D_p} \qquad (1.36)$$

Once we have calculated the rate of turbulent energy dissipation, it can be substituted into Equation 1.37 to calculate G for a given kinematic viscosity.

$$G = \left(\frac{\varepsilon}{\upsilon}\right)^{1/2} \qquad (1.37)$$

Blend time

Experimental data reveals that an HEV static mixer with fluid injected into the centerline of the pipe will fully be mixed within six pipe diameters. Before blending begins, the coefficient of variation is 1 and after 4 pipe diameters the coefficient of variation drops to below 0.002 if the Reynolds number is greater than 10 000 (refer to Figure 1-32). If the coefficient of variation is less than 0.002, a system is more than 95% mixed; therefore, a conservative estimate of the blend time may be determined by calculating how long it will take for the fluid to flow six pipe diameters. An illustration of the chemical plume profile for a HEV

static mixer in a pipe is in Figure 1-33. The blend time for static mixers can be calculated from Equation 1.38

$$\theta_b = \frac{6D_p}{u_b} \qquad (1.38)$$

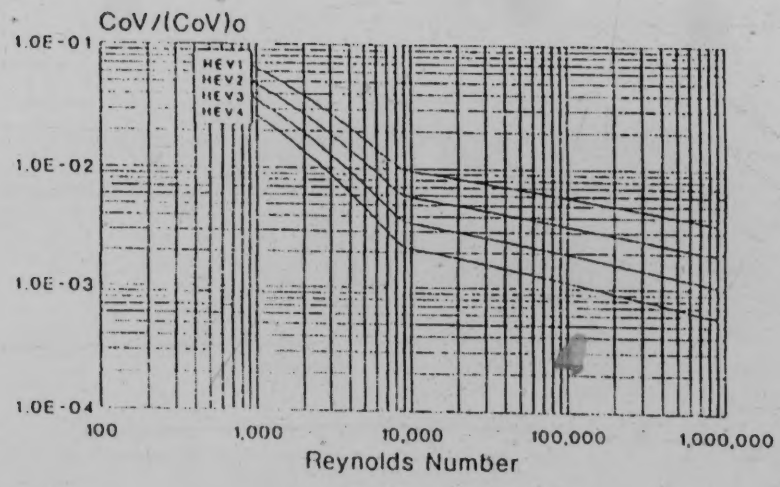

Figure 1-32 Mixing in an HEV static mixer after 3 pipe diameters with 2 sets of tabs (HEV2). If Re>10,000, the coefficient of variation is <0.006 (Courtesy of Chemineer, 2003)

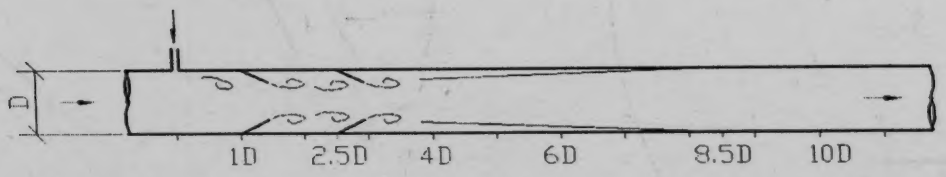

Figure 1-33 Plume profile in an HEV static mixer with chemical injection inline with the top tab of an HEV static mixer (tabs not drawn to scale) (drawn by Louis Kennedy, 2003).

Dispersion

The HEV static mixer has radial mixing much faster than a pipe and minimal axial mixing thus negligible backmixing. For turbulent flow with a Reynolds number greater than 10 000, the injected chemical will be fully mixed six pipe diameters from the HEV static mixer. Once fully mixed, the dilution will simply be the rate of injected liquid divided by the fluid flowrate in the pipe.

1.7.2.2 Turbulent Mixing in a Pipe

The transition from laminar to turbulent flow in a circular pipe occurs as the Reynolds' number (Equation 1.35) exceeds the 2000-3000 range (Perry, 1973). As discussed in Section 1.7.1.1, the velocity profile for a pipe with turbulent flow is essentially flat and plug flow may be assumed; therefore, axial mixing can be assumed negligible and dispersion may be assumed to occur only in the radial direction.

Pressure Drop

The pressure drop is calculated using Equations 1.32–1.34. The Fanning (Darcy) friction factor for smooth pipes can be estimated from the following correlation (Perry, 1973):

$$f = 0.79\,\mathrm{Re}^{-1/4} \qquad (1.39)$$

Characteristic Shear Rate, G

The calculation of G in pipes is the same as for static mixers.

Blend time

Experiments by Brodkey (1975) have shown that if a fluid is injected into the center of a pipe, the intensity of segregation is 0.02 at 40 pipe diameters from the injection point at a r/r_0 of 0.73 (Brodkey, 1975). Brodkey's intensity of segregation data is combined with an assumption that the quantity of injected fluid in regions where the intensity of segregation is <0.3 is negligible, this reveals that the boundary of the injected plume is linear between the point of injection and 50 pipe diameters away. The profile of this plume for a pipe in turbulent flow is illustrated in Figure 1-34. Since Brodkey's experiments show that injected fluid is fully mixed after 50 pipe diameters the blend time can be calculated by Equation 1.40.

$$\theta_b = \frac{50 D_p}{u_b} \qquad (1.40)$$

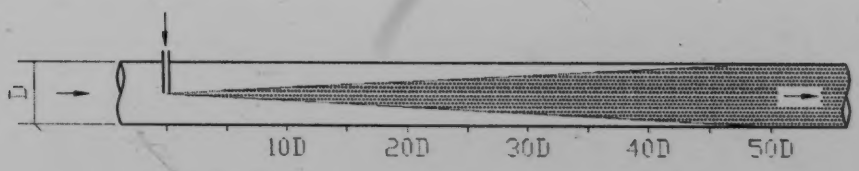

Figure 1-34 Profile of injected alum plume in a turbulent pipe (drawn by Louis Kennedy, 2003).

Dispersion

As described Section 1.7.1.1, dispersion in a pipe may occur in the axial or radial direction, but if the flow is turbulent, plug flow may be assumed and only dispersion in the radial direction is significant. The plume profile of solute injected into the center of a pipe is discussed in the previous section and is illustrated in Figure 1-34. Since the slope of this plume has been defined, the solute concentration throughout the plume and thus the extent of dilution can be calculated. The local concentration (Y_p) can be estimated by multiplying the final concentration obtained after 50 pipe diameters by the ratio of the cross-sectional area of the plume to the cross-sectional area of the pipe with Equation 1.41, where x is the distance along the pipe from the injection point.

$$Y_p(x) = Y_p(50D)\frac{\left(\frac{D_p}{2}\right)^2}{\left(\frac{1}{100}x\right)^2} \qquad (1.41)$$

for

$0 < x < 50D$

Where:

D_P= pipe diameter (m)

If the solute undergoes a reaction, in addition to Equation 1.41, the reaction time and the distance the solute travels in this time must also be taken into account. For example, if the precipitation of liquid alum occurs in one second, the concentration of liquid alum in the plume may only be calculated for distances shorter than the distance the fluid travels in one second.

1.7.2.3 Continuous Stirred Tank (CST)

A CST has mixing conditions of high mixing intensity, high dispersion and high backmixing. For an ideal continuous stirred tank, the flow fed to the tank is instantaneously mixed with the volume of fluid that is in the tank. A CST has high macro and micromixing and fast dilution rates.

Power

The energy for mixing is generated by the rotation of the impeller in the tank. The power transferred from the impeller to the fluid has been shown to be: (Holland and Chapman, 1966)

$$P = N_p \rho N^3 D^5 \qquad (1.42)$$

Where:

N_p= impeller power number

N= rps

D= impeller diameter (m)

The power number is dependent upon the type of impeller and the structure of the tank. For a marine impeller centered in a baffled cylindrical tank with the fluid height equal to the tank diameter, the power number is approximately 0.87 (Oldshue, 1983).

Characteristic Shear rate, G

The equation for G may be written as (Amirtharajah *et al,* 1991):

$$G = \left(\frac{P}{\mu V} \right)^{1/2} \qquad (1.43)$$

Since we know the volume of the tank and the power input, G can be calculated. A local G at the impeller can also be calculated by using the impeller swept volume instead of the volume of the tank.

$$G_{imp} = \left(\frac{P}{\mu V_{swept}} \right)^{1/2} \qquad (1.44)$$

Where the swept volume is related to the diameter of the impeller by the following equation (Paul *et al.*, 2003), where D is the impeller diameter:

$$V_{swept} = \left(\frac{\pi D^2}{4} \right) \frac{D}{5} \qquad (1.45)$$

Blend time

Since the CST is not ideal, the feed is not instantaneously mixed with the fluid in the tank. The time required for complete mixing may be estimated from the blend time correlation developed by Grenville et al. (1995) (as cited in Chapter Nine of Paul *et al.*, 2003).

Grenville's (1995) correlation was developed from experiments done on a cylindrical baffled tank with a tank height equal to the tank diameter. Grenville (1995) used vessels of 0.3, 0.61, 1.83 and 2.97 meters in diameter. The variety of impellers tested were hydrofoils, pitched and flat blade turbines and disc turbines with diameter ranging from one third to one half the vessel diameter (Grenville and Nienow, 2003 as cited in Chapter Nine of Paul *et al.*, 2003). The impeller was always placed one third of the liquid depth above the vessel base.

Application of Grenville's correlations to square vessels was analyzed internally by Kresta *et al.* (2003). In all cases Kresta *et al.* (2003) found that if the width of the vessel was used as the tank diameter (T), the Grenville correlations could be used for a square tank.

The Grenville equations for calculating blend time in fully turbulent and transitional flow are given in Equations 1.47 and 1.48. The flow regime can be determined by calculating the Reynolds number for a stirred tank in Equation 1.46. If the Reynolds number is between 200 and 10 000 the flow is transitional. The flow becomes fully turbulent once the Reynolds number exceeds 10 000. The Reynolds number of a stirred tank can be calculated from Equation 1.46.

$$\mathrm{Re}_i = \frac{\rho N D^2}{\mu} \qquad (1.46)$$

Once the flow regime is known, the Grenville correlation can be used to estimate the blend times in a stirred tank. The blend time for transitional flow is given in Equation 1.47 (Grenville et al, 1995 as cited in chapter nine of Paul *et al.*, 2003).

$$\theta_b = \frac{33856}{\mathrm{Re}\, N_p^{2/3} N}\left(\frac{T}{D}\right)^2 \qquad (1.47)$$

The blend time for fully turbulent flow is given in Equation 1.48 (Grenville et al, 1995 as cited in chapter nine of Paul *et al.*, 2003)

$$\theta_b = \frac{5.2}{N_p^{1/3} N}\left(\frac{T}{D}\right)^2 \qquad (1.48)$$

Dispersion

The dilution of injected solute in an ideal CST may be calculated. If there is no reaction the dilution is simply the ratio of injected solute to tank volume; however, if a reaction occurs, the reaction time must also be taken into account. For example, if the aluminum hydroxide precipitates after one second the concentration of liquid alum at one second after injection will be the ratio of the volume of alum injected over the period of one second over the volume of the tank for a tank residence time greater than the reaction time. If the tank is not ideal, the percentage of the tank containing solute instead of the total volume of the tank should be used.

1.7.2.4 Jar

The jar is a miniature batch stirred tank. Six jars are used in the jar test, which is a standard test in water treatment. It is lab scale test where coagulation, flocculation and settling are simulated. The quality of the water in the supernatant of these lab scale simulations are analyzed and used to determine process parameters such as coagulant dosage.

The mixing conditions produced in a jar are batch tests not continuous flow tests; therefore, the macromixing and the RTD distributions are different than for a CST, as discussed in Section 1.7.1. The mixing intensity in the jar test could be varied from zero to 300 s^{-1} by changing the RPM of the impeller, as shown in Figure 1-36. The mixing intensity in the jar is relatively low when compared to the capabilities of the static mixer and a CST used in this work.

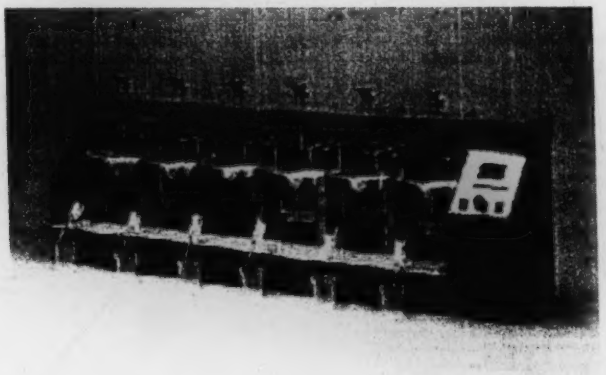

Figure 1-35 The Jar test apparatus (photograph courtesy of Phipps & Bird, Inc., Richmond, VA., 2003)

The process steps simulated in a standard jar test are:

1. Coagulant (Alum) rapid mixing
2. Coagulant (Alum) slow mixing
3. Polymer mixing
4. Flocculation – slow mixing
5. Settling – no mixing

Mixing in the jar is accomplished with a 1 x 3 inch flat blade impeller in a 2 litre, 4.5 inch wide jar with a liquid depth of 6 inches.

Characteristic Shear rate, G

The G value is correlated to the RPM of the impeller as shown in Figure 1-36 (Phipps and Bird website, 2003).

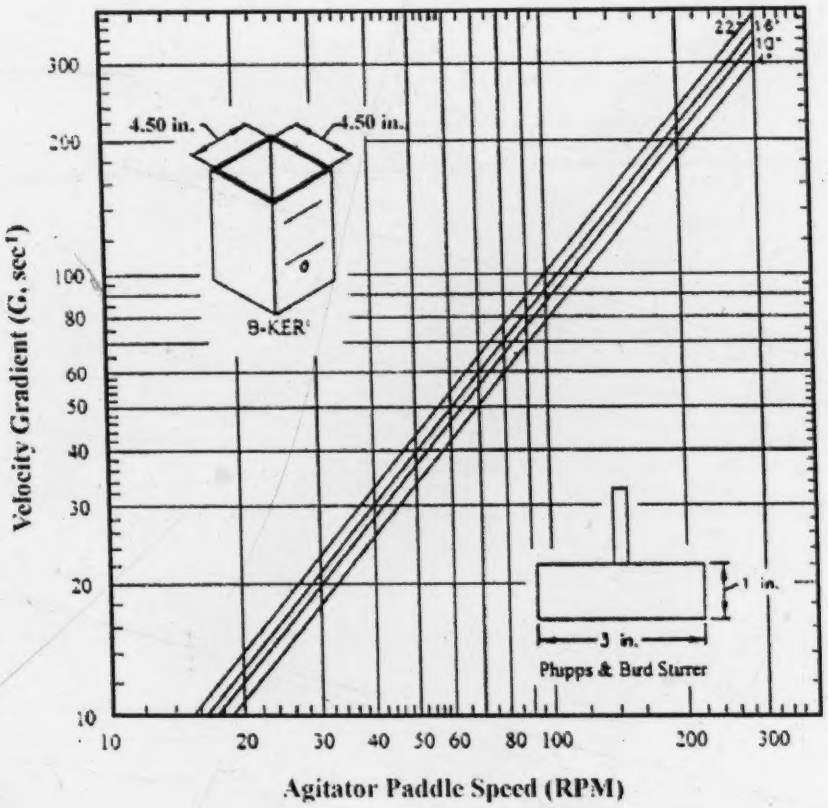

Figure 1-36 The Jar test correlation between impeller speed and G (photograph courtesy of Phipps & Bird, Inc., Richmond, VA, 2003)

Impeller Power

Impeller power is most often calculated from an impeller power number. If this number is not given, it can be back calculated given G and RPM. An equation for power number can be derived by combining the equations for impeller power (Equation 1.42), volume of the jar and G in Equation 1.43 to get:

$$N_p = \frac{G^2 \mu h}{\rho N^3 D^3} \qquad (1.49)$$

Blend time

The correlation developed by Grenville et al (1995), although developed for cylindrical baffled tanks, was used to estimate of blend times for the square jar. These are the same equations used for the CST (Equations 1.47 and 1.48).

Dispersion

The dilution of injected solute in a jar with instantaneous mixing (ideal mixing) may be calculated. If there is no reaction the dilution is simply the ratio of injected solute to tank volume; however, if a reaction occurs, the reaction time must also be taken into account. For example, if the aluminum hydroxide precipitates after one second the concentration of liquid alum at one second after injection will be the ratio of the volume of alum injected over the period of one second over the volume of the tank. If the mixing in the jar is not ideal, the percentage of the jar containing solute instead of the total volume of the jar should be used.

1.7.2.5 Inline Mechanical Mixer

An Inline mechanical mixer is a mixer with one or more impellers mounted so that the impellers are inside the pipe and mix the fluid as it flows through the pipe, producing mixing conditions with a high mixing intensity and a low degree of dispersion.

1.8 Rapid Mixing and Coagulation

The method of rapid mixing of alum in water treatment affects the mixing intensity and dispersion. Mixing intensity and dispersion were discussed in Section 1.7.1. In water treatment, the effects of the mixing intensity, time and the product of the two (Gt) on turbidity removal have been extensively studied. The

effects of dispersion, dilution rates and macromixing on aluminum hydroxide precipitate habit are not. In water treatment, it is believed that alum must undergo rapid mixing immediately upon injection followed by a period of slow mixing. The optimum intensity and duration of the rapid mix period varies between studies. Some studies show that too much rapid mixing is detrimental and that there is actually an optimum rapid mix time (Letterman, 1973 & Kan *et al.*, 2002), the cause of this is outside the scope of this work. It has been proposed that Gt, rather than the initial rapid mixing intensity should be used to design rapid mix systems. Gt was first suggested and experimentally tested by Letterman *et al (1973)*. He showed that regardless of the initial mixing intensity (G), each alum dosage required a corresponding Gt, as illustrated in Figure 1-24. Amirtharajah and Mills (1982) also recognized the importance of Gt. In their 1982 work, they maintained a constant Gt as they varied G, to properly evaluate the effects of varying the initial mixing intensity. They defined the regions of pH and alum dosage where only sweep coagulation was significant and the initial mixing intensity had no effect (Figure 1-25). The importance of the Gt factor is also supported mathematically by the collision rate equation for particle collisions due to fluid shear (Equation 1.16). The collision rate equation predicts the formation of larger flocs as Gt increases, as shown in Equation (1.17). Since the sedimentation process is more effective when larger flocs are formed, positive effects of a higher Gt should be expected.

The importance of the factor Gt is widely accepted and has both experimental and theoretical support. The significance of the initial rapid mixing intensity does not have the same unequivocal support. Rather, the insignificance of the initial mixing intensity has been reported in the literature by numerous sources: Letterman *et al.* (1973), Kawamura (1973), Amirtharajah and Mills (1982), and Charles *et al.* (1987) (as cited in Clark *et al*, 1994).

Letterman *et al.* (1973) showed that turbidity removal was dependent upon Gt and alum dosage. Regardless of the initial mixing intensity, the optimum Gt remained constant for each alum dosage. As alum dosage decreased, the Gt requirement increased (Figure 1-24). Letterman concluded that optimum

turbidity removal does not depend on the aluminum ionic complexes which exist before aluminum hydroxide precipitation (Al^{3+}, Al^{+}...), nor solely on the time required to disperse the alum, but rather upon the formation of larger $Al(OH)_3$ flocs, which in turn settle faster, resulting in better turbidity removal. Letterman based this conclusion upon the observation that the mixing period required for optimum turbidity removal was always substantially higher than the time required for precipitation of aluminum, 1 to 10 seconds.

Kawamura *et al.* (1973) (cited in Clark *et al*, 1994) examined the effect of the initial mixing intensity (G) by injecting alum into an impeller of an inline mechanical mixer. He found that turning the inline impeller off had no effect upon final turbidities

Tests by Amirtharajah and Mills (1982) confirmed the insignificance of the initial rapid mixing intensity when coagulation occured in the sweep zone (Figure 1-25). In their experiments, they varied the initial mixing intensity, but maintained a constant Gt of 16 000. They combined their experiemental results with those of other experimenters and constructed a diagram, in which the pH and alum dosage could be used to predict the mechanism of coagulation; sweep, absorption/charge neutralization or a combination of the two. The operational diagram is found in Figure 1-22.

Charles *et al.* (1987) (as cited in Clark *et al.*, 1994) studied alum performance in a stirred tank. He showed that poorer performance of alum occurs under conditions of maximum macromixing or high dispersion. He observed better alum performance when the alum was added near the surface of the tank (slow dispersion), versus near the impeller (fast dispersion).

Studies show that both G and time are important factors for determining the conditions for optimum water treatment, but alone are not able to completely explain turbidity removal differences between different types of mixing equipment. Vrale and Jordan (1971) studied different methods of mixing with identical mixing intensity and mixing times, but did not get the same turbidity removal (Vrale and Jordan, 1971). This suggests that an additional factor must influence coagulation with alum. This factor may be the rate of change of pH

which is determined by the extent and rate of water dispersion into liquid alum and controls whether the larger or smaller habit of amorphous aluminium hydroxide precipitates.

1.9 Summary

The literature review reveals that unknown variables other than G, time and Gt influence the performance of alum in coagulation, so new mixing methods must be experimentally compared to existing mixing equipment. The effectiveness of the new mixing method: HEV static mixer, may be evaluated by comparing it to existing mixing methods, such as turbulent pipe flow, continuous stirred tanks and inline mechanical mixers.

Historically, comparisons have been made to jar tests, which is a batch test. A batch test has different dispersion characteristics than a pipe and stirred tank in continuous flow, as discussed in Section 1.7.1. The characteristics of macromixing and dilution in a jar, CST and a pipe in turbulent flow are different, thus their local concentrations of liquid alum during aluminum hydroxide precipitation will vary. A comparison between precipitation of aluminum hydroxide in a continuous stirred tank and a stirred tank in batch mode has not been previously made. No experimental data for alum injected into a continuous stirred tank or its reaction rate equations were found during the literature review.

It has been suggested that the conditions of precipitation may influence coagulation if it occurs via the sweep mechanism (Amirtharajah *et al*, 1991). One method of examining this possibility is to compare performance of a CST to a pipe. In the field of reactor modeling, it is known that the overall conversion in a pipe (PFR) is different from a continuous stirred tank reactor (CSTR) because of their different reactant concentrations. Therefore, variations in precipitation pathways and thus precipitate structure should be expected between a PFR and a CSTR. A second method of comparison would be to study the differences in the effects of dispersion between the slow radial mixing in a pipe and the fast radial mixing of a static mixer.

The literature review has revealed that a high degree of supersaturation, which may occur in water treatment with mixing conditions of fast dispersion, will produce precipitates 100 times smaller than a low degree of supersaturation with slower precipitate formation. It was also shown that conditions with a slow rate of precipitation promote the formation of larger and more agglomerated precipitates. Therefore, mixing conditions with little back mixing and slow radial mixing will favor the formation of larger and more agglomerated aluminum hydroxide precipitates. A larger precipitate will require a smaller Gt to form a sufficiently sized floc. The collision rate of the larger precipitate will be 10-10 000 times larger since its collision rate will be affected by turbulence, unlike the smaller precipitate whose collisions are due mainly to Brownian motion, rather than fluid shear.

The literature review reveals a number of variables that control the aluminum hydroxide precipitate size. A fast rate of precipitation, a high solution pH at the time of precipitation, a high degree of supersaturation and a large availability of hydroxide ions, result in the formation of smaller precipitates. It is important to recognize that mixing affects all five of these variables. The method of mixing will determine the rate at which water is dispersed in with the alum. The slower the water is integrated with the alum: the fewer hydroxide ions available during precipitate formation, the lower the local pH at the time of precipitation, and the lower the degree of supersaturation.

If mixing conditions in water treatment affect the initial size of the precipitate, conditions that produce smaller precipitates should be expected to have a higher concentration of suspended aluminum hydroxide particles in the supernatant solution of the jar tests and require a higher Gt to form an effective floc. Based upon the information in the literature review, it should be expected that a CST may produce a greater proportion of smaller precipitate than a pipe with turbulent flow, and the HEV static mixer may produce a greater proportion of smaller precipitate than the empty pipe. This better performance of an empty pipe over a static mixer and CST is opposite to what one may initially expect if the mechanism of coagulation is believed to be adsoption/charge neutralization.

If the mechanism is sweep, a larger initial precipitate would be more beneficial than an increase in collisions between the intermediate hydrolysis products of alum and the negatively charged colloids.

1.10 References

Alwitt, R., 1976, *The Aluminum-Water System*, in J.W. Diggle & Vijh, *Oxides and Oxide Films*, **vol 4**, Marcel Dekker, New York, 169-254

Amirtharajah, A., Clark, M. & Trussel, R., 1991, *Mixing in Coagulation and Flocculation*, American Water Works Association Research Foundation, American Water Works Association.

Amirtharajah, A., Mills, K., 1982, in *Rapid-Mix Design for Mechanisms of Alum Coagulation,* Journal AWWA, **44**, 210-216.

Benefield, L.& Morgan, J., 1991, *Chemical Precipitation*, Chapter 10, in *Water Quality and Treatment*, McGraw-Hill, USA.

Brodkey R., 1975, in T*urbulence in Mixing Operations*, Ch 2, Academic Press, USA

Camp, T.& Stein, P., 1943, *Velocity Gradients and Internal Work in Fluid Motion*, Boston Society of Civil Engineers, **Vol 30**, 4, 219-237.

Chen, J, Shao, L, Guo, F, Wang, X, 2003, *Synthesis of Nano-Fibers of Aluminum Hydroxide in Novel Rotating Packed Bed Reactor*, Chemical Engineering Science, **58**, 569-575.

Clark, M., 1985, *Critique of Camp and Stein RMS Velocity Gradient*, Journal of Environmental Engineering-ASCE, **111(6)**, 741-754

Cleasby, J., 1984, *Is Velocity Gradient a Valid Turbulent Flocculation Parameter?*, Journal of Environmental Engineering, **Vol 110**, 875-897

Fasano, J. & Penney, W., 1991, *Avoid Blending Mix-ups,* Chem. Eng. Prog., **87**, 10, 56-63

Folger, S., 1992, in *Elements of Chemical Reaction Engineering*, Prentice Hall PTR, New Jersey

Fursenko, V., Popov, A., Zenkevich, Y. & Mazurova, O., 1975, *Investigation of Solubility of Aluminum Hydroxide in Water and Its Pickup in High-Pressure Steam*, Thermal Engineering, **22**, Iss 9, 100-104.

Gale, J., Rohl, A., Milman, V. &Warren, M., 2001, *An Study of the Structure and Properties of Aluminum Hydroxide: Gibbsite and Bayerite*, J. Phys, Chem. B, **105**, 10236-10242.

Gerson, A., 2001, *The Role of Fuzzy Interfaces in the Nucleation, Growth and Agglomeration of Aluminum Hydroxide in Concentrated Cautic Solutions*, Progress in Crystal Growth and Characterization of Materials, **43**, 187-220.

Grenville R., Ruszkowski S., Garred E., 1995, *Blending of miscible liquids in the turbulent and transitional regimes*, MixingXV conference, Banff, Alberta, June 20-25, 1995.

Han, M. & Lawler, D., 1992, *The Relative Insignificance of G in Flocculation* , Journal AWWA, **October 1972** , 79-91

Hayden, P. & Rubin, A., 1974, in *Systematic Investigation of the Hydrolysis and Precipitation of Aluminum, Ch 9*,Ann Arbor Science, Mich.

Hayes, R., 2000, Introduction to Chemical Reactor Analysis, University of Alberta, Canada

Hiemenz, P. & Rajagopalan, R., 1997, in *Principles of Colloid and Surface Chemistry*, Ch 1, Marcel Dekker, New York

Holland, F & Chapman, F., 1966, *Power requirements in Liquid Mixing*, Chapter 2 in *Liquid mixing and Processing in Stirred Tanks,* Reinhold Publishing Coorporation, USA.

Jiratova, K., Weiss & Rocek, J., *Effect of Precipitation and Aging on Porous Structure of Aluminum Hydroxide*, Collect. Czech. Chem. Commun., **56**, 1253-1269.

Kan, C., Haung, C. & Pan, J., 2002, Time requirement for rapid-mixing in Coagulation, Colloids and Surfaces A: Physiochemical and Engineering Aspects, 203, 1-9.

Kawano, M. & Tomita, K., 1996, *Amorphous Aluminum Hydroxide Formed at the Earliest Weathering Stages of K-Feldspar*, Clays and Clay Minerals, **44**, 672-676.

Latimer, W & Hildebrand, J., 1964, Reference Book of Inorganic Chemistry, The MacMillan Company, USA.

Lefevre, G., Fedoroff, M., 2002, *Synthess of Bayerite Microrods by nNutralization of Aluminate Ions at Constant pH*, Materials Letters, **56**, 978-983.

Letterman R., Quon, J. & Gemmell, R., 1973, *Influence of Rapid-Mix Parameters on Flocculation*, Journal AWWA, **November**, 716-722.

Martin, B., 1991, *Fe^{3+} and Al^{3+} Hydrolysis Equilibria, Cooperativity in Al^{3+} Hydrolysis Reactions*, Journal of Inorganic Biochemistry, **44**, 141-147.

Misra, C., 1986, *Industrial Alumina Chemicals, Ch 1, in*Ameican Chemical Society, Washington, DC.

Mullin, J.W., 2001, *Crystallization*, 4th ed., Butterworth-Heinemann Ltd., **Oxford**, Great Britain.

Nagai, H., Hokazono, S. & Nagai, H., 1991, *Synthesis of Aluminum Hydroxide by Homogeneous Precipitation Method 1 - Effect of Additives on the Morphology of Aluminum Hydroxide*, Br. Ceram. Trans. J., **90**, 44-48.

Nagai, H., Muta, R., Nagashima, S. & Kato, A., 1993, *Precipitation Behaviour and Coalescence of Aluminum Hydroxide Particles from Aluminum Salt Solutions in the Presence of Sulfate Ion*, Nippon Kagaku Kaishi, **Issue 2**, 173-176.

Nauman, E. & Buffman, B., 1983, *Mixing in Continuous Flow Systems,* John Willey and Sons, New York.

Nienow, A., 1997, *On Impeller Circulation and Mixing Effectiveness in Turbulent Flow Regime*, Chem. Eng. Sci., **52**, 2557-2565.

O'Melia C., 1972, in *Physiochemical Processes for Water Quality Control*, W.J. Weber , Jr. Ed., John Wiley & Sons, New York

Oldshue, J., 1983, *Fluid Mixing Technology,* Ch. 3, McGraw-Hill Publications, New York

Perry, R., 1973, *Flow in Pipes and Channels*, Chapter 5, in *Perry's Chemical Engineer's Handbook*, McGraw Hill, USA.

Paul, E., Atiemo-Oberg, V. & Kresta, S., 2003, *Handbook of Industrial Mixing*, Science and Practice, North American Mixing Forum

Phipp's and Bird Website, www.phippsbird.com/gcurve.html

Richardson, J. & Zaki, W., 1954, Sedimentation and Fluidization: Part 1, Trans. Instn Engrs, Vol 32, 35-51.

Rocek, J., Heinz, K., Steinike, U. &Jiratova, K., 1991, *Porous structure of aluminum hydroxide and its content of pseudoboehmite*, Applied Catalysis, **74**, 29-36.

Rubin A.J., 1976, Aqueous-Environmental Chemistry of Metal, Ann Arbor Science, Michigan, USA.

Saffman, P.G. & Turner, J.S. 1956, *Collision of Drops in Turbulent Clouds*, Journal of Fluid Mechanics, 1:16

Shook, C.A., 1994, *Applications of Fluid Mechanics*, University of Saskatchewan, Saskatoon.

Streiff, F., Jaffer, S. & Schneider, 1998, *The Design and Application of Static Mixer Technology*, 3rd International Symposium on Mixing in Industrial Processes, 107-114.

Trawczynski, 1996, *Effect of Aluminum Hydroxide Precipitation Conditions on the Alumina Surface Acidity*, Ind. Eng. Chem. Res., **35**, 241-244.

Unuma, H., Kato, S., Ota T. & Takahashi M., 1998, *Thomogeneous precipitation of alumina precursors via enzyatic decomposition of urea*, Advanced Powder Technology, **9**, no 2, 181-190.

Violante, A. & Huang, P., 1993, *Formation Mechanism of Aluminum Hydroxide*

Polymorphs, Clays and Minerals, **41**, 590-597.

Vrale, I., & Jordan, R., 1971, R*apid Mixing in Water Treatment*, Journal AWWA, **63**, 52.

Wallis, G.B., 1969, *One Dimensional Two Phase Flow*, McGraw-Hill, New York.

Chapter 2

Experimental Methods

2.1 Introduction

The purpose of this project was to determine whether or not mixing with a HEV static mixer enhances the performance of the coagulant, alum. An HEV static mixer is a vortex mixer with low-pressure drop designed for fully turbulent flow (Re>10,000). It produces fast radial mixing without moving parts. As the flow rate increases so does the pressure drop across the static mixer, thus also the turbulent mixing intensity. Therefore, dispersion due to radial and axial mixing (back mixing) and mixing intensity were chosen as experimental variables along with mixing time and changes in the residence time distribution behaviour. Their impact was tested in a jar test by detecting the extent of particulate removal in the jar's supernatant solution with turbidity and aluminum concentration measurements.

The mixing intensity of an HEV static mixer, if properly sized, can be made comparable to that surrounding impellers in stirred tanks, low lift pumps and inline mechanical mixers. If the intensity of mixing at the time of alum injection is a limiting factor in coagulation, static mixer performance should be comparable to other equipment operated at similar mixing intensities. Experiments were designed to compare static mixers to continuous stirred tanks (CST), low lift pumps and inline mechanical mixers of similar and different mixing intensities. Quantification of mixing intensity, according to turbulent theory, is the rate of turbulent kinetic energy dissipation per unit mass (ε). The term ε, is rarely used to quantify mixing intensity in the water treatment industry. Rather, the term regularly used is G (s^{-1}). G was originally derived to be the mean turbulent velocity gradient for the velocity gradient term in the laminar fluid shear equation (Camp and Stein, 1945). It is defined in Equation 1.15. Its original derivation is debatable and its common name, the "mean velocity gradient" is not physically meaningful for turbulent flow, so for this thesis it will be renamed to the characteristic shear rate. The debate over the validity of the derivation of G and its ability to quantify flocculation and mixing intensity was reviewed in Section 1.5.1.

In addition to mixing intensity, dispersion due to back mixing and radial mixing will be addressed. The degree of influence of mixing intensity or dispersion in coagulation with alum is dependent upon the mechanism of coagulation. It has been shown that mixing intensity is a limiting factor when the mechanism of coagulation is "Charge Neutralization" (Amirtharajah and Mills, 1982). If the mechanism of coagulation is "Sweep", the total number of collisions between precipitates and colloids, and the conditions during precipitate formation are more important than the ion/colloid collision frequency (Amirtharajah and Tambo, 1991). The collision rate, time, and initial precipitate size determine the final floc size and thus efficiency of particulate removal. The final floc size is a function of Gt and precipitate size: precipitate size is determined by supersaturation, as introduce in Section 1.3.2 and 1.4.3 and is controlled by dispersion as presented in Section 1.7.1. Therefore, the variables of Gt and dispersion should be expected to be more influencisal than initial mixing intensity, if the mechanism of coagulation is "Sweep".

The mechanism of coagulation determines the importance of each factor; therefore, experiments were designed with the intent of examining both mechanisms of coagulation, "sweep" and "charge neutralization". The mechanism of coagulation was estimated from the operational diagram in Figure 1-22 (Amirtharajah and Mills, 1982). According to the operational diagram, two operational zones were possible for Edmonton's winter water: "sweep" and "combination" (sweep & charge neutralization). Experiments were designed to test coagulation in the sweep and combination zones by changing the alum dosages: experiments with alum dosages of 15–45 mg/L tested the static mixer during sweep coagulation, and 7-10 mg/L of alum tested the combination zone (sweep and charge neutralization).

The experiments were designed to be comparative. Different pumps allowed for comparisons between continuous and intermittent chemical injection. Tests on empty pipes, CST (continuous stirred tank), jar tests (batch), inline mechanical mixers and actual plant mixing conditions permitted comparisons of different degrees of radial mixing, back mixing, mixing time (t), mixing intensity (G

or ε) and Gt with static mixers. Different combinations of mixers separated the effects of dispersion and initial mixing intensity. A static mixer in series with pipe followed by a CST or empty pipe followed by a CST were both compared to a CST alone: then the performance of the static mixer could be attributed either to its ability to achieve a high mixing intensity or to its lack of back mixing. The mixing intensity of the CST and static mixer were comparable, but the extent of back mixing ranges from large for the CST to essentially none for the static mixer and empty pipe. Comparison between an empty pipe and a static mixer was used to answer questions on the effect on the rate of dispersion due to radial mixing. An empty pipe has much slower rate of radial mixing than a static mixer.

2.2 Analytical Methods

The role of alum is to enhance the removal of particulate matter from natural water. The efficiency of particle removal in the supernatant of the jar test is then a logical choice for comparison of alum performance. The extent of particle removal by itself does not tell us which mechanism of coagulation or which mixing variable dominates. Each mechanism of coagulation depends upon different variables, so different analytical methods may be used depending upon the dominating mechanism. If the size of the initial precipitate is thought to be important, precipitate isolation and analysis could be done using a centrifuge, ultrasonic agitation and a scanning electron microscope. If double layer compression was assumed to be relevant, streaming current or electrophoretic mobility measurements could be made. Measurements of mechanisms, such as the number of collisions between the colloids and precipitate's preexisting ions, which exist for seconds or less, are almost impossible to measure directly. Since the dominant mechanism and the limiting factor for this project were not clear, a measurement capable of detecting improvements, regardless of the mechanism, was chosen. This measurement was the extent of particulate removal: both particles of naturally occurring colloids and the aluminum hydroxide precipitates formed from alum.

Two analytical methods were chosen to compliment each other: Turbidity, which is based upon the extent of light scattering, can trend the total concentration of particulate matter in solution, while aluminum concentration provides a direct measurement of the quantity of aluminum hydroxide present as particles in solution. Based upon the settling velocity calculations in Table 1-2, majority of the particles to be measured in the supernatant solution would be smaller than 1 micron, since the particles were allowed to settle for 10 minutes in the jar test and samples of the supernatant were withdrawn from 6 centimeters below the surface. Particles smaller than one micron in the supernatant will consist of naturally occurring colloids such as clay, humic and fulvic acids, and possibly the precipitate of alum, aluminum hydroxide. The aluminum concentration measurements detected the amount of aluminum hydroxide precipitate in the supernatant of the jar, while the turbidity measured the overall particle concentration: both aluminum hydroxide precipitate and naturally occurring colloids.

2.2.1 Turbidity

Turbidity measures the optical clarity of a solution by detecting the extent of light scatter and absorption caused by the sample. As the concentration of the sample increases, so will the amount of light scatter and absorption and vice versa.

Theories of light scattering, based upon knowledge of sample parameters and laws of electromagnetism, predict the angular distribution of light scattered by the sample. The light scattering calculations are complicated even further when absorption occurs together with scattering. When scattering is large compared to absorption, Lambert's law states that the intensity of electromagnetic radiation traversing a medium in direction x becomes (Vanous *et al*, 1982), where the turbidity coefficient, τ, is a property of the scattering ability of the sample material.

$$I = I_0 e^{-\tau x} \quad (2.1)$$

Where:

I= intensity of electromagnetic radiation at x

I_o = incident intensity at x=0

For the more complex equations that arise once absorption becomes significant, refer to Vanous *et al*, 1982. There are a number of methods for measuring the total light scattered. One is to measure the attenuation of the incident beam as it passes through the sample. Another is to detect all light scatter by using a integrating sphere or thirdly by using the nephelometic method which only detects scatter at a given angle to the incident beam (Vanous *et al., 1982*).

The instrument used to measure turbidity was a Hach 2100N turbidimeter. It operated on the principles of nephelometric measurement. A 90 degree detection angle was used. This allowed for a simple optical system, less sensitive to scattering and variations in particle size. A 90 degree detection angle minimized detection of scattering and reflection due to the passage of the light beam through the entrance and exit windows of the sample cell and is less sensitive to variations in particle size (Vanous *et al.*, 1982). A light source and photocell provide the beam of light and the apparatus for detection of light scatter. Both the photocell and light beam source are isolated from the sample. The sample was contained in a glass vial and placed into the turbidimeter where a beam of light passed through the sample, and the scattered light was detected by the photocells. The accuracy of the turbidimeter was ±0.01 NTU (nephelometric turbidity units), the resolution was 0.01 NTU, and the repeatability was within 0.01 NTU (Hach, 2003).

Although turbidity measurements are accurate and repeatable, more than one variable can influence the turbidity. The size, structure and concentration of particles all affect how light is scattered and absorbed, thus all affect turbidity readings. Only if the size and structure of the particles remains constant between samples can changes in turbidity be attributed solely to a change in

concentration. Since the size and composition of particles in Edmonton's winter river water is relatively constant, then the composition of the particles under 1 micron in size in the jar's supernatant is also relatively constant and observed changes in turbidity may be attributed to changes in natural particle concentration. If aluminum hydroxide precipitates remain suspended in the supernatant, this assumption is no longer valid. Aluminum hydroxide precipitates are not similar in size and composition to the naturally occurring colloids. Aluminum hydroxide precipitates are not present in raw water: only in the supernatant samples. Also, the amount of aluminum hydroxide precipitate remaining in the supernatant varied between samples. No attempts were made to correlate turbidity due to aluminum hydroxide precipitate concentration, but a measurement of aluminum hydroxide precipitate concentration was used to compliment turbidity measurements to remove this potential source of error.

Turbidity is better than direct particle count if the particle size to be measured is small, less than 1 micron (Van Gelder *et. al*, 1999). The expected size of the unsettled particulate matter in the jar test was determined by calculations assuming the suspended particles would be composed of clay with a specific gravity of 2.65. Since the particle volume concentration in Edmonton's North Saskatchewan River winter water was low (<5 NTU) the equation for the settling velocity of a single particle in a large body of fluid (Equation 1.3) was adequate. The particles in the jar tests were allowed to settle for 10 minutes and supernatant solution was withdrawn from 6 cm below the water surface, so the likelihood of particles which could settle 6 cm in 10 minutes being left behind in the supernatant was small. The results of the settling velocity calculations in Table 1-2 revealed that the particle size to be expected to remain in the supernatant would be smaller than 10 microns.

2.2.1.1 Aluminum Concentration

An increase in turbidity may be indicative of an increase in aluminum hydroxide precipitates, naturally occurring colloids or a combination of the two. A measurement of natural colloid concentration or aluminum hydroxide precipitate

allows us to distinguish between the causes of turbidity. Direct measurement of the concentration of naturally occurring particles is difficult because of the complexity and diversity of natural particles, so the measurement of aluminum hydroxide precipitate concentration was selected. The concentration of aluminum hydroxide precipitate was quantified with a total aluminum concentration measurement. Since the amount of aluminum in untreated water and the quantity soluble in the treated water are negligible when compared to the quantity of aluminum present as aluminum hydroxide precipitate, aluminum concentration is essentially equal to the concentration of aluminum hydroxide present as precipitate (aluminum hydroxide solubility was discussed in Section 1.3.1). In addition to determining whether increases in turbidity were due to poor precipitate removal or poor natural colloid removal, aluminum concentration in the supernatant was used to determine the amount of alum not contributing to the formation of effective flocs.

The measurement of aluminum concentration was done using an Inductively Coupled Plasma Spectrometer, which detected atomic emissions. The sample standard deviation of the apparatus was 0.01 mg/L and it was able to detect 91-114% of the aluminum present in a sample, averaging 106% detection. The operating procedures of the Leeman Labs PS 1000 ICP spectrometer for aluminum are provided in Appendix B.

2.3 Jar Test

The jar test is well established in the water treatment industry. It provides a controlled environment for lab scale simulations of the sedimentation process. In this work, the sedimentation process includes alum injection, alum mixing, polymer injection, polymer mixing, flocculation and settling. During this project, well-mixed samples of alum and water from the pilot plant were put through a jar test to simulate the sedimentation steps following the initial alum mixing period. The supernatant of the jar was tested for natural and aluminum hydroxide particles. The coagulant, alum and polymer, Magnafloc LT27S were used for this project. The jar test procedures were based upon those developed by Epcor's

E.L. Smith Water Treatment Plant. Epcor's jar test procedures include the following steps: alum injection, alum rapid mix, alum slow mix, polymer injection, polymer rapid mix, polymer slow mix, flocculation and settling, as summarized in Table 2-1.

Table 2-1 Summary of standard jar test procedures for Epcor and project jar test procedures

Step #	Epcor's Standard Jar Test Procedures			This Project's Jar Test Procedures		
	Step	N (RPM)	Time (min.)	Step	N (RPM)	Time (min.)
1	Alum injection	300	---	Alum injection	---	---
2	Alum Rapid Mix	300	0.5	Initial Alum mixing	25-300	2 sec–30 min
3	Alum Slow Mix	100	3	Additional Alum Mixing	25	6-10
4	Polymer Injection	300	---	Polymer injection	200	----
5	Polymer Rapid Mix	300	0.5	Polymer mixing	200	5
5	Polymer Slow Mix	100	0.5			
6	Flocculation	25	15	Flocculation	25	15
7	Settling	0	10	Settling	0	10
8	Sampling	0	---	Sampling	0	-----

The jar test procedures for the alum and polymer mixing steps were modified from the standard jar test procedures as outlined in Table 2-1. Alum mixing was modified because it was an experimental variable. The experiments often involved a slow mix period that preceded or even replaced the rapid mix period. To avoid confusion, the procedures referred to as "Alum Rapid Mix" and "Alum Slow Mix", were renamed "Initial Alum Mix" and "Additional Alum Mix". Initial alum mix refers to the alum mixing that occurred at the alum injection point. In some experiments, the initial alum mix step took place in the pilot plant and for others in the jar. Additional alum mix refers to the additional alum mixing that occurred after the sample was put into the jar.

The polymer used in this project is discussed in Section 1.6.3. The polymer mixing steps were modified based on results shown in Figure 2-1 and

Figure 2-2. Variability due to polymer mixing had to be eliminated in order to ensure experimental repeatability. This was accomplished by combining and extending the rapid and slow polymer mix steps into one step of mixing at 200 RPM for 5 minutes. The jar tests results plotted in Figure 2-1 and Figure 2-2 followed the procedures in Table 2-1. The tests were done on samples taken from sample point three (refer to Figure 2-5), with alum injection into the center of a 4 inch pipe. The pilot plant set-up will be discussed in more detail in Section 2.4. The Gt for the alum mixing step was held constant (additional alum mixing was zero), and only the polymer mixing was varied. Long polymer mixing times were also observed for polymers used before the filtration system (Hemsing, 2001). Hemsing attributed mixing times 10-100 times the blend time, to the high dissolution time of the polymer.

The polymer dosages were chosen so that the control experiment would have final turbidities slightly greater than the actual plant. Since the plant was operating at a polymer dosage of 0.26 and clarifier overflow turbidities of 0.2NTU, a polymer dosage of 0.2 mg/L giving a final turbidity of 0.4NTU, left room for improvements to the alum mixing methods.

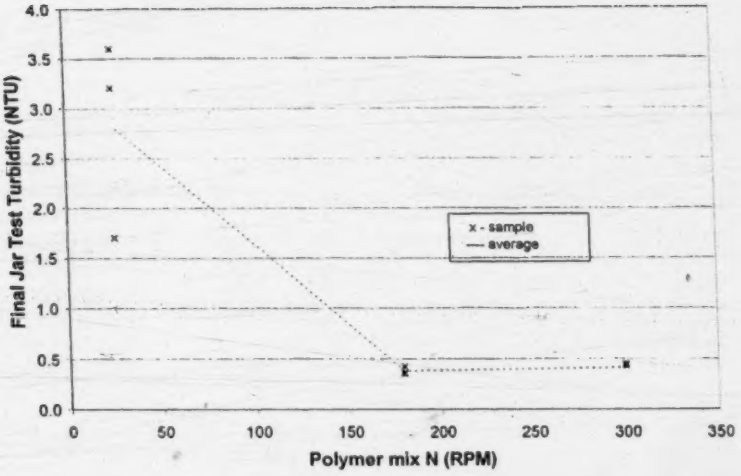

Figure 2-1 Effects of polymer mix intensity on turbidity removal, when mixing 35 mg/L of alum for 10 minutes in untreated water of 4 NTU in a Jar Test. Maximum turbidity removal achieved when the RPM was greater than 175.

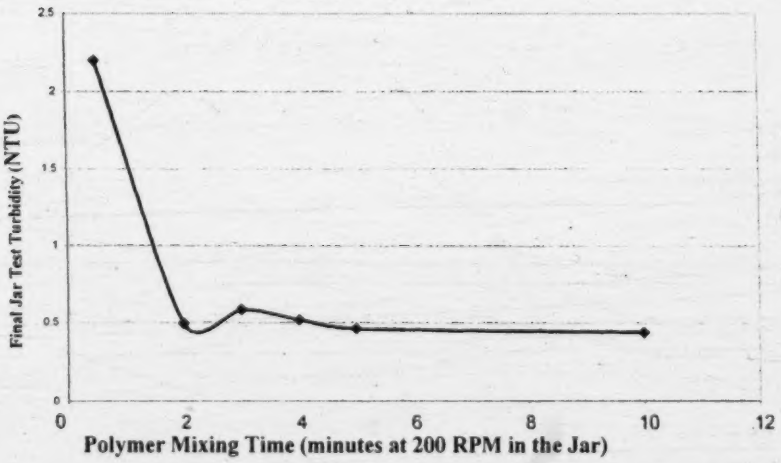

Figure 2-2 Effect of polymer mixing time at 200 RPM on turbidity removal in a Jar test. Maximum turbidity removal achieve when mixing exceeds 2 minutes.

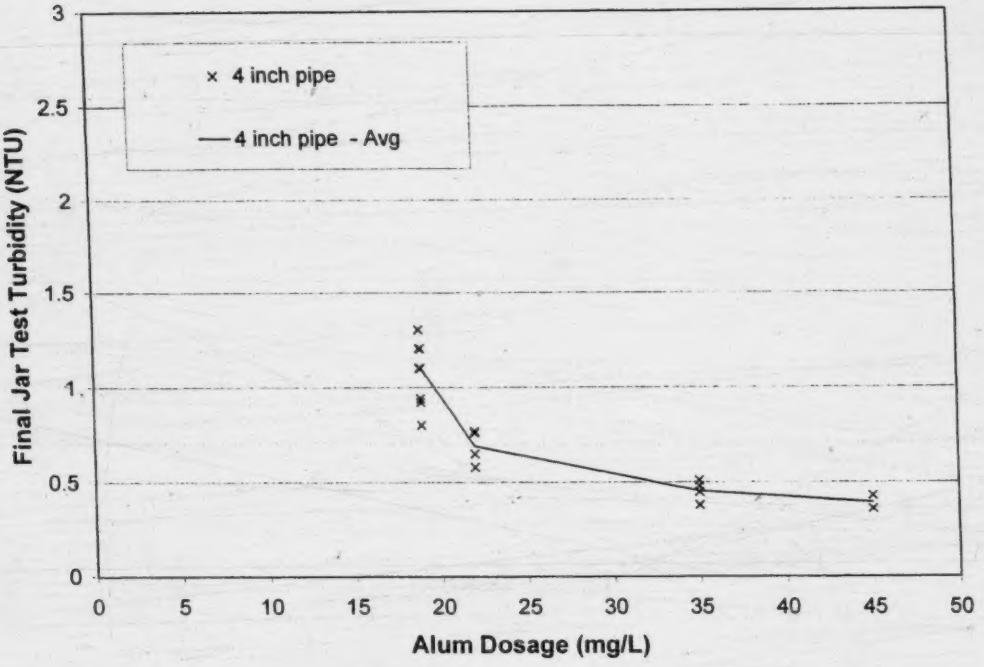

Figure 2-3 Dependency of turbidity on alum dosage when alum is injected with a diaphragm pump into a 4 inch pipe at an Re=5,800 (Data taken from block 4).

Alum dosages chosen were based upon theoretical and experimental results in the pilot plant control experiments and the jar test experiments. The experimental results of alum injection into a 4 inch empty pipe with the inline mechanical mixer off, showed that turbidity removal remained constant for alum dosages of 25-40 mg/L. They also showed that poorer turbidity removal resulted as the alum dosage fell below 25 mg/L (Figure 2-3). Experiments in the jar with a lower raw water turbidity and alum concentrations of 33, 15 and 8 mg/L showed that turbidity removal dropped off below 15 mg/L, as shown in Figure 2-4.

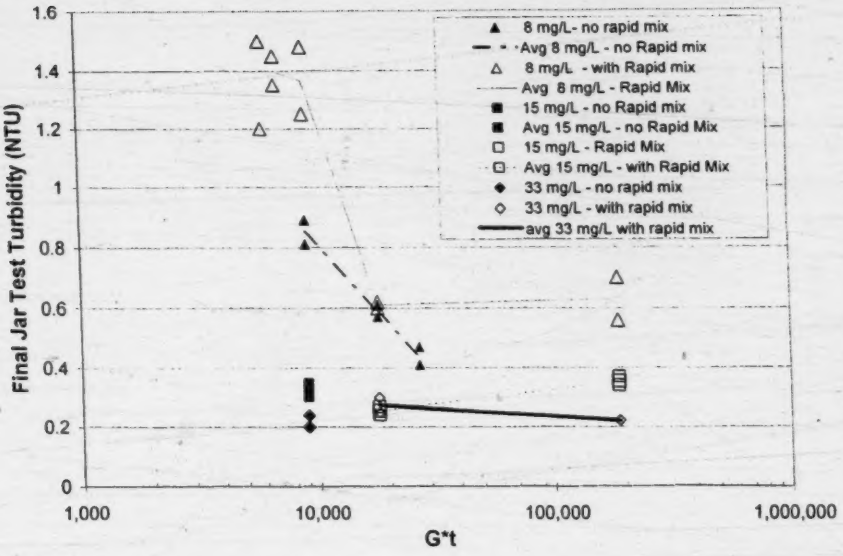

Figure 2-4 Effect Alum dosages of 8-33 mg/L with changes in total Gt before polymer addition (the sum Gt from rapid and slow alum mixing steps) (25 RPM upon alum addition = no initial rapid mix, 300 RPM upon alum addition= with initial rapid mix. Data taken from block 8)

In addition to detecting differences in turbidity due to alum dosage, attempts to detect differences due to changes in coagulation mechanisms were also made by setting alum so that both coagulation mechanisms of sweep and combination would occur according to Figure 1-22. According to this design and operation diagram the sweep and combination zones could be tested if alum dosages greater and less than 10 were tested; therefore alum dosages of 8, 15 and 20 mg/L were chosen for the test line experiments.

For all jar tests, chemical (alum and/or polymer) was injected into the jar, four centimeters from the impeller shaft and six centimeters below the water surface using an Eppendorf pipette. Samples of the supernatant solution were withdrawn with a pipette tip placed 6 cm below the surface of the water in the center of the jar.

2.4 Initial Alum Mixing Conditions

The experiments were set up to study various alum-mixing methods. The methods of mixing tested in the pilot plant were static mixers, pipes in turbulent flow, continuously stirred tanks and inline mechanical mixers. The possible alum injection points were as follows:

Train one

- Into the center of a 2 inch pipe
- Into the bottom of a pipe (1 inch or 2 inch in diameter)
- 2 inches before and centered on the top tab of an HEV static mixer (1 inch or 2 inches in diameter)

Train Two

- Into the center of straight pipe (4 inches in diameter)
- At the impeller of an inline mechanical mixer
- At the impeller of a CST

Jar

- Near the impeller in a jar test

2.4.1 Pilot Plant

The pilot plant consisted of two parallel test trains with untreated river water feed. Each train consisted of three sequential parts, illustrated in the schematic in Figure 2-5:

1. Straight pipe
2. Stretch of pipe with bends
3. Continuous stirred tank

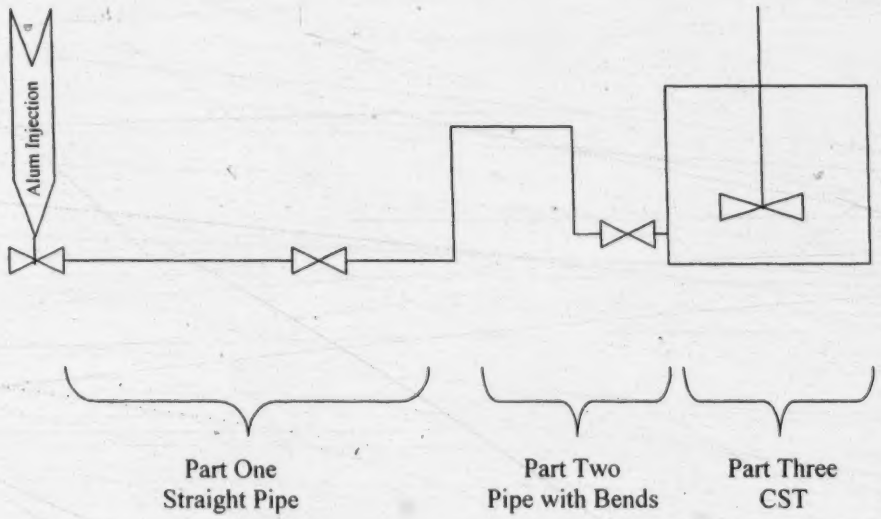

Figure 2-5 The three parts of each pilot plant train.

River water was continuously pumped to the pilot plant where it then flowed through the stretch of straight pipe followed by the length of pipe with bends and then into a continuous stirred tank (CST). The pipe diameters, lengths and number of pipe bends are summarized in Table 2-2. It was possible

to withdraw samples from each train at several locations. How the samples were withdrawn is detailed in Section 2.4.1.1.

Table 2-2 Summary of pipe diameters, lengths and bends for each train.

Section	Pipe Diameter (inches)	Length (m)	Number of bends
Train one			
Straight pipe	1 or 2	5	0
Pipe with bends	2	14	13
Train two			
Straight pipe	4	2	10
Pipe with bends	2	8	11

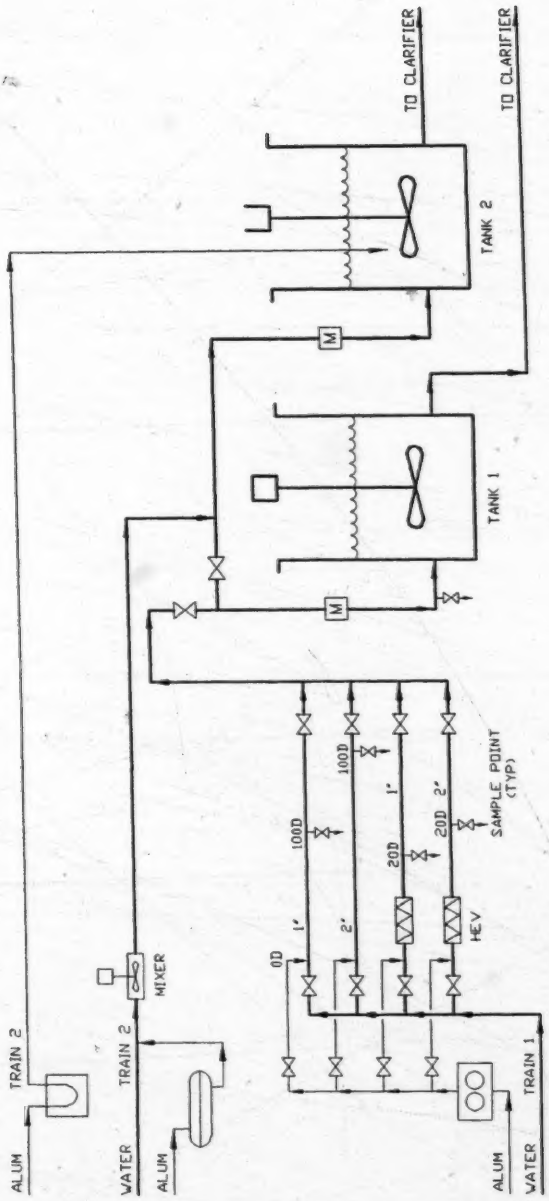

Figure 2-6 Schematic of trains one and two (train one is on the bottom). (drawn by Louis Kennedy, 2003)

2.4.1.1 Train one

Train one was used to study alum mixing with pipes and static mixers (Figure 2-6). In train one alum injection always occurred along the section of straight pipe. A manifold allowed for four choices of straight pipe: 5 meters of empty pipe of diameter 1 or 2 inches, and 1 or 2 inch diameter static mixers followed by 5 meters of straight pipe, 1 or 2 inches in diameter, respectively. The sample valves for the lines with empty pipe were located 100 pipe diameters from the alum injection point. The sample valves for the static mixer lines were located 20 pipe diameters from the alum injection point.

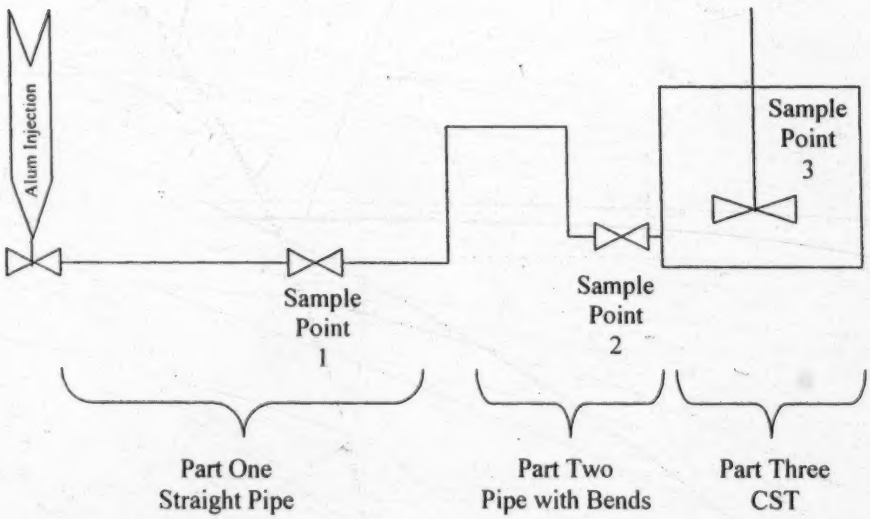

Figure 2-7 A schematic of the sample points in train one.

Alum injection into train one was achieved with a gear pump. Since a gear pump provides continuous flow, it was possible to withdraw a fully mixed sample from valves along the pipe or from the continuously stirred tank. The three sample points used were one from the valve along the stretch of straight

pipe (Point 1), a second from the valve just before the CST (Point 2) and the third from the top of the CST (Point 3), all illustrated in the schematic in Figure 2-7. Samples from the CST were taken by dipping a 2L pitcher into the top of the tank. The pitcher was dipped approximately 20 centimeters below the surface between the shaft and the edge of the tank. The water flow rates in train one ranged from 1.5 to 4.9 m^3/hr.

2.4.1.2 Train two

Train two was used to test alum mixing in pipes, inline mechanical mixers and continuous stirred tanks (refer to Figure 2-6). Alum injection could be done either in the section of straight pipe or directly into the CST. The straight pipe was 4 inches in diameter with an alum injection point into the center of the pipe followed by 2 meters of straight pipe. An inline mechanical blender was located immediately after the alum injection point. Alum was injected into the center of the water flow, which was set at 1.5 m^3/hr, so the retention time in the section of straight pipe was 37 seconds, well above the time required for precipitation (1-7 seconds). The inline mechanical mixer could be turned off or set at a maximum of 1800 RPM. The pumps used for alum injection in train two were different from train one. The pump used for alum injection into the straight 4 inch pipe was a diaphragm pump. The pump used for chemical injection into the CST was a peristaltic pump. Therefore, train two always had intermittent alum flow, making it impossible to withdraw a fully mixed sample from along the pipe, so only samples from the top of the CST were taken.

2.4.1.3 Continuous Stirred Tank

The continuous stirred tank was a square unbaffled tank with a single 13" marine impeller set at 200 RPM. The dimensions of the tank are drawn to scale in Figure 2-8 and summarized in Table 2-3.

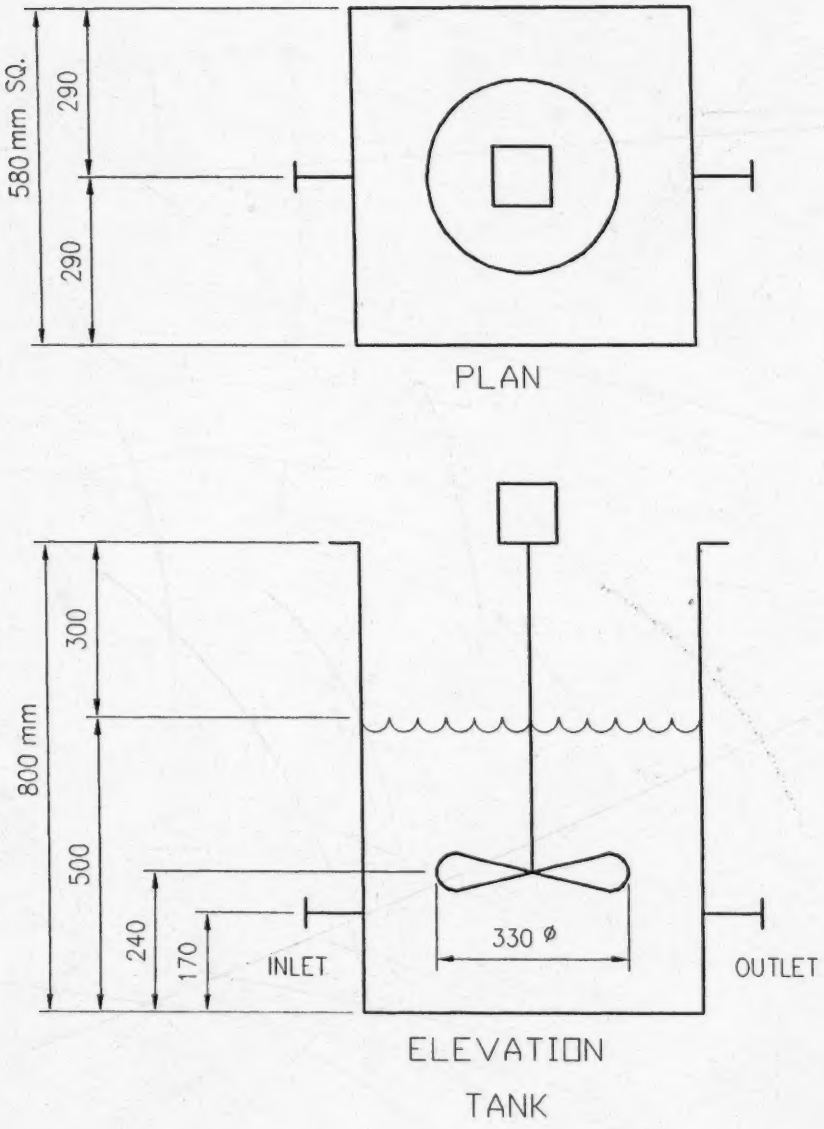

Figure 2-8 Diagram of CST in the Pilot Plant. Dimensions are in millimeters (drawn by Louis Kennedy, 2003)

Table 2-3 Properties and Dimensions of the CST

Variable	Description	Dimensions (cm)
Tank Type	Box	
Impeller type	marine	
Baffles	none	
C	Impeller off bottom of tank clearance	24
D	Impeller diameter	33
H	Height of liquid level in tank	50
h	Height of tank	80
I	Inlet pipe off bottom of tank clearance	17
O	Outlet pipe off bottom of tank clearance	17
T	Tank width	58
W	Width of square tank	58
Q	1.5 m^3/hr	
V	168 Litres	

Summary With Tank Diameter = Width of the Tank (T)

Variable	Ratio
C/T	0.4
D/T	0.6
H/T	0.9

2.4.1.4 Pipes

PVC piping was used throughout the Pilot Plant. The inner diameters of the 1, 2 and 4 inch diameter pipes were 1.049, 2.067 and 4.026 inches respectively. The chemical was injected into the center of the 2 and 4 inch pipes and into the bottom of the 1 inch pipe. The plume of alum for injection at the center of the pipe is illustrated in Figure 2-9., the shape of which was discussed in Section 1.7.2.2.

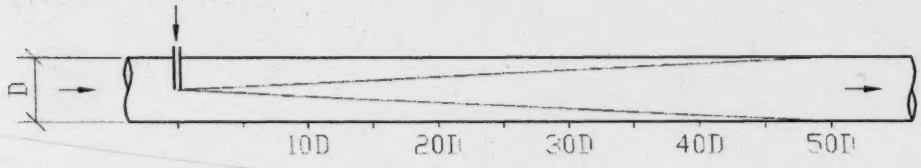

Figure 2-9 Alum plume with chemical injection into the center of a pipe. (drawn by Louis Kennedy, 2003)

2.4.1.5 Static Mixers

The static mixers used were high efficiency vortex (HEV) mixers, 1 and 2 inches in diameter. The chemical was injected 2 inches before the first tab and the injection point was inline with the static mixer's top tab. The HEV and its tabs are described and illustrated in Section 1.7.2.1.

2.4.1.6 Inline Mechanical Mixer

The inline mechanical mixer consisted of two 3.6 inch A100 impellers mounted inside a 4 inch pipe. The chemical injection point was at the center of the pipe, just before the impellers.

2.4.2 *Mixing Conditions*

The mixing and flow conditions in the empty pipes and pipes with static mixers were chosen to ensure fully turbulent flow by setting the Reynolds number to be greater than 10 000 (Table 2-4). The effects of alum mixing time were evaluated by varying the combined alum mixing time of the initial and additional alum mixing steps from seconds to several minutes. The detailed conditions for each set of experiments are given in Appendix A.

Table 2-4 Summary of mixing conditions (0 °C and $\nu = 9 \times 10^{-7}$ m^2/s).

Initial Mixing Method	Injection Pump	Flow rate range (m^3/hr)	Initial G (s^{-1})	Total Alum Mixing time	Total G t	Re in Pipe (thousands)
2" Pipe (center)	Gear	1.5-4.8	50 – 260	2 min – 11 min	250 - >100 000	11-37
1" Static Mixer	Gear	3.8	11 000	1 sec – 20 min	1 000 - >100 000	58
2" Static Mixer	Gear	4.8	1 500	2 sec – 14 min	3 000 – 10 000	11-37
2" Pipe (bottom)	Gear	4.8	260	8 sec – 14 min	6 000 - >100 000	11-37
1" pipe (bottom)	Gear	3.8	2 000	1 sec- 15 min	9 000 - >100 000	58
4" pipe (center)	Diaphragm.	1.5	5	8 min	>100 000	6
CST	Peristaltic.	1.5	>1 200	7 min	>100 000	
Inline blender	Diaphragm.	1.5	N (RPM) 0-1 800	8 min	>100 000	Tank Re 403

2.4.3 Pumps

The three types of pumps used in this experiment were diaphragm, gear and peristaltic. The gear pump used was a Micropump Model 180 series magnetically driven gear pump, and the diaphragm pump was a Liquid Metronics A771-152-C pump. The diaphragm and peristaltic pumps produced an intermittent chemical injection stream, while the gear pump provided a continuous injection of chemical. The difference between continuous and intermittent chemical injection into a pipe is illustrated in Figure 2-10 and Figure 2-11.

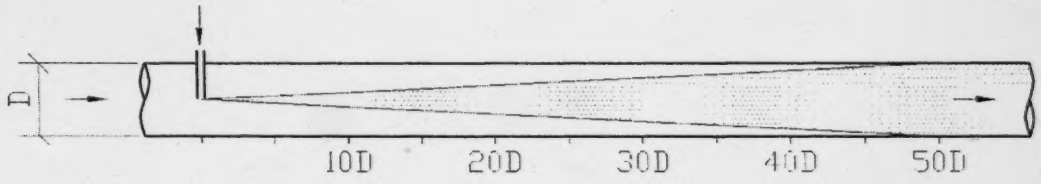

Figure 2-10 Continuous injection into center of pipe (drawn by Louis Kennedy)

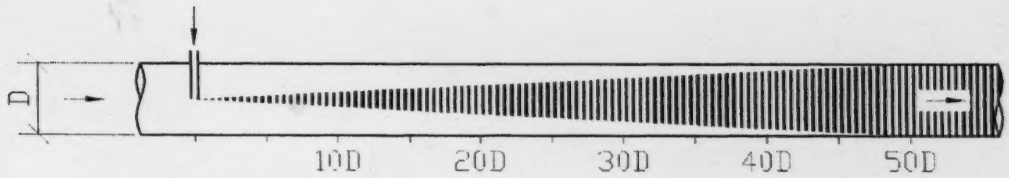

Figure 2-11 Intermittent Injection into center of 4 inch pipe with 1 stroke per second. Only solid black areas contain injected alum (drawn by Louis Kennedy).

Pump calibration curves were established for each pump. The gear and diaphragm pump flow rates were established by doing "draw downs" with a graduated cylinder and stop watch. The flow rates for the peristaltic pump were

found by doing "bucket tests" with a graduated cylinder and a stop watch. The stroke length and the frequency of the stroke could be set on the diaphragm pump by changing the percentage of maximum stroke or percentage of maximum speed settings respectively. The correlation between actual frequency and the diaphragm pump's dial setting of percentage of maximum speed is shown in Figure 2-13. The resulting pump calibration curves are given in Figure 2-12, Figure 2-14, Figure 2-15 and Figure 2-16.

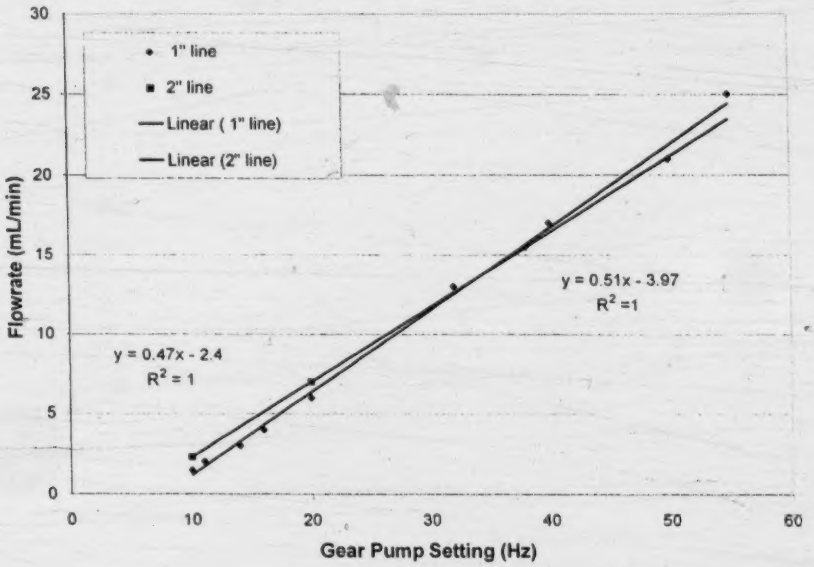

Figure 2-12 Pump calibration curves for the gear pump for line pressures used for "Test Line" experiments.

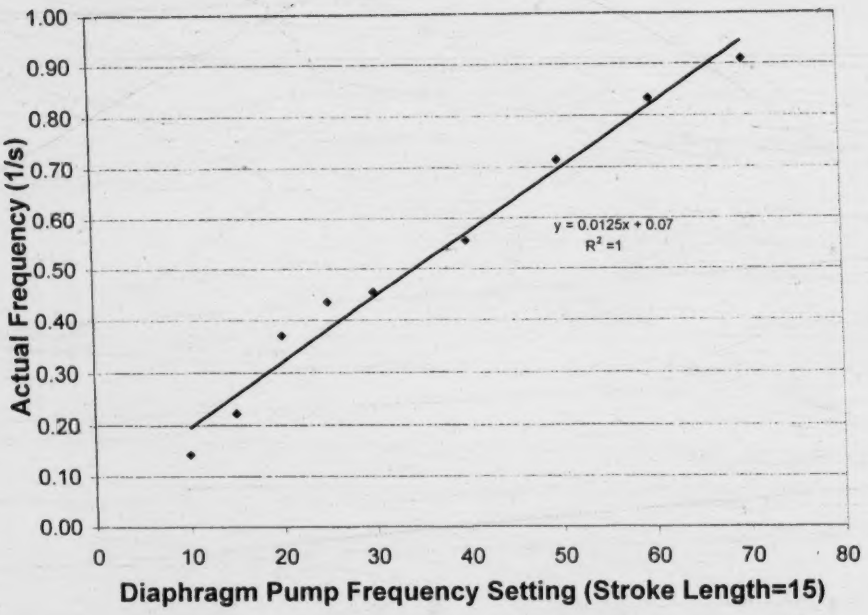

Figure 2-13 Actual frequency curve for the diaphragm pump.

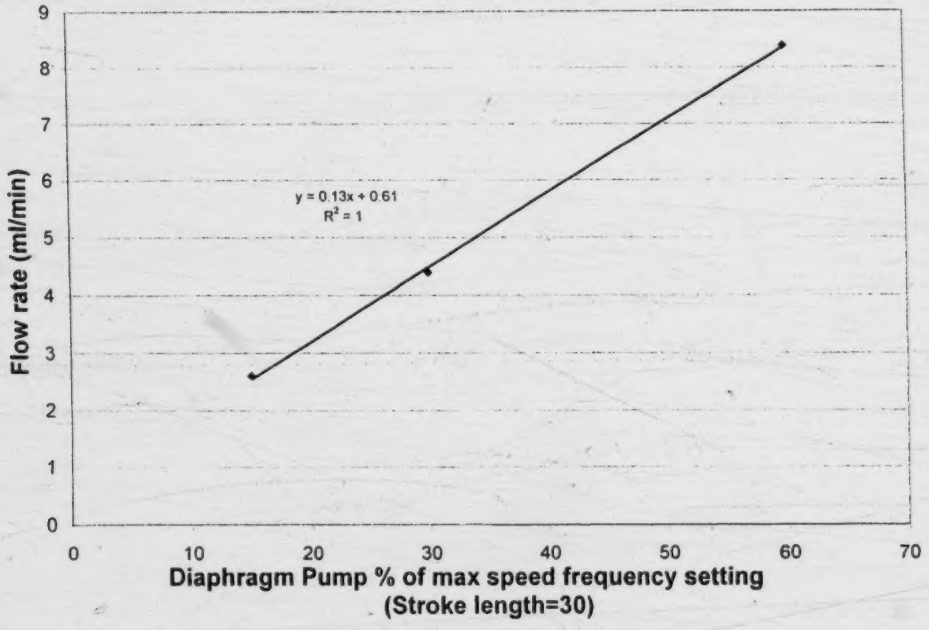

Figure 2-14 Diaphragm pump calibration at a stroke length setting of 30.

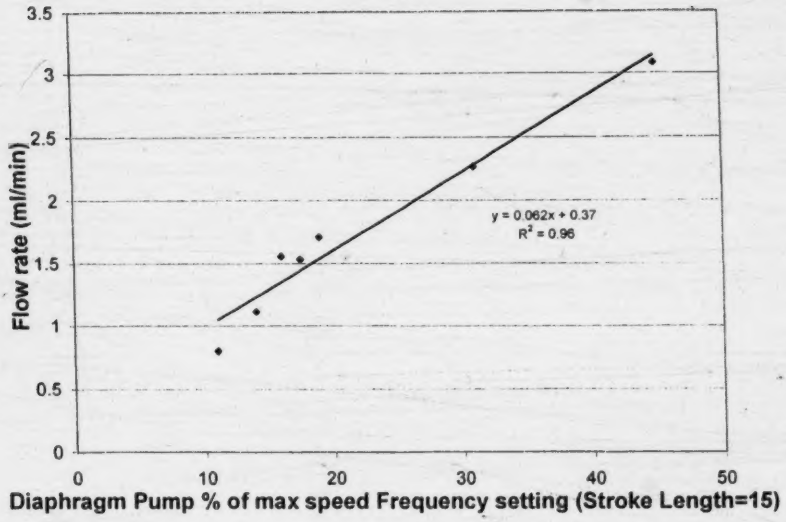

Figure 2-15 Diaphragm pump flowrate calibration at stroke length setting of 15.

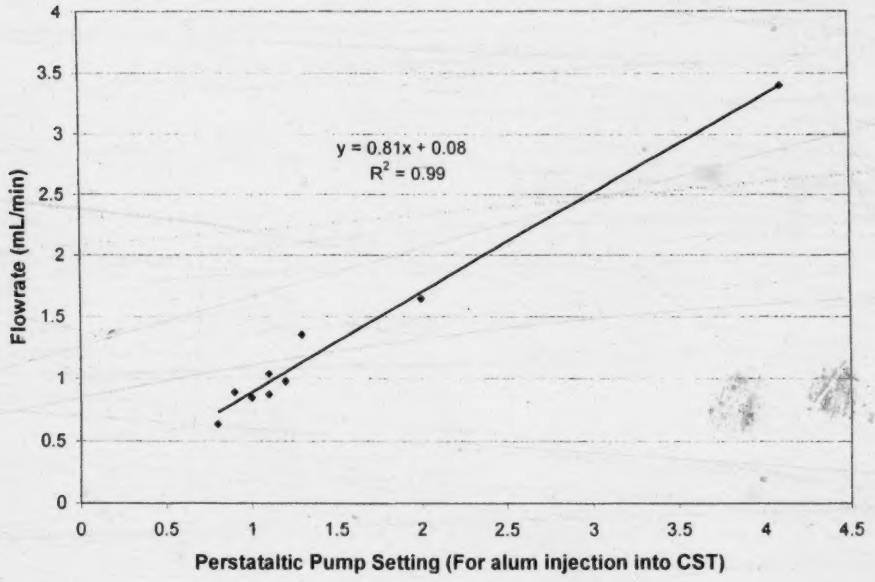

Figure 2-16 Flowrate calibration for the Peristaltic Pump.

Validation of the pump curves was achieved by comparing the alum dosages in the feed to those calculated from pump curve data and an analytical measurement of aluminum in a feed sample. The data for the calculations are in appendix B. There is a ±3-13% difference between alum dosages calculated from the gear pump curve and the total aluminum concentration measurement. The average error of the total aluminum concentration measurement is ±6%, so there exists experimental error in both methods. Since the aluminum concentrations in the supernatant will be used to analyze alum performance, the alum dosages calculated from the aluminum concentration in the feed sample were taken to be the true values and the pump curve calculations were used to identify outliers.

2.5 Experimental Procedures

As shown in the experimental set-up section, alum was injected with various pumps and mixed with various mixing apparatus under continuous (CST, Pipe, Static Mixer & Inline Mechanical Mixer) and batch (Jar) conditions. The experimental procedures for the continuous conditions in the pilot plant train, the straight section of pilot plant pipe and the batch jar tests were all slightly different. Numerous experiments were done, examining various combinations of "Initial Alum Mix" and "Additional Alum Mix" steps. In order to clarify the purpose and avoid confusion, all experiments will be categorized into three groups. These three groups of experiments, from now on, will be referred to as the "Jar", "Pilot Plant Train" and "Isolation Test Line" experiments. The purpose of each and the reason for its slightly different procedures is discussed in this section.

2.5.1 Jar

The "Jar" experiments are the tests where all sedimentation steps, from alum injection to settling, were simulated in the jar. The purpose of the "Jar" experiments was to establish how alum dosage affects the mixed solution pH, the optimum Gt, and the influence of the initial G on coagulation with alum in Edmonton's winter river water. The influence of the initial G is used to identify

whether the mechanism of coagulation, sweep or a combination of sweep and charge neutralization, took place. The procedures for the jar test in the "Jar" experiments were outlined in Section 2.3.

2.5.2 *Pilot Plant Train*

The "Pilot Plant Train" experiments will refer to mixing tests done using either train 1 or train 2. The alum/water samples taken from all three possible sample points along the pilot plant train were put into jars where polymer was added, mixed, flocculated and settled. The schematic in Figure 2-7 illustrates the 3 sample locations used in this project. The main purpose of the "Pilot Plant Train" experiments was to look for differences between static mixers and pipes, inline mechanical mixers and continuous stirred tanks (CST).

The procedures for the "Pilot Plant Train" were similar to the procedures for the "Jar" experiments, except that alum injection and mixing took place in the pilot plant instead of the jar. Additional alum mixing in the jar was optional. A summary of the procedures is given in Table 2-5. The differences in the alum mixing procedures between the Jar and Pilot Plant Train experiments are summarized in Table 2-6.

Table 2-5 Mixing Conditions for Pilot Plant Train experiments

Step Number	Sedimentation Process Step Description	Location	N (RPM)	Time (min.)
1	Alum injection	Pilot plant	Varied	Varied
2	Initial Alum mixing	Pilot Plant	Varied	Varied
3	Additional Alum Mixing	Jar	0 or 120	0 or 5
4	Polymer injection	Jar	200	----
5	Polymer mixing	Jar	200	5
6	Flocculation	Jar	25	15
6	Settling	Jar	0	10
7	Sampling	Jar	0	-----

2.5.3 Isolation Test Line

Finally, the last set of jar test experiments were done on samples taken solely from the straight pipe section of the pilot plant train. Increments of additional alum mix were done in the jar to determine a minimum Gt requirement for optimum turbidity removal. The purpose of the "Isolation Test Line" experiments was to better determine the effects of Gt and which of the two, the static mixer or pipe, required a lower Gt for optimum turbidity removal. The second purpose of the "IsolationTest Line" tests was to examine coagulation in two operational zones, "sweep" and the "combination" zone of charge neutralization and sweep.

Like the "Pilot Plant Train" experiments, the first few mixing steps took place in the pilot plant and the remaining steps in the jar. The differences between the "Isolation Test Line", "Jar" and "Pilot Plant Train" experiments are summarized in Table 2-6.

Table 2-6 Differences between Jar, Pilot Plant Train and IsolationTest Line experiments. Total Gt is the total Gt of the initial alum mix and additional alum mix steps.

Category	Initial Alum Mix N (RPM)	Initial Alum Mix time	Additional Alum Mix N (RPM)	Additional Alum Mix time (min)	G (s^{-1})	Total G x t (thousands)
Jar	25-300	2sec-30min	25	6-10	15 to 300	6-180
Pilot Plant Train	---	1.2 sec-7min	120	0 or 5	5 to 11 000	1 to ->300
Isolation Test Line	---	1.2 sec – 25 sec	25	2-20	50 to 11 000	2-20 000

The flowrates and Reynolds numbers for the pilot plant experiments are summarized in Table 2-7.

Table 2-7 Flow rate and Reynolds numbers for continuous flow experiments in the IsolationTest line and Pilot Plant Train experiments.

Experimental Group	Test Line	Pipe Diameter		Water Flowrate	Bulk velocity in Pipe	Reynolds # in Pipe
		(in.)	(m)	(m^3/hr)	u_b (m/s)	
Isolation Test Line	2" static	2	0.05	1.5	0.21	11 609
Isolation Test Line	2" empty pipe	2	0.05	1.5	0.21	11 609
Isolation Test Line	1" static	1	0.03	3.8	2.08	58 821
Isolation Test Line	1" empty pipe	1	0.03	3.8	2.08	58 821
Control	Train 2 – Pipe	4	0.10	1.5	0.05	5 805
Pilot Plant Train	2" static	2	0.05	4.8	0.66	37 150
Pilot Plant Train	2" empty pipe	2	0.05	4.8	0.66	37 150
Pilot Plant Train	1" static	1	0.03	3.8	2.08	58 821
Pilot Plant Train	1" empty pipe	1	0.03	3.8	2.08	58 821

2.6 Experimental Design

The experiments were designed to isolate the effects of the first part of the sedimentation process, the injection and mixing of alum. The variables to be isolated were alum dosage, mixing intensity, time and dispersion. The differences in dispersion between mixing methods are discussed in Section 1.7.1. The effect of variables in other steps in the sedimentation process and the variable feed water were taken into account and removed by reproducible experimental procedures and using the statistical method of blocking. What could not be blocked was randomized. A sample standard deviation for each mixing method at numerous alum dosages was established. The method with the lowest sample standard deviation was used as the control experiment. The control experiment also showed the expected effect of improvement of turbidity removal as the alum dosage increases. The establishment of a reliable control permitted comparison between blocks. The low standard deviation of most mixing methods also provided repeatability and reliability of the experimental data.

Blocking is an important statistical tool. A block is a portion of an experimental material that is expected to be more homogeneous than the aggregate (Box *et al.*, 1978). In this project, the experimental material is untreated North Saskatchewan River water and the block was the group of paired experiments conducted during one or more days with similar river water turbidity. A pair is the smallest block. The parallel set up of the pilot plant allowed for paired experiments to be done, but since the experimental conditions remain constant for more than one pair, the size of the block was made larger. If the conditions remain constant for an entire day, all the paired experiments of the same day are blocked together. If water conditions remained constant for more than one day the block size was increased even further (multiply by the number of constant days). Therefore, depending upon the consistency of the water

conditions, the block was as small as one day of experiments or as large as the number of experiments conducted on days with identical water conditions.

In addition to blocking experiments, it is important that the experiments be made comparative (Box *et al*, 1978). If a modification is being tested, it should be compared side by side with old methods. This was achieved in this project by using both of Epcor's pilot plant trains. Each train was capable of continuously feeding coagulant chemicals and mixing them with natural untreated water. The new method of initial alum mixing, static mixers, was tested in one train, while an unmodified method of chemical injection, pipes, CST or inline mechanical mixers could be tested simultaneously in the other train.

Comparison was also achieved by choosing a daily control experiment. The control experiment was chosen for its consistency and repeatability. Since the water conditions remained constant throughout each day, it was not necessary to pair each experiment with the control, instead it was conducted at least once in each block; therefore, once daily. The samples taken for the daily control experiment is summarized in Table 2-8.

Table 2-8 Control experiment used for this project

Control	**Sample location**
Train two – injection into 4 inch empty pipe	CST of train two (sample point 3 in Figure 2-7)

In addition to comparison, replication and randomization methods were used. Replication was achieved within each paired experiment by taking more than one sample from each test run. Since the jar test apparatus could hold 6 jars at a time, multiple samples could be tested simultaneously. For example, 3 samples from 2 different sample points could be tested at the same time. Replication was also achieved between blocks by repeating the same experiments on days with different natural water conditions. Randomization was achieved by ensuring that pairs of opposite extremes were in the same block.

Pairs were chosen to be the two conditions giving the extreme values or combined effects of each dependent variable of interest: G, time, alum dosage and dispersion. The effects of these dependant variables on the minimum Gt, rate of change of pH, supersaturation, hydroxide ion concentration and evidence of floc breakage were tested in pairs. The pairs are summarized in Table 2-9. The purpose of each pair will be now be discussed.

The opposite extremes of each dependent and independent variable were identified as follows:

- Mixing Intensity: The mixing intensity changes the rate of particle collisions, so the extreme cases for mixing intensity, high and low mixing intensity (G or ε), will result in the least and most particle collisions. Therefore, the comparisons were made between the high G of the 1 inch static mixer and the low G of the 4 inch or 2 inch pipes, and between the high G of a CST with the low G of a pipe.
- Mixing time and Gt: The extremes of mixing time ranged from seconds to minutes. The low Gt was set to be of the order of magnitude of 1 000 and the high Gt was greater than 300 000 for the "Pilot Plant Train" experiments and 20 000 for the "Isolation Test Line" experiments, by varying the additional alum mixing time.
- Initial Mixing Intensity: The importance of collisions between naturally occurring colloids and the ionic aluminum species that exist prior to aluminum hydroxide precipitation (less than 10 seconds) was studied by examining the effects of continuous versus intermittent alum injection. With intermittent alum injection, much of the untreated water can not contact the ionic aluminum species, which only exists for seconds. The white area in Figure 2-10 and Figure 2-11 illustrates the quantity of water that never contains the aluminous ions that only exist for seconds. The importance of the collision frequency between the ionic species and colloids was also studied by testing alum injection with an inline mechanical mixer both on and off. The number of collisions with the inline mixer on would be higher.

- Radial dispersion: The rate of radial dispersion was examined by comparing a pipe to a static mixer. The rate of radial dispersion in a pipe differs from that in a static mixer as discussed in Section 1.7.2. It is minimal in a pipe and maximal in static mixer; therefore, a 2 inch pipe was compared to a 1 inch static mixer.
- Dispersion: Dispersion was examined by comparing a CST and pipe. As discussed in Section 1.7.1, the macromixing and local concentration differences in a CST and a pipe in turbulent flow are of opposite extremes. Macromixing is high in a CST and minimal in a pipe. The dispersion in a pipe results in high local concentrations and a slow rate of change of pH and vice versa for the CST.
- The rate of change of pH: The rate of change of pH is controlled by dispersion; therefore the experimental pair for the rate of change of pH is identical to the pair for dispersion.
- Local hydroxide ion concentration: The local hydroxide ion concentration at the time of precipitation is controlled by dilution of the liquid alum with water; therefore, the experimental pair for local hydroxide concentration is identical to the pair for dispersion.
- Local supersaturation: As discussed in Section 1.7.1, local supersaturation is dependent on dispersion rates. The supersaturation may be inferred from a local concentration, but is a complex non-linear function of the concentration, pH and solubility.

Table 2-9 Paired extremes of experimental variables. (PP – Pilot Plant Train, ITL – Isolation Test Line, JT- Jar Test)

Variable	Low Extreme	High Extreme
Initial G (PP)	4" Pipe $G=5\ s^{-1}$	1" Static Mixer $G=11\ 000\ s^{-1}$
Initial G (PP, ITL)	2" empty pipe $G=50\ s^{-1}$	1" Static Mixer $G=11\ 000\ s^{-1}$
G t (PP)	Mixed sample taken in straight pipe	Mixed sample taken from CST
G t (PP, ITL)	No additional alum mixing in jar	Additional alum mixing in jar.
Collision frequency (colloids and hydrolysis ions) (PP)	Intermittent alum injection at low G (4" pipe/diaphragm)	Continuous alum injection at high G (1" static/gear)
Collision frequency (colloids and hydrolysis ions) (PP)	Inline Mechanical mixer ON	Inline Mechanical Mixer OFF
Radial mixing (ITL)	2" pipe (G=50)	1" static mixer (G=11 000)
Back mixing (PP and JT)	Plug Flow or Batch (pipe or jar)	CST
Local pH at time of Aluminum Hydroxide precipitation (PP)	Low pH (Cationic) Pipe	High pH (Anionic) CST

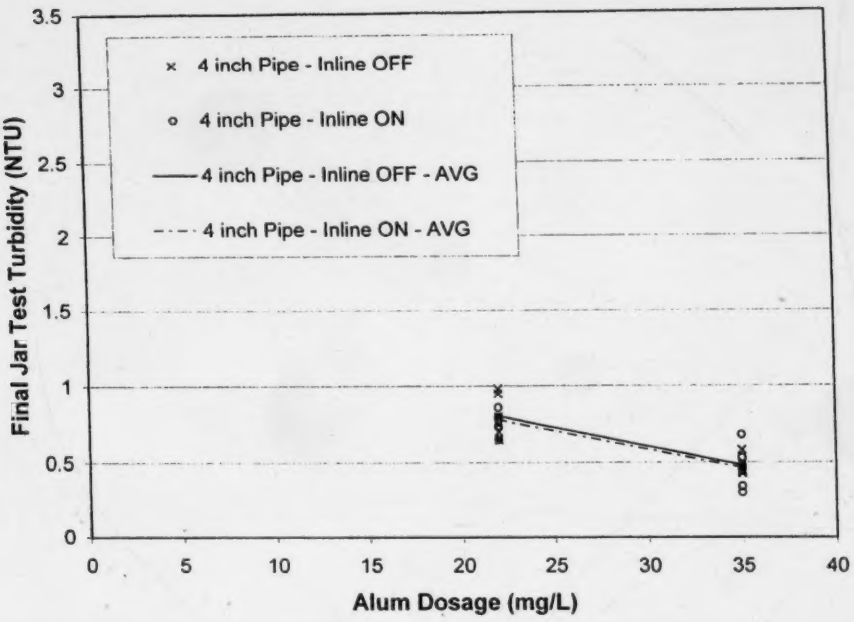

Figure 2-17 Effects of the inline mechanical mixer on turbidity removal. (Total Gt for alum mixing= 37.5±0.5 data taken from block one)

The control experiment was chosen from three existing mixing methods in the pilot plant: alum injection at the center of 4 inch pipe just before the impeller of the inline mechanical mixer with the impeller off; or with the impeller on; and injection the impeller of a continuous stirred tank in fully turbulent flow. The inline mechanical mixer used in the Epcor Pilot plant was a Lightning Line Blender, which consisted of two 9 centimeter in diameter A100 impellers which rotated at 1800 RPM. Samples from train two were always taken from the top of the CST with a 2 litre pitcher. This sampling method assumed that the tank was uniformly mixed. Samples from the pipe on train 2 could not be taken, since the alum injection pump on train two was not continuous, as the diaphragm pump only injected alum on the upward stroke and not the downward stroke. The results of these samples, for when alum was injected in the center of the pipe directly

before the impellers, are shown in Figure 2-17. They show that turbidity removal improves as the alum dosage increases. This trend is what would be expected. The same trend was observed with the inline mechanical mixer both on and off.

Since the understanding of dispersion in an empty 4 inch pipe is more established than the dispersion by the inline mechanical mixer (Brodkey, 1978), alum injection into the center of a 4 inch pipe was chosen as the control experiment.

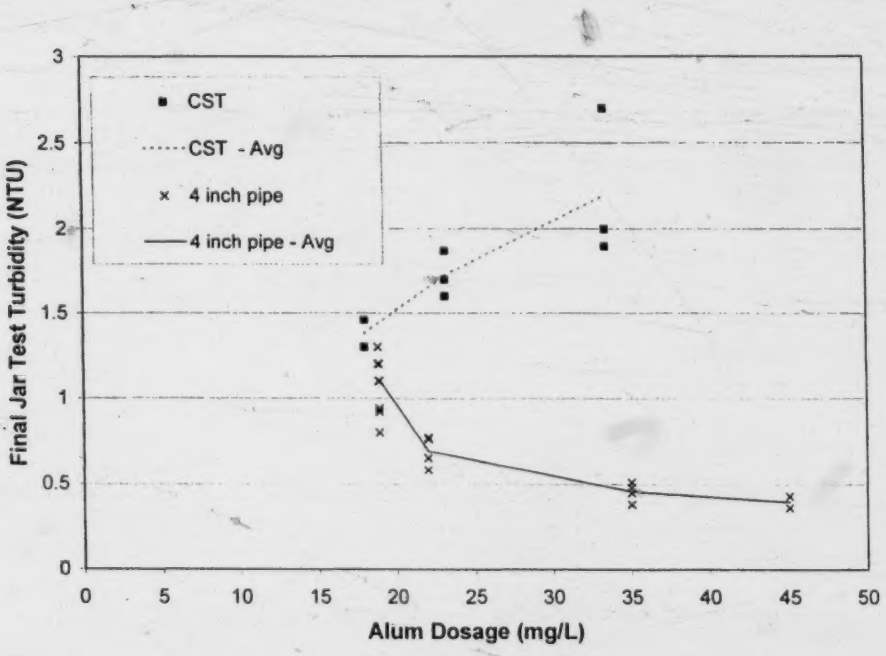

Figure 2-18 Changes in sample variation with alum dosage for alum injection into a 4 inch pipe and at the impeller of a CST, the 4 inch pipe sample standard deviation is between 0.03-0.1 while the CST is between 0.1-1.1 (data taken from block 4)

A CST is capable of a higher initial mixing intensity than the 4 inch empty pipe, so it may have potentially been a good control experiment. As defined earlier, the two requirements for the control experiment are low variability and the

ability to detect improvements in turbidity removal as the alum dosage increases. Figure 2-18 shows that the CST met neither of these two requirements. Turbidity removal improved as alum dosage was lowered and the sample scatter was larger than for the 4 inch empty pipe. The cause of the poor turbidity removal when alum was added to the CST will be discussed in Chapter Three.

The alum mixing conditions in Epcor's E.L Smith water treatment plant were also tested. In the plant, alum is injected at the impeller of the low lift pump. The results will be discussed in Section 3.11.

2.7 Determining the Mechanism of Coagulation

Two mechanisms of coagulation with alum have been established in the literature: sweep and charge neutralization (Section 1.6). Both mechanisms are inferred from the effects of increasing the collision frequency of the ionic aluminum species and naturally occurring colloids. Since the ionic aluminous species of interest only exist for seconds or less, variations in the collision frequency immediately after alum injection are significant for the mechanism of charge neutralization. If an increase in the collision frequency during the seconds after alum injection improves turbidity removal, the mechanism of coagulation is assumed charge neutralization, and if no improvement is detected, the mechanism of coagulation of alum can be assumed as sweep. It has been shown that the combination of pH and alum dosage determine the mechanism of coagulation with alum; therefore, the resulting mixed solution pH for each alum dosage had to be measured. In addition to alum dosage, pH and initial G, the mixing time was also varied. It has been experimentally shown that turbidity removal is dependent upon a minimum Gt and alum dosage, so improvements in turbidity removal could be due to increases in Gt rather than G. Experiments were performed in the jar to examine the effect of G at the time of alum injection; and thus the mechanism of coagulation with alum. Alum injection and alum mixing were done in the jar. The mixing intensity in the jar was set at either 15 or 300 s^{-1} for a set of incremental time periods. The total Gt versus final turbidity of the supernatant solution was then plotted so that the effects of increasing G

could be examined at values of Gt ranging from 6 000 to 180 000 with varying initial G. The range of alum dosages tested was 8 -35mg/L, resulting in a mixed solution pH of 7.9 to 7.4 respectively. If the mechanism of coagulation is sweep, there will be no difference in turbidity removal between alum injected into at jar at a G of 15 or 300 s^{-1}. The results of these experiments are plotted in Figure 2-4, tabulated in Appendix A and discussed in Chapter Three.

2.8 References

Amirtharajah, A. & Tambo, N., 1991, *Mixing in Water Treatment*, Chapter one, Mixing in Coagulation and Flocculation, American Water Works Association Research Foundation, American Water Works Association.

Amirtharajah, A. & Mills, K., 1982, *Rapid-Mix Design for Mechanisms of Alum Coagulation,* Journal AWWA, **44**, 210-216

Camp T and Stein P, 1943, *Velocity Gradients and Internal Work in Fluid Motion*, Boston Society of Civil Engineers, vol 30, 4, 219-237

Box G., Hunter W. & Hunter S., 1978, *Statistics for Experimenters*, Ch 4 & 6, John Wiley & Sons, USA.

Clark M., 1985, *Critique of Camp and Stein RMS Velocity Gradient*, Journal of Environmental Engineering-ASCE, **111(6)**, 741-754

Hemsing, J., 2001, *Kinetics of Blending Soluble Polymer Additives*, Masters Thesis, U of A

Minear, R. & Keith, L., 1982, *Water Analysis*, Acedemic Press, New York

Van Gelder, A., Chowdhury, Z. & Lawler, D., 1999, *Conscientious Particle Counting,* Journal AWWA, **85(12)**, 64-76

Vanous, R., Larson, P. & Hach, C., 1982, *Theory and Measurement of Turbidity*, Ch 5, in Water Analysis, Acedemic Press, New York

Vanous, R., Larson, P. & Hach, C., 1982, *Theory and Measurement of Turbidity*, Ch 5 in Water Analysis, Acedemic Press, New York

Hach Website, www.hach.com/Spec/2100N

Chapter 3

Results and Discussion

3.1 Introduction

In the literature review two distinct habits of amorphous aluminum hydroxide were shown: one 100 times larger than the other. The degree of supersaturation determines the habit of the precipitates: a low degree of supersaturation produces aluminum hydroxide precipitates 100 times bigger than a high degree of supersaturation (Section 1.4). The impact of initial precipitate size on collision rate is severe. For precipitates of the size of 0.01 micron, particle collisions due to Brownian motion dominate and the collision rate remains low. If the initial precipitate is 100 times larger, collisions due to fluid shear become significant and the collision rate is much larger (Section 1.5.1); thus drastically reducing the required flocculation time.

In addition to precipitate size, solubility changes due to alkalizing reagents can be significant (Section 1.3.1, Figure 1-4). Both the aluminum solubility and the local aluminum concentration determine the degree of supersaturation and both are influenced by the rate at which water is dispersed through the injected liquid alum. Evidence of changes in precipitate size and aluminum solubility with variations in the extent and rate of dispersion between alum injection methods will be presented.

The dominant mechanism of coagulation for Edmonton's North Saskatchewan River water in the winter, charge neutralization or sweep, will be determined. This is a key question because the alum injection conditions that encourage the formation of larger precipitate for sweep coagulation are opposite to the conditions that promote coagulation due to charge neutralization. A high initial G will increase the degree of supersaturation and thus form smaller precipitates, thus a high G is poor for sweep coagulation. In charge neutralization, however, a high G is beneficial, as it will increase the number of collisions between the cationic hydrolysis products and colloids.

Alum injection into an empty pipe, static mixer, inline mechanical mixer and CST will be compared. Finally, the results of this work will be used to make

recommendations on the optimum mixing conditions for alum precipitation and turbidity removal of Edmonton NSR water in the winter.

3.2 Blocking of Experimental Results

In order to eliminate the effects of variable feed water, the experiments were blocked. Each block was based upon date, experimental procedures and experimental conditions. For each block the experimental procedures were the same and the difference between the minimum and maximum daily average raw water turbidity was less than 1 NTU. The raw water conditions for each block of experiments are summarized in Table 3-1 and the NTU ranges are shown in Figure 3-1.

The pilot plant train experiments in the first three blocks were used to establish a base line for optimum turbidity removal and the control experiment. The first block of experiments was to determine the effectiveness of the inline mechanical mixer. The second compared the plant conditions to the conditions in block one. The third and fourth added the comparison of the continuous stirred tank to the pipe line injection with the inline mechanical mixer both on and off. The pilot plant train experiments in block 5 and 6 were used to compare the static mixer and empty pipes to the baselines established in blocks 1 to 4. The isolation test line experiments in blocks 7 and 8 were used to establish the minimum Gt required for the static mixers and empty pipes at lower alum dosages. The jar experiments in block 8 were used to determine the mechanism of coagulation: sweep or charge neutralization, by examining the effects of the initial mixing intensity (G) on turbidity removal.

Table 3-1 Block summary of raw water turbidity, experimental procedures and alum injection methods (PP train= pilot plant train). All tests were done on Edmonton's winter water at a temperature of 3.0±2 ° C.

Block	*Raw Turbidity*	*Dates*	*Test Procedures*	*4 " P - Inline on*	*4 " P - Inline off*	*Plant*	*Tank*	*2" P bottom*	*2" P center*	*2" SM*	*1" P*	*1" SM*
1	3.1	Nov 6	PP Train	x	x							
2	4.4	Nov 18	PP Train		x	x						
3	3.4-4.2	Nov 25, Nov 29	PP Train		x	x	x					
4	2.7-3.3	Nov 15, Dec 4	PP Train		x	x	x					
5	3.1-4	Dec 6, Dec 9-11	PP Train		x	x	x	X				
6	2.3-2.4	Dec 13, Dec 16, 18	PP Train		x	x	x	x		x	x	x
7	2.3	Mar 18	Test line			x			X	x	x	x
8	1.1-1.8	Mar 11-13	Test line			x			X			x
8	1.1-1.8	Mar 5-11	Jar									

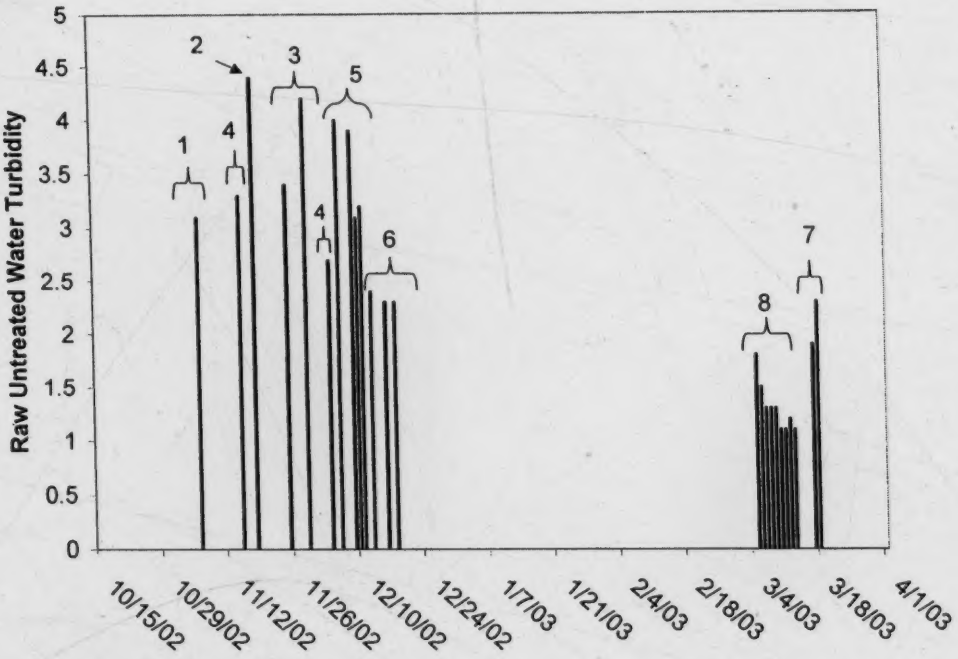

Figure 3-1 Daily average raw water turbidity in each block.

3.3 The Relationship between Turbidity and Aluminum Concentration.

A high degree of supersaturation produces aluminum hydroxide precipitates under 0.01 microns in size: at this size, collisions due to Brownian motion dominate over those due to fluid shear and the collision frequency drops by several orders of magnitude. Injection conditions with instantaneous dilution create regions of high local supersaturation and form smaller precipitates as discussed in Section 1.7.1 and Section 1.3.2. Under conditions of high supersaturation and low solubility, smaller precipitates form and remain suspended. This appears as an increase in final turbidity and aluminum concentration in the jar tests. A direct correlation between final aluminum

concentration and final turbidity will be seen if the suspended particles are small aluminum hydroxide precipitate. The plot in Figure 3-2 shows that this is indeed the case: final turbidity increases as the final aluminum concentration increase. Therefore, it can be assumed that turbidity may be used as a rough index for fine aluminum hydroxide precipitate concentration. Figure 3-2 shows that the CST has the highest values for final turbidity and aluminum concentration of all the injection methods, thus the CST forms the largest quantity of smaller precipitate. The CST, at the point of alum injection, has a high rate of dilution due to back mixing, thus creating a high degree of supersaturation.

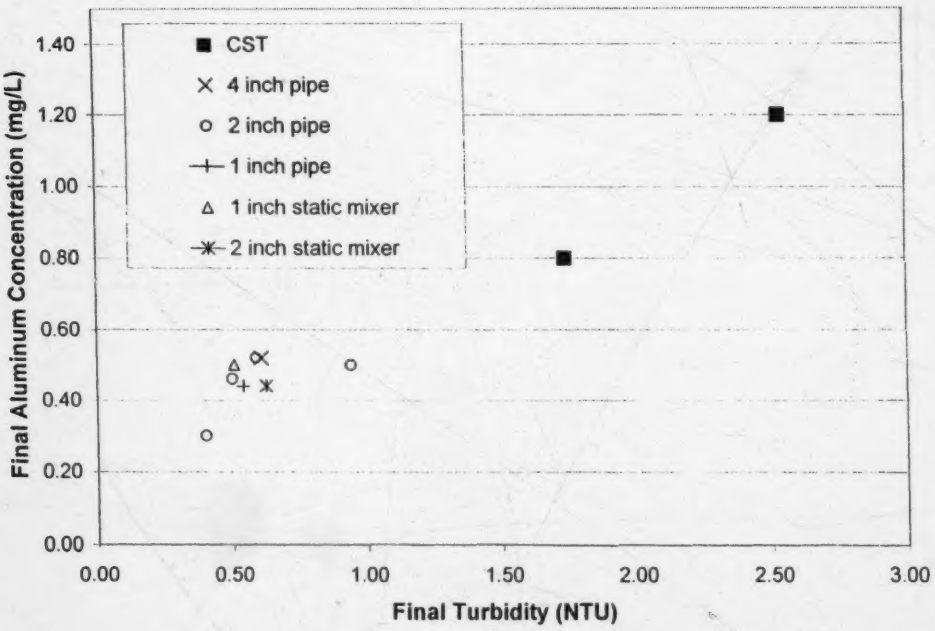

Figure 3-2 Relationship between final turbidity and final aluminum concentration for CST and pipeline injection. (Data taken from block six.)

3.4 The Effects of Alum Dosage

The effects of alum dosage on turbidity removal (Section 1.6.4) and the final solution pH (Section 1.3.3) discussed in the literature review were confirmed in the experiments. As the alum dosage decreased, the final pH increased (Figure 3-3) and as the alum dosage decreased, turbidity removal dropped and was less repeatable (Figure 3-4).

The pH results can be used to predict alum solubility. The results indicated that the minimum alum dosage resulting in precipitation without the use of an acidifying reagent was 8 mg/L. As the alum dosage is decreased to 8 mg/L the pH increases to 7.8 (Figure 3-3). Figure 1-10 shows that at 8 mg/L, alum becomes fully soluble when the pH increases above 7.9. So instant dilution can lead to full solubility in the limits of these experiments.

The pH data can also be used to predict the mechanism of coagulation using Figure 1-25. At a solution pH of 7.8 and alum dosage of 8 mg/L the mechanism of coagulation according to Amirtharajah and Mills (1982) is a combination of sweep and charge neutralization. As the alum dosage increases to 10, 20 and 30 mg/L the pH drops to 7.75, 7.53 and 7.4 respectively. The corresponding mechanisms of coagulation according to Figure 1-22 should be combination (10mg/L) and sweep (20 and 30 mg/L), thus the experiments were intended to straddle the mechanisms of interest; however, the results in Figure 2-4 showed no evidence of charge neutralization. As discussed in Section 1.6.4, turbidity removal should be improved as the intensity of the initial rapid mix period increases if the mechanism of coagulation with alum is charge neutralization. The opposite effect was observed at 8mg/L of alum in the jar test results plotted in Figure 2-4. In Figure 2-4, the open triangles represent conditions with a higher initial G but had higher turbidity in the supernatant solution of the jar test, thus poorer turbidity removal. From this result, it was inferred that the sweep mechanism dominated, even at the lowest concentration of alum.

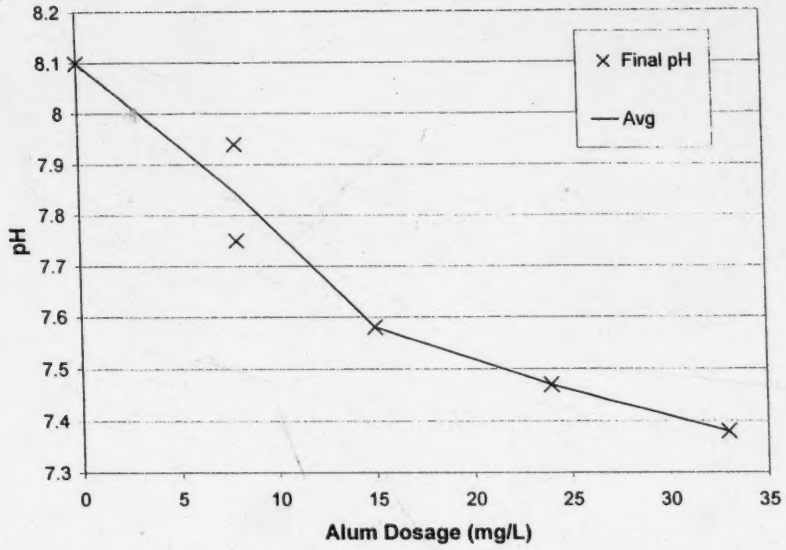

Figure 3-3 Effect of alum dosage on final pH. Test results from alum injection directly into the jar. (Total Gt of alum mixing=189 000, Block 8)

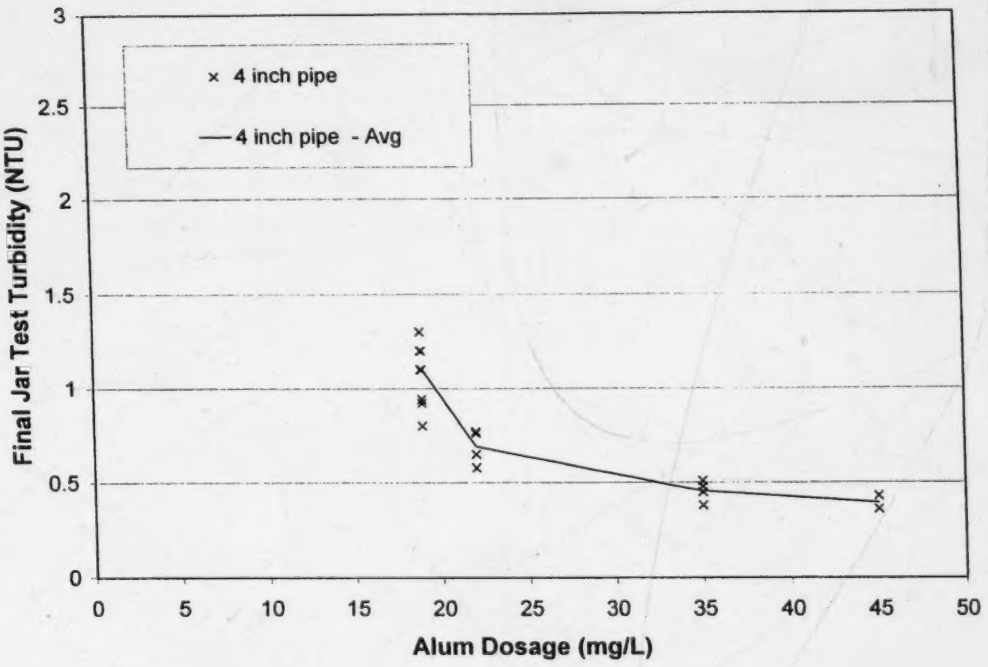

Figure 3-4 Effect of alum dosage on turbidity removal (total Gt from initial and additional alum mixing=37.5±0.5 10^4, data taken from block 4 in Table A-4)

3.5 Initial Mixing at all Injection Locations

Alum injection at the pipe wall of the 2 inch pipe resulted in poor initial mixing for the pilot plant train tests in blocks 5 and 6, as shown in Figure 3-5. Figure 3-5 is plot of alum dosages measured from the aluminum concentration in the pilot plant train and isolation test line samples and the calculated alum dosages from the water and alum flowrates. These calculations were compared to the measured aluminum concentration in samples. The calculated and measured values agreed for sample locations of the CST, the 1 inch empty pipe, and the 1 and 2 inch static mixers, but not for sample locations 1 and 2 of the 2 inch pipe with injection at the pipe wall. This showed that even at 100 pipe diameters from the injection point, the sample was still not fully mixed. This

demonstrates that correct design and installation is critical for the successful operation of mixing equipment. For blocks 7 and 8 the injection point was moved to the center of the 2 inch pipe.

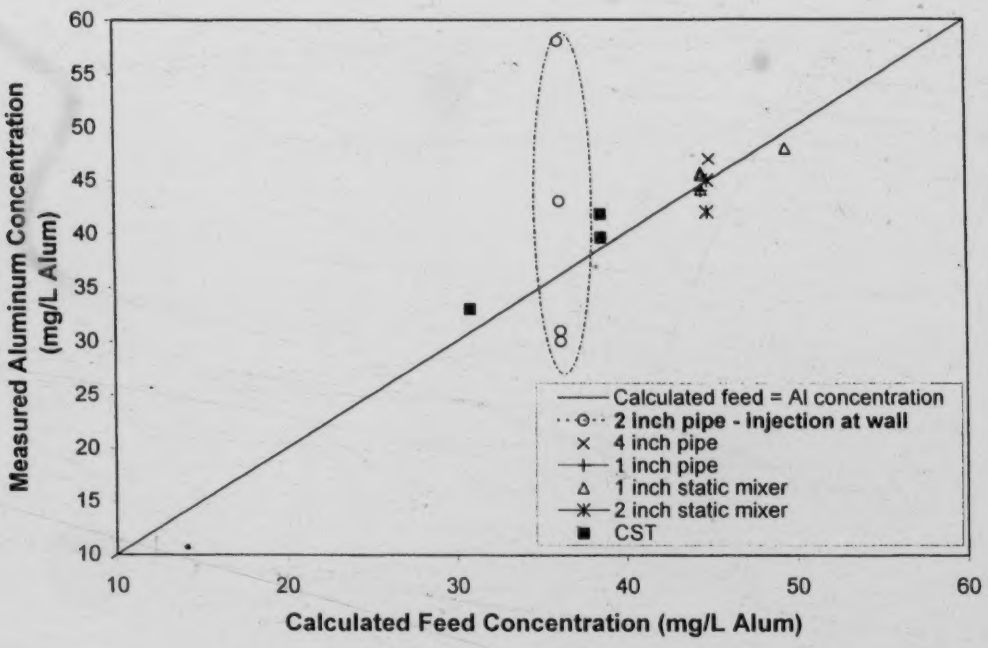

Figure 3-5 Comparision of calculated and measured alum concentration of pilot plant train samples. (Data taken from Table A-6 block 6, sample points 1 and 2 for pipeline injection and sample point 3 for the CST. Total Gt from alum mixing = $37.4 \times 10^4 \pm 5 \times 10^4$). The plot reveals that alum injection at the wall of the 2 inch pipe results in samples with much higher alum dosages than calculated at sample point one: thus the alum is not fully mixed at 100 pipe diameters from the injection point.

3.6 Effectiveness of Inline Mechanical Mixer

Prior to this study, the pilot plant alum injection was done with a diaphragm pump into the center of a 4 inch pipe just before an inline mechanical mixer. The literature review revealed (Section 1.8) that others had observed no detrimental effect when the plant's inline mechanical mixer was turned off. This test was repeated on the pilot plant at high and low alum dosages. It was observed that the inline mechanical mixer had no effect upon turbidity removal regardless of alum dosage as shown earlier in Figure 2-17. The initial mixing intensity and the additional Gt created by the inline mixer were both insignificant since the mechanism of coagulation was sweep (Section 3.7) and the additional Gt created by the inline mechanical mixer is negligible when compared to the total Gt.

3.7 Determining the Mechanism of Coagulation with the Jar Test

Jar tests were done at a low and high G, to examine the effects of initial G on turbidity removal at alum dosages of 8-35 mg/L. If the mechanism of coagulation is charge neutralization, jar tests at 300 RPM should outperform those at 25 RPM. The results in Figure 2-4 are opposite from what should be expected from charge neutralization: a higher G at 8 mg/L resulted in poorer turbidity removal, even at a high Gt of 200 000, suggesting that small precipitates unaffected by Gt formed and that the coagulation mechanism is sweep. This verifies that the observations and conclusions made in Section 3.6.

3.8 Continuous Stirred Tank Results

Alum injection into the CST in train 2 was achieved with a peristaltic pump. The pilot plant's existing alum injection method, the inline mechanical mixer in a 4 inch pipe, was then compared to injection near the impeller in a continuous stirred tank. The experiments were repeated at various alum dosages and raw water turbidities. Under all conditions, injection directly into the continuous

stirred tank had poorer results than any form of pipeline injection, as shown in Figure 3-6.

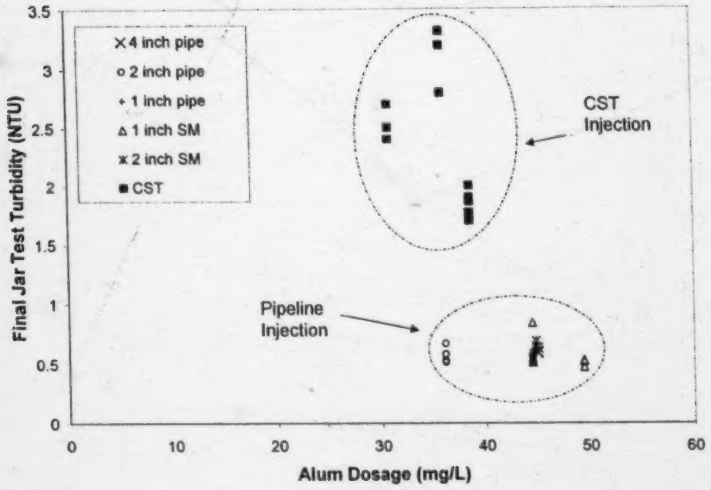

a)

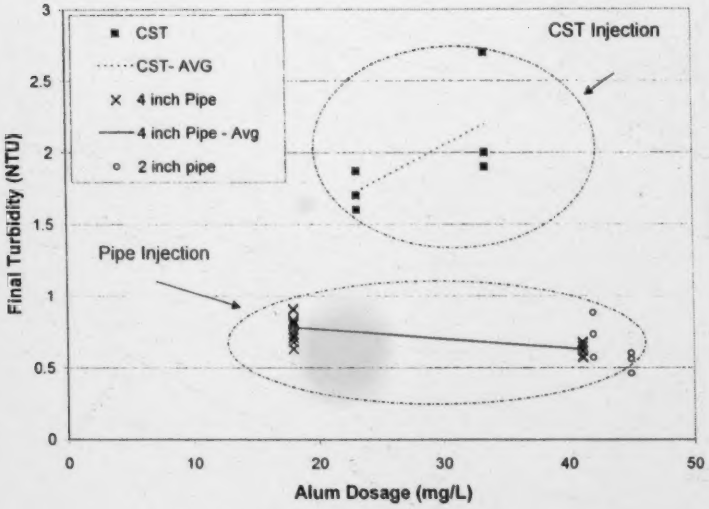

Figure 3-6 Comparision of turbidity removal with alum injection into a CST and a 4 inch pipe at high raw water turbidity (Total Gt from alum mixing = 37.4×10^4 $\pm 5 \times 10^4$, Alum dosage = 30-50 mg/L) a) Block 6 Raw Water NTU = 3.1-3.3 b) Block 5 Raw Water NTU = 3.1- 4.0 (Data taken from Table A-6 and A-5) The CST has poorer turbidity removal than all pipeline injection methods, even at high Gt)

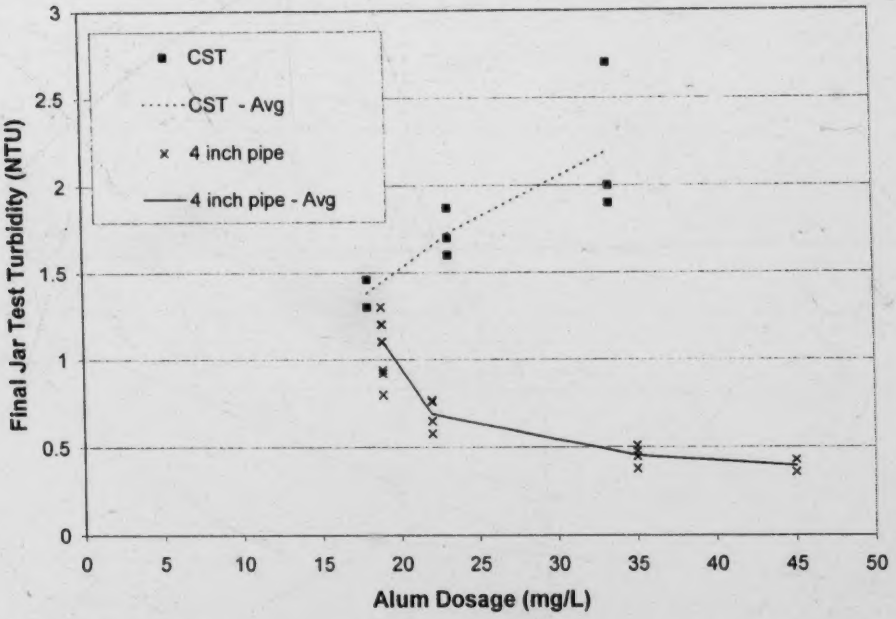

Figure 3-7 Comparision of turbidity removal with alum injection into a CST and a 4 inch pipe at lower raw water turbidity (Total Gt from alum mixing = 37.4×10^4 $\pm 5 \times 10^4$, Alum dosage = 30-50 mg/L) (data from Block 4 in Table A-5, Raw water NTU = 2.7-3.3)

A CST has a much faster rate of dilution and thus a much higher degree of supersaturation than all of the pipeline injection methods: this results in the formation of smaller aluminum hydroxide precipitates and a consistently high turbidity in the supernatant solution of the jar test, as shown in Figure 3-6. The poor results of the CST, even at an extremely large Gt of 370 000, suggest that precipitate collisions are unaffected by Gt. Since smaller precipitates dominated by Brownian motion, are unaffected by Gt (Figure 1-20), this result provides evidence of the formation of smaller precipitates in the CST.

In addition to the ineffectiveness of Gt, the high final aluminum concentrations in the CST provide evidence of the formation of the smaller

aluminum hydroxide precipitates. Figure 3-2 shows that the CST always has a large final turbidity as well as a large final aluminum concentration. The final aluminum concentration is essentially equal to the concentration of aluminum hydroxide precipitates, as discussed in Section 2.2.1.

3.8.1 Pipe line Injection with and without Static Mixers

According to literature (Section 1.6.4), the mechanism of coagulation should be sweep for alum dosages greater than 12 mg/L and a combination of sweep and charge neutralization for alum dosages between 7-12 mg/L. Thus, as the alum dosage falls below 15 mg/L, improvements as the initial G increases from 5 s^{-1} in the 4 inch empty pipe to 11,000 s^{-1} in the 1 inch static mixer should be observed. If the alum dosage is greater than 12 mg/L the mechanism is sweep and the initial G will have no effect as confirmed by the results for alum dosages greater than 30 mg/L plotted in Figure 3-8. To eliminate the possibility of the high Gt masking beneficial effects of the initial G, a plot of Gt versus turbidity removal in Figure 3-8 b was created. This plot reveals that at a Gt of 10,000 s^{-1}, the higher initial G of the 1 inch static mixer (triangles) has a poorer turbidity removal than the lower G of the 2 inch (circles). The fact that the higher initial G in pipeline injection gives poorer results is contradictory to what should be expected if the mechanism of coagulation is charge neutralization. This result confirms that the mechanism of coagulation for alum dosages greater than 30 mg/L is sweep.

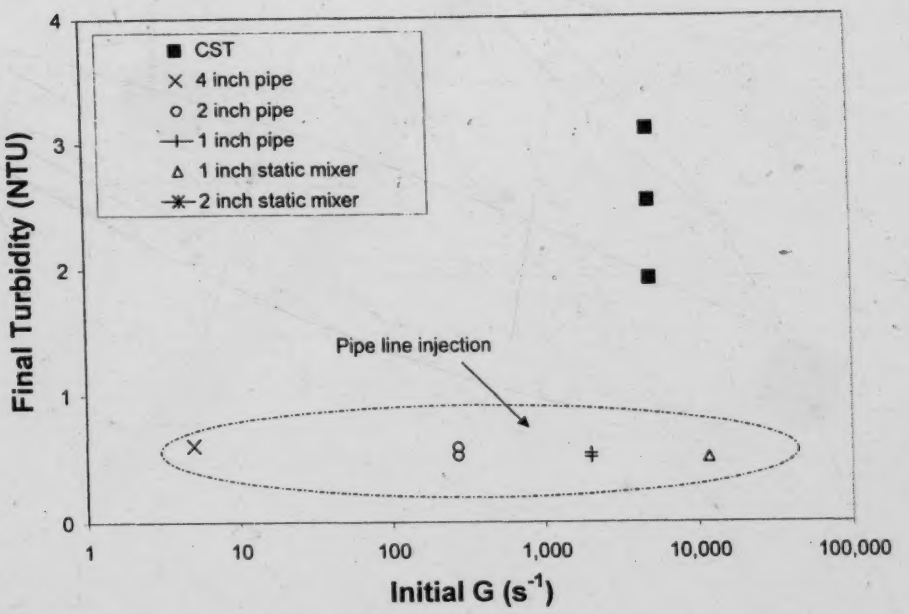

a)

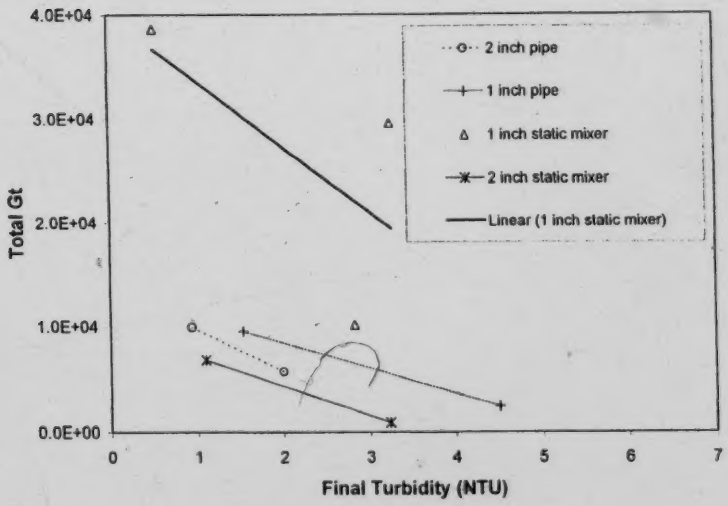

b)

Figure 3-8 a) Regardless of the initial G, good turbidity removal is achieved with pipeline injection and poor results are seen with CST injection ($Gt=37.4x10^4 \pm 5x10^4$, data taken from block 6) b) differences between pipeline injection methods are seen if Gt is plotted instead of initial G (data taken from block 6).

It should be noted that the initial G of the CST is between the extremes of G tested for pipeline injection methods (Figure 3-8); therefore, the initial G of the CST does not explain its poor performance even at the extremely high Gt of 370 000. In addition to the low initial G, the 4 inch pipe also had intermittent instead of continuous alum injection. As illustrated in Figure 2-11, the majority of the raw water will not contact the alum during precipitation, therefore Figure 3-8 also supports the conclusion in Section 3.7, since the lack of contact with colloids during precipitation appears to have no negative effect.

3.9 How Total Gt Affects Turbidity Removal

Effect on Sample Scatter

The sample scatter decreases as the Gt increases beyond 10^5, as shown in Figure 3-9.

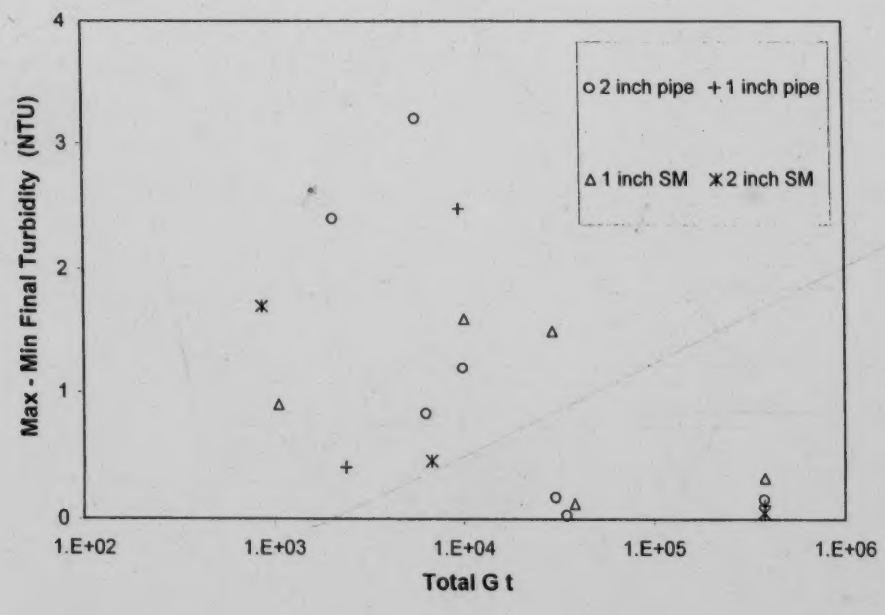

Figure 3-9 Minimum final turbidity and sample scatter decrease as Gt increases for all pipeline injection methods.

The Effect of Pipe Diameter on Minumum Gt

A bigger pipe diameter is better for injection methods tested with and without a static mixer, as illustrated in Figure 3-10.

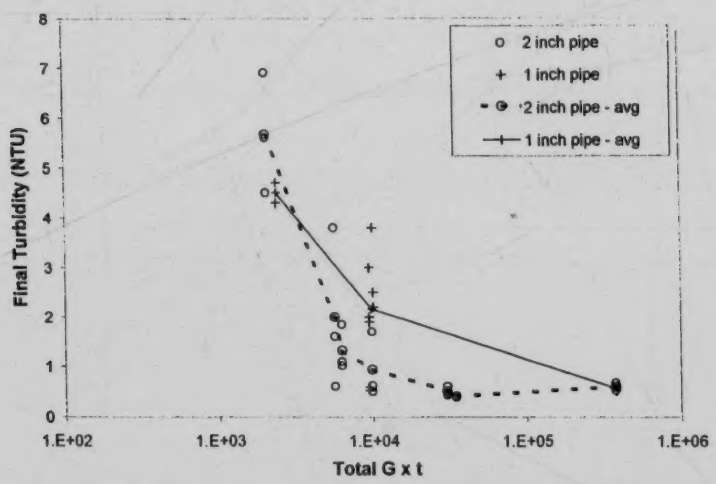

a)

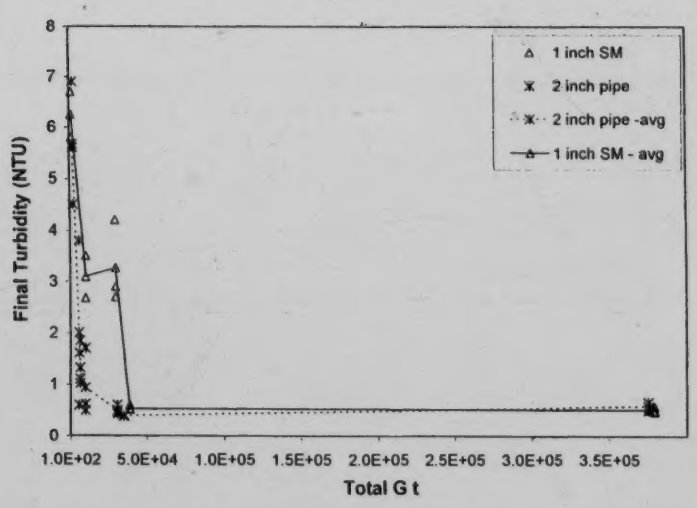

b)

Figure 3-10 Effect of pipe diameter on final turbidity a) without static mixers b) with static mixers (Gt= total Gt from initial and additional alum mixing)

The Effect of Alum Dosage on Minimum Gt

The minimum Gt required for optimal turbidity removal increases as the alum dosage decreases. This is shown in the test results for blocks 7 and 8 illustrated in Figure 3-11, where the minimum Gt increased as the alum dosage was decreased from 20 to 7mg/L. At 20 mg/L (Figure 3-11a) the minimum Gt for all types of pipeline injection tested, including static mixers, appears to be the same. As the alum dosage drops to 15 and 7 mg/L (Figure 3-11 b) the minimum Gt increases and the differences emerge between types of mixing. The 2 inch pipe at 15 mg/L shows similar behaviour to the 20 mg/L tests: as the alum dosage is dropped to 7 mg/L the minimum Gt increases to 10 000. The 1 inch static mixer, with a much higher initial G follows similar trends to the 2 inch pipe, but requires a higher total Gt in all cases for the same turbidity removal. This suggests that the 1 inch static mixer produces a larger quantity of smaller precipitate than the 2 inch pipe. The better performance of the 2 inch pipe over the 1 inch static mixer is also seen in block 6, shown in Figure 3-12 for a higher alum dosage.

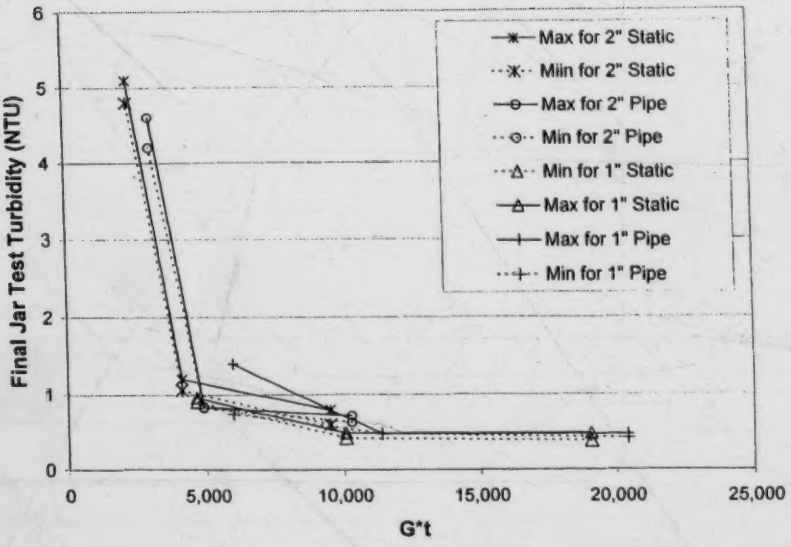

a)

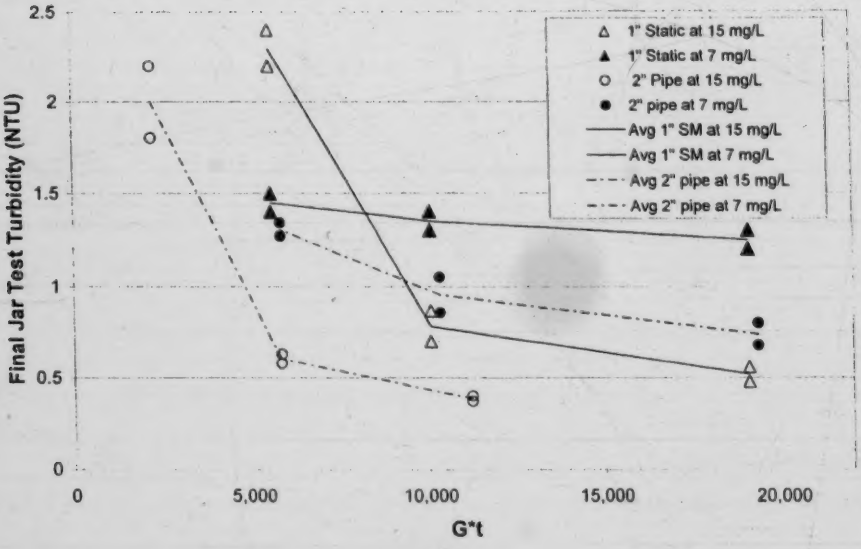
Final Jar Test Turbidity (NTU)
G*t
1" Static at 15 mg/L
1" Static at 7 mg/L
2" Pipe at 15 mg/L
2" pipe at 7 mg/L
Avg 1" SM at 15 mg/L
Avg 1" SM at 7 mg/L
Avg 2" pipe at 15 mg/L
Avg 2" pipe at 7 mg/L

b)

Figure 3-11 Effect of alum dosage on the minimum Gt in pipeline injection. a) Alum dosage =20 mg/L, data taken from block 7 b) Alum dosage = 7-15 mg/L, data taken from block 8. Test procedures in Section 2.5.3.

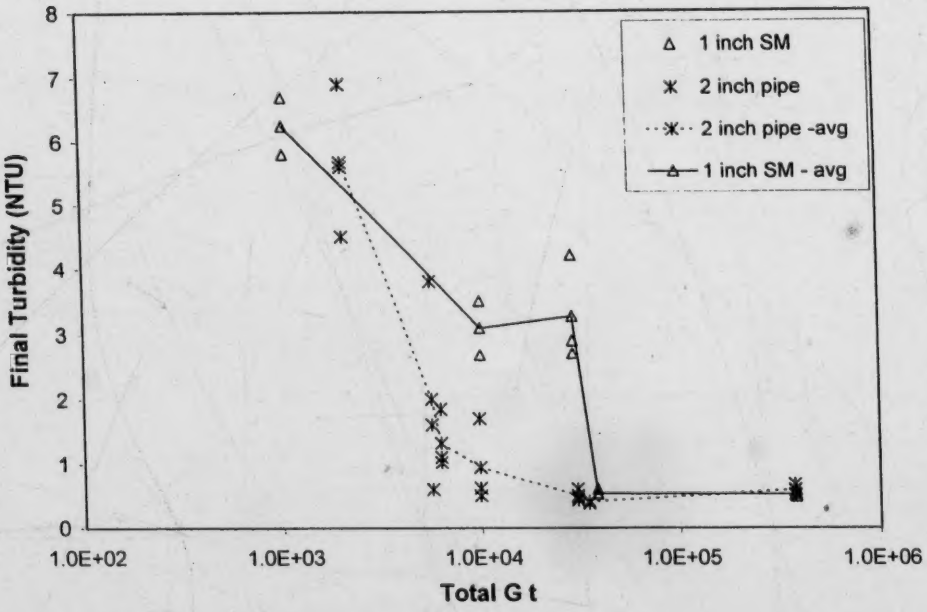

Figure 3-12 Effect of a 2 inch Pipe and 1 inch static mixer on minimum Gt. (Alum dosage = 30-50 mg/L data from block 6)

3.10 Dispersion

At lower alum dosages the 2 inch pipe outperformed the1 inch static mixer (Figure 3-11 and Figure 3-12) and pipeline injection methods always result in a much lower final turbidity than a CST (Figure 3-6). The rate and extent of dilution of the injected alum may account for both observations, thus dispersion for each injection method may trend the degree of supersaturation and thus the quantity of smaller precipitate formed.

In addition to trending precipitate formation, dilution may also quantify the negative effects of too much water dispersion into the liquid alum plume. An increase in dilution will increase the amount of water from which the aluminum

may take a hydroxide ion. Increasing the dilution will increase the hydroxide ion availability and the local pH during precipitation, both of which favor the formation of the smaller precipitate (Section 1.3 and 1.4.3).

Dispersion is an informative calculation, but it fails to quantify the degree of supersaturation of each injection method. If the exact time of precipitation and local aluminum concentrations were measured for each injection method, a better relationship between supersaturation and precipitate formation could be established. Since the time of precipitation was not measured in this work, it was assumed that precipitation occurred at one second for all injection methods. This is a reasonable assumption, since it has been reported that aluminum precipitation occurs in 1-7 seconds (Section 1.4.2). The degree of supersaturation will affect the rate of precipitation; therefore, the time of precipitation will vary between injection methods, but for an initial hypothesis test, the error will be assumed negligible. The equations for blend time are in Section 1.7.2 and the equation for the fraction of the jar or tank containing alum for a period of time shorter than the blend time, is described below.

3.10.1 CST

Dispersion in a CST is fast and large, as discussed in Section 1.7.1 and 1.7.2.3. For an ideal CST the injected alum would be instantaneously mixed throughout the tank, but the tank used was not ideal, so a blend time had to be calculated and a relationship for the fraction of the tank containing alum had to be established. For a period of time shorter than the blend time, the percentage of the vessel containing injected liquid alum was calculated assuming that dispersion in the vessel followed the exponential relationship in Equation 1.50. The results are plotted in Figure 3-13.

$$x_b = 1 - e^{\frac{-3t}{\theta}} \qquad (1.50)$$

Where:

θ = blend time (s)

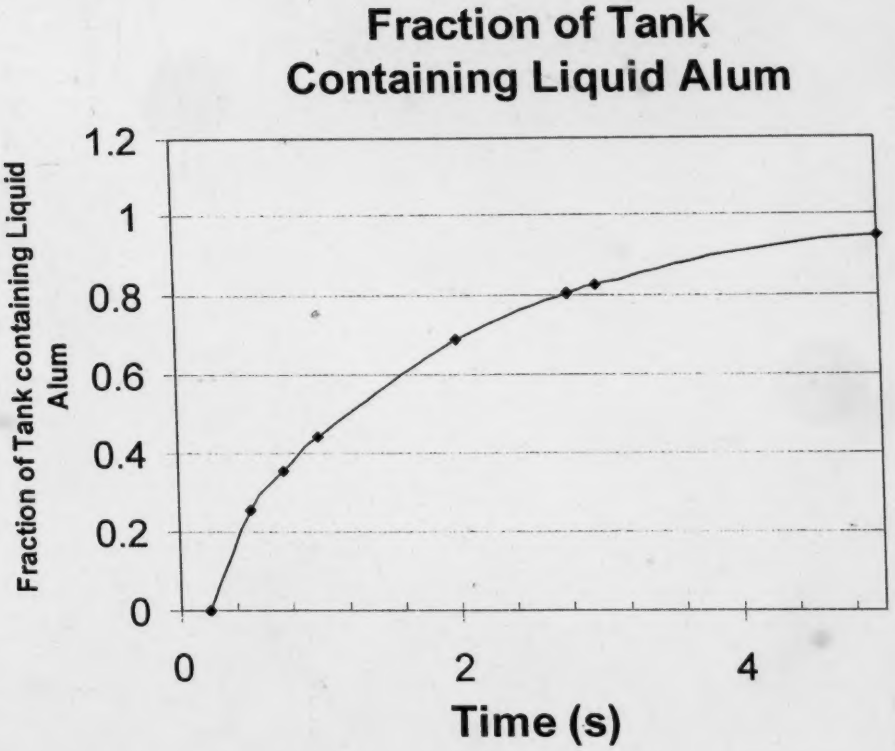

Figure 3-13 Fraction of vessel containing alum for the period of time shorter than the blend time for the CST. Blend time, θ = 5s, at an impeller speed of 200 RPM. CST was operated at 200 RPM during the pilot plant experiments.

3.10.2 Jar

Just like the CST, if the mixing in the jar were ideal, the injected alum would be instantaneously mixed throughout the jar. The jars used in this work were not ideal, so the blend time had to be calculated and the change in the fraction of the jar containing injected alum had to be estimated. For the period of time the jar is not fully mixed, the dispersion of the injected fluid can be estimated from an assumed fraction of the jar containing the injected fluid. The increase of the fraction of the jar containing injected fluid (x_b) with time was estimated with a linear relationship assuming the vessel was 95% blended after one blend time,

as shown in Figure 3-14. The blend time was calculated with the Grenville correlations as discussed in Section 1.7.2.3.

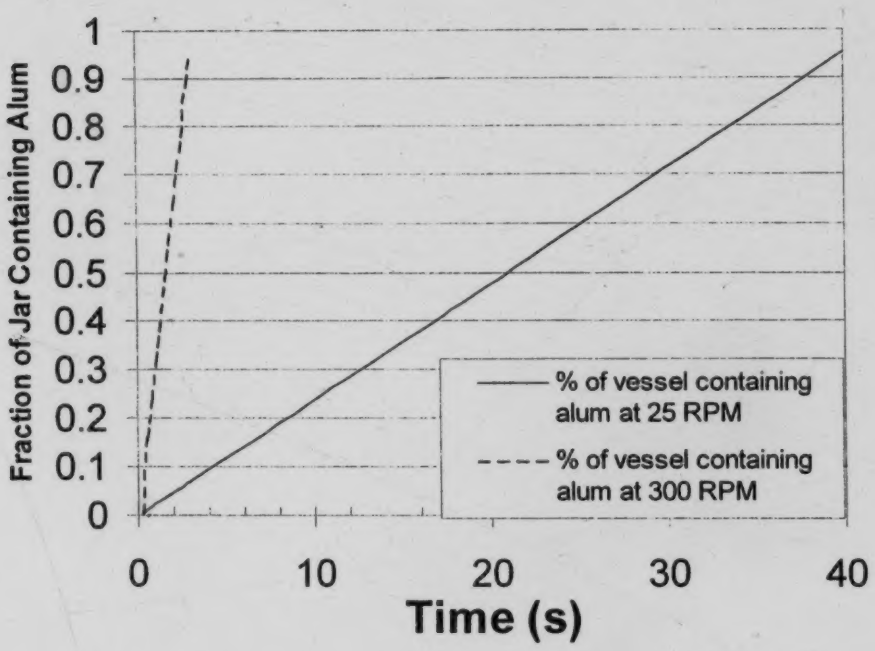

Figure 3-14 Fraction of vessel containing alum for the period of time shorter than the blend time for the jar. The blend time was 40 seconds at 25 RPM and 1 second at 300 RPM.

3.10.3 Pipe and Static Mixer

The concentration in the alum plume with time can be calculated using the equations given in Section 1.7.2. The concentrations of reactants in the pipe, CST or jar one second after alum injection are tabulated in Tables 3-2 and 3-3 and plotted in Figure 3-15. The results show that the reactant concentration in the CST is much higher than for all pipe line injection methods (empty pipe and static mixers). Figure 3-15 shows that as the reactant concentration (liquid alum) 1 second after injection falls below 25 mg/L, poorer turbidity removal results.

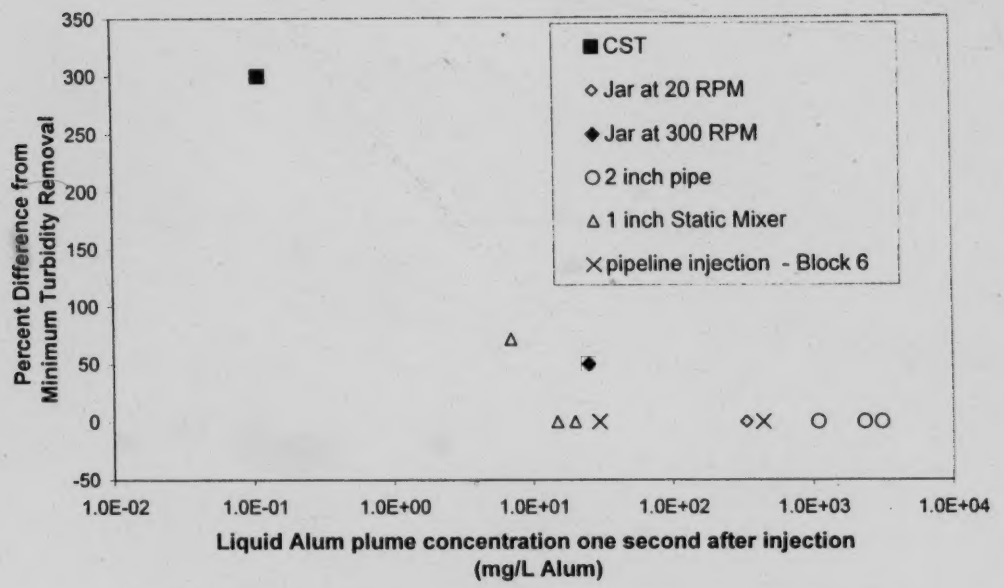

Figure 3-15 Alum plume concentration one second after alum injection. Higher liquid alum concentration upon precipitation results in better turbidity removal, data taken from block 7 and 8 with alum dosages for Jar = 8mg/L, for pipeline injection=7-30 mg/L and for CST=20 mg/L, all Gt>20,000.

Table 3-2 Dispersion calculation results for pipe line injection

	1 Second after Alum Injection		
	Distance traveled (pipe D)	*Cross sectional area ratio (plume/pipe)*	*Plume Liquid Alum Concentration (mg/L of Alum)*
Block 6			
2 inch pipe - 30 mg/L	13	0.06	440
2 inch SM - 30 mg/L	13	1	30
1 inch pipe - 30 mg/L	80	1	30
1 inch SM - 30 mg/L	80	1	30
Block 7 and 8			
2 inch pipe - 7mg/L	4	0.006	1093
2 inch pipe -15mg/L	4	0.1	2343
2 inch pipe - 20 mg/L	4	0.1	4687
1 inch SM - 7 mg/L	80	1	7
1 inch SM - 15 mg/L	80	1	15
1 inch SM - 20 mg/L	80	1	20

Table 3-3 Dispersion calculation results for the CST and Jar

	1 Second after Alum Injection	
	% of vessel with alum	*Liquid Alum Concentration (mg/L of Alum)*
CST - 20 mg/L	44	0.1
Jar at 25 RPM- 8 mg/L	2	336
Jar at 300 RPM- 8 mg/L	31	25

3.10.4 *Effect of Gt on Final Aluminum Concentration*

The higher final turbidity of the CST is attributed to smaller aluminum hydroxide precipitates remaining suspended in solution (Figure 3-2). Evidence of smaller aluminum hydroxide precipitate formation with alum injection into a 1 inch static mixer is shown in Figure 3-16. At an alum dosage of 15 mg/L, the final aluminum concentration for a 1 inch static mixer was higher than the 2 inch pipe. The final aluminum concentrations in Figure 3-16 follow the same trends as the plot of turbidity removal in Figure 3-11 b.

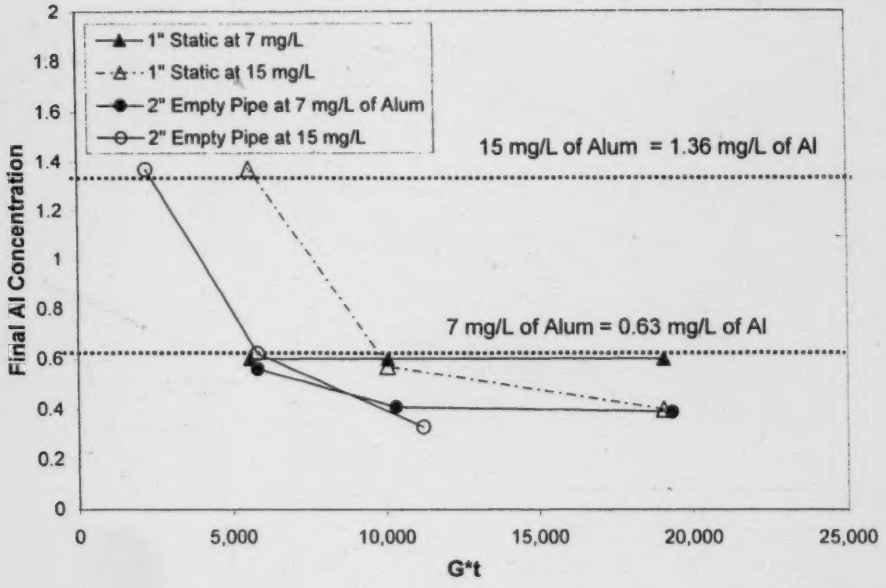

Figure 3-16 The effect of Gt on final aluminum concentrations at low alum dosages (Alum dosage = 7 & 15 mg/L, data taken from block 8)

The aluminum concentration results at 7 mg/L require further explanation. At 7 mg/L the aluminum is fully soluble for the 1 inch static mixer but for not the 2 inch pipe, so for this case, the dissolved aluminum hydroxide takes up a significant fraction of the final aluminum concentration. The results for the static

mixer in Figure 3-16 show that all aluminum injected remained in the supernatant at 7 mg/L, but the lack of an increase in turbidity in Figure 3-11 b reveals that no precipitates formed. This result may possibly be explained by changes in solubility due to the local concentrations of water and thus hydroxide ion availability during the hydrolysis reactions of aluminum. The results documented by Fursenko (1975) in Figure 1-4 and previously discussed in Section 1.3.1 identify the possibility that a change in solubility may arise from a competition for hydroxide ions. If this hypothesis is correct, it would help explain the apparent difference in aluminum hydroxide solubility that occurred between the two different mixing methods that are plotted in Figure 3-16. The difference in radial mixing between the static mixer and empty pipe show that water is dispersed water concentration during the time of hydrolysis of aluminum would be greater for the 1 inch static mixer, thus more hydroxide ions would be available during precipitation.

3.11 Comparison to Plant

At the E.L Smith water treatment plant alum is injected at the impeller of the low lift pump. The low lift pump consists of a long vertical pipe submersed in a large sump with the pump impeller located just above the bottom of the pipe. The alum injection point is only inches from the bottom of the pipe, so it is possible that a of the injected alum was dispersed in the sump, before it traveled up the pipe to the plant. If back mixing in the sump occurred, the liquid alum would have been rapidly diluted, thus poorer turbidity removal results should be expected. If a majority of the alum travels directly up the pump pipe, turbidity removal should be better than a CST. The plant experiments in blocks 7 and 8 are compared to the pipeline injection results at a Gt of $20x10^3 \pm 3x10^3$ in Figure 3-17. The pipeline injection methods outperformed the plant conditions; however, the plant achieved better turbidity removal than the CST, which consistently had final turbidities greater than 1.5 NTU (Figure 3-6). The plant's low lift pump mixing conditions and turbidity removal performance are a combination of pipeline and CST conditions. It may be the presence of back

mixing at the pump suction, rather than the initial G created by the pump's impeller that explains the performance of the plant's alum injection method. The G in the plant pipe is 900 s^{-1}, well above the initial G of 5 s^{-1} of the 4 inch pipe, but the 4 inch pipe had no back mixing, while back mixing is very likely in the sump of the low lift pump.

The total Gt achieved in the plant was calculated using the pressure drop in the pipes from the point of alum injection to the sample point, which was located just before the clarifier. Neglecting the energy initially dissipated as heat, the total Gt for alum mixing in the plant is 22 000. This is well above the minimum Gt requirement of 10 000 observed for pipeline injection in the pilot plant, as illustrated in Figure 3-11. At a Gt of 20 000±3 000 the pipeline injection method and the jar tests consistently give better turbidity removal than the plant, as illustrated in Figure 3-17.

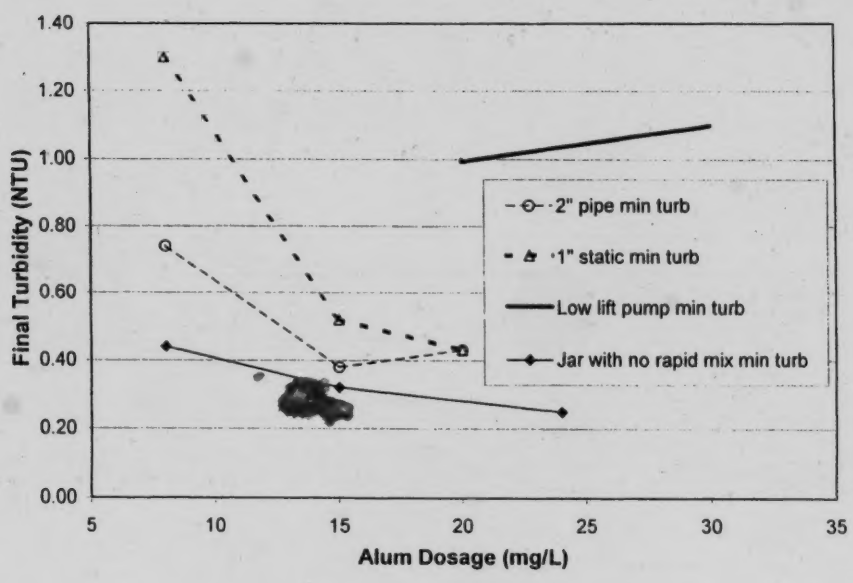

Figure 3-17 Comparision of Plant results to pipeline injection and jar tests (G x t =$20x10^3 \pm 5x10^3$, data from blocks 7 and 8)

3.12 Conclusions

It was found that turbidity could be used to detect small aluminum hydroxide precipitate that remained suspended in the supernatant of the jar tests. This measurement was used to explain the experimental results, which differ from what was initially expected.

The mechanism of coagulation with alum for Edmonton's winter water was determined to be sweep by the lack of positive effects of rapid mixing in the jar tests illustrated in Figure 2-4. This conclusion was confirmed by the fact that both the inline mechanical mixer and the intermittent alum injection had no detrimental effects on turbidity removal.

Evidence of smaller precipitate formation was observed in mixing conditions with fast dispersion: the CST and the 1 inch static mixer. As explained in Section 1.3.2, mixing conditions that cause the water to disperse quickly into the liquid alum produce local regions of high supersaturation and thus smaller precipitate formation. Of all the mixing methods tested, the CST had the largest extent and rate of dispersion and the results indicate that it formed a very fine aluminum hydroxide precipitate (Figure 3-2 and Figure 3-6). The combination of extremely high Gt and poor turbidity removal suggest that the precipitate was so small that the dominant collision mechanism was Brownian motion rather than fluid shear. The negative effects of dispersion by a static mixer only became evident at lower alum dosages. The results indicated that the fast radial mixing of a 1 inch static mixer formed more small aluminum hydroxide precipitates at 15 mg/L than the 2 inch pipe (Figure 3-11), thus explaining the higher minimum Gt requirement for the 1 inch static mixer.

The literature review revealed that an optimum Gt for turbidity removal rather than minimum Gt should be observed (Section 1.8), but all of the experiments for this thesis showed no detrimental effect of the high Gt in the stirred tank or a high Gt from additional mixing in the jar. One big difference between this work and literature data was the use of polymer. No tests were

done without the polymer, so the definite cause of an observed minimum rather than an optimum Gt cannot be given at this time.

It has been shown that some mixing conditions produce evidence of more small precipitate formation than others. Some of the results, such as those in Figure 3-16, indicate that the mixing method may also affect the aluminum solubility. At low alum dosages, the fast radial mixing of the 1 inch static mixer resulted in a higher aluminum solubility and prevented precipitation at 7 mg/L of alum (Figure 3-16).

The apparent formation of the smaller precipitate by the CST and 1 inch static mixer was detrimental to turbidity removal, which may be explained by the slower collision rates, thus agglomerate formation, of its dominating collision mechanism, Brownian motion. Only if the initial precipitates are larger than 1 micron will aluminum hydroxide agglomerates form mainly due to collisions created by fluid shear. Therefore, the degree of supersaturation must be minimized throughout precipitation to ensure the formation of precipitate larger than 1 micron and thus a lower Gt requirement. As the number of smaller precipitates increases, the minimum Gt required also increases as the fraction of small precipitate becomes larger. This severe consequence was observed by the poor performance of the CST, even at an extremely large Gt.

In addition to the negative effects of dispersion on precipitate size, there is some evidence that it may also affect aluminum solubility. The alkalizing reagent influences the solubility of aluminum hydroxide and thus the degree of supersaturation and the pH range of precipitate formation (Figure 1-4 and Section 1.3).

Implications

- Initial mixing conditions should be designed to optimize the formation of larger aluminum hydroxide precipitates by controlling the rate of precipitation of aluminum hydroxide from alum. The mixing conditions should control the rate of change of pH. The pH may be controlled by the quantity and rate of water mixed with liquid alum or possibly by acid additives. The initial mixing

conditions must provide adequate mixing of alum and water to reach a solution pH where precipitation can occur, while preventing a fast rate of precipitation and the formation of the detrimental smaller precipitates.

- The rate of precipitation may be reduced with a reduction in back mixing, or the rate of dispersion or dilution. This can be achieved in the plant by moving the alum injection point away from potential locations of back mixing, such as the large open sump, and into a properly sized pipe or static mixer. The pipe diameter should be large enough to ensure a high liquid alum concentration at the time of precipitation, yet small enough to ensure turbulent flow.
- The rapid mix stage in water treatment may be improved if proceeded by a short slower mix period designed to produce larger aluminum hydroxide precipitates. Larger precipitate will reduce required flocculation and retention times.
- The rate of change of pH and its effects on supersaturation during alum injection into a CST should be investigated if considering adding liquid alum to a CST. Injection of liquid alum into a CST with Edmonton's NSR water in the winter should be avoided. Properly sized pipeline injection with or without a static mixer results in more efficient turbidity removal.
- Without further data, alum injection into a CST without an additional acidifying reagent should be avoided. Properly sized pipeline injection is recommended.

Recommendations for Future research

- Tests with static mixers on high turbidity water should be done. This work only evaluated static mixers with low turbidity waters. At higher raw water turbidity, it may be more important to evenly disperse the alum throughout the natural particles. This may be achieved with a static mixer. Since the static mixer in this work performed much better than the CST and their performance is essentially identical to an empty pipe at higher alum dosages, it warrants more research.

- The effects of initial mixing conditions on the rate of precipitation, aluminum solubility and precipitation formation should be studied further.
- A more detailed study of the relationship between precipitate size and local alum concentrations at the time of precipitation should be done to establish the fine line between the formation of larger 1 micron precipitates and the detrimental smaller 0.01 micron precipitates.
- The effects of polymer mixing time should be further evaluated.
- The effects of rate of water dispersion in the alum plume on aluminum solubility should be studied further, since Figure 1-5 suggests that the availability of the hydroxide ion during precipitation affects the solubility of aluminum.

3.13 References

Amirtharajah, A. & Tambo, N., 1991, *Mixing in Water Treatment*, Ch 1 in Mixing in Coagulation and Flocculation, American Water Works Association Research Foundation, American Water Works Association.

Appendix A

Experimental Data

Table A-1 Block one data

Alum Dosage (mg/L)	*Test ID*	*Test Date*	*Daily Avg Raw Water Turbidity (NTU)*	*Final Turbidity (NTU)*	*Avg Final Turbidity (NTU)*
4 inch Pipe - Inline Mechanical Mixer OFF					
22	Test 3	6-Nov	3.1	0.7	0.81
				0.8	
				0.95	
				0.65	
				0.75	
				0.98	
35	Test 2	6-Nov	3.1	0.5	0.48
				0.58	
				0.49	
				0.44	
				0.45	
				0.43	
4 inch Pipe - Inline mechanical mixier ON at 1800 RPM					
22	Test 4	6-Nov	3.1	0.86	0.78
				0.78	
				0.74	
				0.65	
				0.86	
				0.8	
35	Test 1	6-Nov	3.1	0.45	0.46
				0.68	
				0.48	
				0.3	
				0.34	
				0.53	

Table A-2 Block two data

Alum Dosage (mg/L)	*Test ID*	*Test Date*	*Daily Avg Raw Water Turbidity (NTU)*	*Final Turbidity (NTU)*	*Avg Final Turbidity (NTU)*
4 inch Pipe					
22	Test 10	18-Nov	4.4	0.58	0.58
				0.54	
				0.59	
				0.62	
35	Test 11	18-Nov	4.4	0.41	0.49
				0.52	
				0.51	
				0.53	
Plant					
30	Test 12	18-Nov	4.4	1.25	0.95
				1.15	
				0.53	
				0.85	

Table A-3 Block three data

Alum Dosage (mg/L)	*Test ID*	*Test Date*	*Daily Avg Raw Water Turbidity (NTU)*	*Final Turbidity (NTU)*	*Avg Final Turbidity (NTU)*
4 inch Pipe					
36	Test 16	29-Nov	4.2	0.66	0.62
				0.58	
				0.62	
37	Test 14	25-Nov	3.4	0.57	0.58
				0.52	
				0.61	
				0.6	
CST					
36	Test 13	25-Nov	3.4	0.9	0.93
				0.8	
				1.1	
Plant					
30	Test 13	25-Nov	3.4	0.77	0.76
				0.7	
				0.8	

Table A-4a Block four data – pipeline injection

Alum Dosage (mg/L)	*Test ID*	*Test Date*	*Daily Avg Raw Water Turbidity (NTU)*	*Final Turbidity (NTU)*	*Avg Final Turbidity (NTU)*
4 inch Pipe					
19	Test 23	4-Dec	2.7	1.1	1.18
				1.2	
				1.2	
				1.3	
				1.1	
				1.2	
19	Test 24	4-Dec	2.7	0.94	1.03
				1.1	
				0.92	
				0.8	
				1.2	
				1.2	
22	Test 6	15-Nov	3.3	0.76	0.69
				0.77	
22	Test 7	15-Nov	3.3	0.58	0.62
				0.65	
35	Test 5	15-Nov	3.3	0.38	0.46
				0.45	
				0.51	
				0.48	
45	Test 8	15-Nov	3.3	0.36	0.40
				0.43	

Table A-4b Block four data - CST

Alum Dosage (mg/L)	*Test ID*	*Test Date*	*Daily Avg Raw Water Turbidity (NTU)*	*Final Turbidity (NTU)*	*Avg Final Turbidity (NTU)*
CST					
18	Test 9	15-Nov	3.3	1.46	1.38
				1.3	
23	Test 27	4-Dec	2.7	1.87	1.72
				1.7	
				1.6	
33	Test 26	4-Dec	2.7	2	2.20
				2.7	
				1.9	

Table A-5 Block five data

Alum Dosage (mg/L)	Test ID	Test Date	Daily Avg Raw Water Turbidity (NTU)	Final Turbidity (NTU)	Avg Final Turbidity (NTU)
4 inch Pipe					
18	Test 28	6-Dec	4	0.68	0.72
				0.76	
				0.73	
18	Test 29	6-Dec	4	0.8	0.71
				0.71	
				0.63	
18	Test 31	6-Dec	4	0.83	0.8
				0.81	
				0.76	
18	Test 34	9-Dec	4	0.9	0.88
				0.91	
				0.82	
41	Test 42	10-Dec	3	0.57	0.61
				0.67	
				0.58	
41	Test 46	10-Dec	3	0.65	0.65
				0.68	
				0.62	
CST					
23	Test 27	4-Dec	3	1.87	1.72
				1.7	
				1.6	
33	Test 26	4-Dec	3	2	2.2
				2.7	
				1.9	
2 inch Pipe					
42	Test 46	11-Dec	3.2	0.57	0.73
				0.88	
				0.73	
45	Test 35	9-Dec	3.9	0.46	0.54
				0.56	
				0.6	

Table A-6: Block Six Data

Alum Dosage (mg/L)		Test Identification			Test Conditions				Additional Mix		"G x t"	Jar Supernatant Results		
Calculated	Measured	Test #	Test Date	Sample Point	Daily Avg Raw Turb (NTU)	Alum Flowrate (mL/min)	Water Flowrate (m3/hr)	Initial G (s^{-1})	RPM	Time (min)	Total	Turbidity (NTU)	Avg Turb (NTU)	Al (mg/L)
4 inch pipe														
45	47	55	13-Dec	3	2.4	1.8	1.5	5			373,200	0.63	0.61	0.5
												0.59		
												0.60		
Plant														
29	29	56	13-Dec	plant	2.4		183 MLD	910			22,800	1.09	1.00	0.7
												0.91		
												1.01		
29	32	61	16-Dec	plant	2.3		183 MLD	910			22,800	1.10	1.70	1.1
												2.40		
												1.60		
CST														
31	33	59	16-Dec	3	2.3	1.1	1.5	4,990			369,000	2.50	2.53	1.2
												2.70		
												2.40		
36	--	63	16-Dec	3	2.3	1.4	1.5	4,990			369,000	3.20	3.11	--
												2.80		
												3.32		
39	40	64	16-Dec	3	2.3	1.5	1.5	4,990			369,000	2.00	1.92	--
												1.86		
												1.90		
39	42	67	17-Dec	3	2.4	1.5	1.5	4,990			369,000	1.77	1.74	0.8
												1.70		
												1.75		
2 inch Static Mixer														
45	42	66	17-Dec	1	2.4	5.0	4.3	1,480			870	2.30	3.23	--
												3.40		
												4.00		
45	42	66	17-Dec	2	2.4	5.0	4.3	1,480			6,760	1.10	1.22	--
												1.05		
												1.50		
45	45	67	17-Dec	3	2.4	5.0	4.3	1,480			375,760	0.60	0.63	0.4
												0.65		

Alum Dosage (mg/L)		Test Identification			Test Conditions				Additional Mix		"G x t"	Jar Supernatant Results		
Calculated	Measured	Test #	Test Date	Sample Point	Daily Avg Raw Turb (NTU)	Alum Flowrate (mL/min)	Water Flowrate (m3/hr)	Initial G (s^{-1})	RPM	Time (min)	Total	Turbidity (NTU)	Avg Turb (NTU)	Al (mg/L)
1 inch Static Mixer - continued														
49	48	59	16-Dec	3	2.3	5.0	3.9	11,700			379,100	0.52 0.53 0.47	0.51	0.5
45	--	64	17-Dec	3	2.4	4.5	3.9	11,700			379,100	0.84 0.52 0.59	0.65	--
45	46	65	17-Dec	1	2.4	4.5	3.9	11,700	120	5	29,560	4.20 2.70 2.90	3.27	4.7
45	45	65	17-Dec	2	2.4	4.5	3.9	11,700	120	5	38,600	0.52 0.60 0.48	0.53	--
45	44	70	17-Dec	2	2.4	4.5	3.9	11,700			10,100	2.50 2.20 3.60	2.83	--
45	44	70	17-Dec	3	2.4	4.5	3.9	11,700			379,100	0.60 0.55 0.51	0.55	0.4
1 inch Pipe														
45	44	68	17-Dec	1	2.4	4.5	3.9	2,000			2,400	4.30 4.70	4.50	--
45	44	68	17-Dec	1	2	5	4	2,000	0	0	9,500	1.90 0.58	1.24	
45	44	68	17-Dec	3	2.4	4.5	3.9	2,000			378,500	0.50 0.52	0.51	--
45	44	69	18-Dec	2	2.3	4.5	3.9	2,000			9,500	0.52 2.00 3.00	1.84	--
45	44	69	18-Dec	3	2.3	4.5	3.9	2,000			378,500	0.61 0.50 0.51	0.54	0.4

Alum Dosage (mg/L)		Test Identification			Test Conditions				Additional Mix		"G x t"	Jar Supernatant Results		
Calculated	Measured	Test #	Test Date	Sample Point	Daily Avg Raw Turb (NTU)	Alum Flowrate (mL/min)	Water Flowrate (m3/hr)	Initial G (s^{-1})	RPM	Time (min)	Total	Turbidity (NTU)	Avg Turb (NTU)	Al (mg/L)
2 inch pipe														
36	58	54	13-Dec	1	2.4	20.0	4.8	270			2,060	4.50 5.60 6.90	5.67	4.4
36		54	13-Dec	2	2.4	20.0	4.8	270			6,300	1.10 1.85 1.02	1.32	1.0
36	43	53	13-Dec	1	2.4	20.0	4.8	270	120	5	30,560	0.47 0.60 0.43	0.50	0.5
36		53	13-Dec	2	2.4	20.0	4.8	270	120	5	34,800	0.41 0.41 0.38	0.40	0.3
36	31	57	13-Dec	1	2.4	20.0	4.8	270	20	5	5,660	0.60 1.61 3.80	2.00	--
36	30	57	13-Dec	2	2.4	20.0	4.8	270	20	5	9,900	0.62 1.70 0.50	0.94	0.5
36	30	55	13-Dec	3	2.4	20.0	4.8	270			375,300	0.58 0.67 0.52	0.59	0.5
36	28	56	13-Dec	3	2.4	20.0	4.8	270			375,300	0.52 0.52 0.53	0.52	--
1 inch Static Mixer														
71	72	60	16-Dec	1	2.3	8.8	3.9	11,700			1,060	6.30 6.80 6.40	6.50	4.0
71	72	60	16-Dec	3	2.3	8.8	3.9	11,700			10,100	2.50 3.80 3.00	3.10	0.6
61	61	62	16-Dec	1	2.3	7.5	3.9	11,700			1,060	6.70 5.80	6.25	--
61	61	62	16-Dec	2	2.3	7.5	3.9	11,700			10,100	3.50 2.68	3.09	--

Table A-7: Block seven and eight data (All samples, except for plant samples taken from sample point 1)

Alum Dosage (mg/L)		Test Identification			Test Conditions				IT Line G	Additional Mix		" G x t"	Jar Supernatant Results		
Calculated	Measured	Test #	Test Date	Daily Avg Raw Turb (NTU)	Injected Solution Composition (Wt % Alum)	Alum Flowrate (mL/min)	Water Flowrate (m^3/hr)	Initial G (s^{-1})	Gt in Pipe	RPM	Time (min)	Total	Turbidity (NTU)	Avg Turb (NTU)	Al (mg/L)
Plant															
20.0	21.6	112	11-Mar-03	1.1	48		185 MLD	900	22,800	25	10	31,800	0.64	0.515	0.3
									22,800	25	10	31,800	0.39		0.3
									22,800	25	5	27,300	0.8	0.725	0.48
									22,800	25	5	27,300	0.65		0.48
									22,800	25	0	22,800	1.05	1.015	0.73
									22,800	25	0	22,800	0.98		0.73
24.0	26.4	124	18-Mar-03	2.3	48		185 MLD	900	22,000	25	10	31,000	0.66	0.72	0.61
									22,000	25	10	31,000	0.78		
									22,000	25	4	25,600	1.07	1.025	0.84
									22,000	25	4	25,600	0.98		
									22,000	25	0	22,000	3.2	2.8	1.53
									22,000	25	0	22,000	2.4		
2 inch Static Mixer															
22.4	23.3	118	18-Mar-03	2.3	7	8	1.5	260	521	25	10	9,521	0.6	0.7	0.4
									521	25	10	9,521	0.8		
	22.7					8	1.5		521	25	4	4,121	1.06	1.1	0.73
									521	25	4	4,121	1.2		
	25.2					8	1.5		521	25	2	2,321	5.1	5.0	
									521	25	2	2,321	4.8		
2 inch Empty Pipe															
22.4	20.3	120	18-Mar-03	2.3	7	8	1.5	50	1,300	25	10	10,300	0.66	0.6	0.44
									1,300	25	10	10,300	0.59		
	20.0					8	1.5		1,300	25	4	4,900	2.9	2.2	0.91
									1,300	25	4	4,900	1.4		
									1,300	25	2	3,100	6.9	5.4	1.72
									1,300	25	2	3,100	3.8		
14.7	15.4	113	11-Mar-03	1.1	2.3	16	1.5	50	1,330	25	11	11,230	0.4	0.4	1.5
									1,330	25	11	11,230	0.37		1.5
									1,330	25	5	5,830	0.63	0.6	1.5
									1,330	25	5	5,830	0.58		1.5
									1,330	25	1	2,230	1.8	2.0	1.5
									1,330	25	1	2,230	2.2		1.5
7.4	6.3	114	11-Mar-03	1.1	2.3	8	1.5	50	1,330	25	20	19,330	0.68	0.7	1.5
									1,330	25	20	19,330	0.8		1.5
									1,330	25	10	10,330	0.86	1.0	1.5
									1,330	25	10	10,330	1.05		1.5
									1,330	25	5	5,830	1.34	1.3	1.5
									1,330	25	5	5,830	1.27		1.5

Alum Dosage (mg/L)		Test Identification		Test Conditions				IT Line G		Additional Mix		" G x t"	Jar Supernatant Results		
Calculated	Measured	Test #	Test Date	Daily Avg Raw Turb (NTU)	Injected Solution Composition (Wt % Alum)	Alum Flowrate (mL/min)	Water Flowrate (m^3/hr)	Initial G (s^{-1})	Gt in Pipe	RPM	Time (min)	Total	Turbidity (NTU)	Avg Turb (NTU)	Al (mg/L)
1 inch Static Mixer															
19.6	20.9	122	18-Mar-03	2.3	15.5	8	3.8	11,800	1,063	25	20	19,063	0.38	0.4	
		122					3.8		1,063	25	20	19,063	0.48		
		122					3.8		1,063	25	10	10,063	0.49	0.5	
		122					3.8		1,063	25	10	10,063	0.42		
		122					3.8		1,063	25	4	4,663	0.91	0.9	
		122					3.8		1,063	25	4	4,663	0.96		
16.4	16.7	116	13-Mar-03	1.1	13	8	3.8	11,800	1,063	25	20	19,063	0.56	0.5	3.9
		116					3.8		1,063	25	20	19,063	0.48		3.9
		116					3.8		1,063	25	10	10,063	0.87	0.8	3.9
		116					3.8		1,063	25	10	10,063	0.7		3.9
		116					3.8		1,063	25	5	5,563	2.2	2.3	3.9
		116					3.8		1,063	25	5	5,563	2.4		3.9
6.9	6.7	117	13-Mar-03	1.1	5.5	8	3.8	11,800	1,063	25	20	19,063	1.3	1.3	3.9
		117					3.8		1,063	25	20	19,063	1.2		3.9
		117					3.8		1,063	25	10	10,063	1.3	1.4	3.9
		117					3.8		1,063	25	10	10,063	1.4		3.9
		117					3.8		1,063	25	5	5,563	1.5	1.5	3.9
		117					3.8		1,063	25	5	5,563	1.4		3.9
1 inch Empty Pipe															
19.6	20.5	121	18-Mar-03	2.3	15.5	8	3.8	2,000	2,400	25	20	20,400	0.47	0.4	0.3
		121					3.8		2,400	25	20	20,400	0.42		
	20.3	121					3.8		2,400	25	10	11,400	0.48	0.5	0.45
		121					3.8		2,400	25	10	11,400	0.48		
	20.0	121					3.8		2,400	25	4	6,000	1.4	1.1	0.69
		121					3.8		2,400	25	4	6,000	0.75		

Appendix B

Spectrometer Procedures for Aluminum

EPCOR
QUALITY ASSURANCE SECTION
WATER LAB

LAST REVISED: Apr. 04, 2003
AUTHOR: N. Best
DATE : May 26, 1997
APPROVED

03.91 METHOD: OPERATION OF LEEMAN LABS PS1000 ICP

SCOPE

This operating procedure will give information on the operation of the Leeman Labs PS 1000 ICP with the ultrasonic nebulizer.

This procedure is for analysts who are familiar with ICP instrumentation technology and who have had training on this instrument.

PURPOSE

The purpose of the procedure is to establish condensed but precise instructions in the operation of the instrument as it is set up in the Water Laboratory.

Additional information, if needed must be obtained from the instrument operations manual.

SAMPLE COLLECTION AND STORAGE

Samples must be collected in clean polypropylene containers. Cleaning of polypropylene containers and all glassware is described in SOP 01.02. After collection samples should be inhibited with a high purity HNO_3 acid at an equivalent of 5 mL/L. Maximum storage length is 6 months for samples containing concentration in mg/L values.

Sample preparation for those samples requiring digestion can be found in SOP 02.11.

REAGENTS

Concentrated nitric and hydrochloric acids.
Metals standards (1000 mg/L) - SCP Science.
Distilled deionized water.
Sodium borohydride.
Potassium iodide.
Argon, prepurified, 99.998%

PROCEDURE

Turn on monitor, printer and computer.
Press Cancel when log on window appears.
Open the WinICP icon.
When the WinICP Runner page comes up choose a protocol from the pull down menu.

Results are stored in datasets. To open an existing dataset use the pull down menu. To open a new dataset use File...New Dataset. Name the new dataset using no more than 8 characters.

Press the DB↓ to open the WinICP Database. Once the database is open press the RN↓ button to load information to the database. Press the RN↑ button to load database information to the WinICP Runner.

The WinICP Runner consists of 9 tabbed pages.
On the MAIN page, enter user name from the pull down menu. Also, make sure real-time printing is on.

Turn on argon, cooling water and ensure exhaust fan is working.
Start the ICP by pressing Cold Autostart on the CONTROL page of the WinICP Runner.
When the ICP has ignited successfully go to the SAMPLE page and using the Move Tip portion of the page place the sample tip in rinse water. Allow instrument to warm up for 1 hour.

On the SAMPLE page turn on elements required for the current run.

On the STANDARDS page, turn on which standards are to be run by turning on the radio buttons. Also, turn on radio buttons for how many replicates are to be run (NOTE: if 3 replicates are to be run turn on radio button for Rep 1, Rep 2 and Rep 3). Turn on which check standards are to be run. Press APPLY.
Once this is done press DB↓ to move to database then RN↓.

The database consists of 12 tabbed pages.
On the PROTOCOL page, choose the Report Spec called Main from the pull down menu.
Also on this page enter the frequency of Peak Optics. When this is done press APPLY (lower right corner) or no changes will be made. Press RN↑ to return to the WinICP Runner.

To enter a sample list, open the rack editor by pressing the Rack Editor button on the MAIN page of the WinICP Runner or on the toolbar at the top of the page.
When the Rack Editor opens choose File...New. Make sure 44 cups per rack is selected then press OK.
Enter sample names in column 1. Add an extended ID, if desired, in column 2. Column 5 is where you enter the frequency of check standards (ie. If you want to run check standard 3 every 12 samples you enter C3 in column 5 of lines 12, 24, 36 etc.). Save the rack editor file using a name no longer than 7 characters.

To peak optics go to the SCAN page of WinICP Runner. Leave the tip in the rinse press the Peak Optics button. Choose FULL peak optics.

To position the plasma go to the SCAN page of WinICP Runner. Move the tip to the cup containing the peak solution and press Position Plasma. A Position Plasma window will open. Press Run Manual. Watch the scans on the Monitor window to see if they are OK. If so, press the Accept button. If not, press the Accept button anyway and then Run Manual again. When the scans are acceptable close the Position Plasma window.

When ready to calibrate go to the STANDARD page of WinICP Runner and press Stnd Auto. (For As and Sb run Sb calibration and samples first. Go to Sample page and check off metals required.) This will run all standards previously selected. To view the intensities go to the REPORT page of WinICP Runner. When the calibration is finished press DB↓. When the WinICP Database opens press RN↓ then go to the CAL CURVE page and check all calibration lines and accept them. Press RN↑.

Now that the calibrations are done the samples can be run.
Go to the SAMPLE page on the Win ICP Runner. Open a rack editor file from the pull down menu, enter the start and end cups and press Run Auto. To view results go to the REPORT page on WinICP Runner.

When samples are complete and satisfactory rinse the ICP with DI water for at least 10 minutes. To extinguish the plasma use the Extinguish Now button on the CONTROL page of WinICP Runner or on the toolbar at the top of the page.

Real-time printing allows the report to print when a page is full. If the sample run is finished and the final page is not full enough to print out go to the MAIN page of WinICP Runner and press Form Feed.

To print out a post-run report, go to the REPORT page on the WinICP Database. Turn on all the results that you want printed and press Generate Report. The Generate Report window will open. Choose viewer if you just want to look at the results.

The data is stored in the software using a dataset name as described above. Data is also transferred to the lab notebook and is entered into LIMS following SOP 11.06.

There are 5 protocols that are used for the monthly metals. All protocols use the above procedure for running the ICP. Additional information is given below.

1. USNLOW

This is the protocol is used for low level analysis of Fe, Al, Ba, Zn, Cu, Cd, Cr and Mn. The procedure for sample and standard preparation is given on the protocol sheet at the end of the METHOD. This protocol uses the ultrasonic nebulizer and the organics torch. The autosampler on the ICP is used to pump sample. The ultrasonic nebulizer should be turned on about 10 minutes before the plasma is ignited to allow the temperatures to stabilize. At the end of the day the ultrasonic nebulizer is rinsed as for the autosampler and allowed to run dry before extinguishing the plasma.

2. MAJION2

This is the protocol used for the analysis of low levels of Na and K. The procedure for sample and standard preparation is given on the protocol sheet at the end of the METHOD. This protocol uses the Hildebrand nebulizer and the aqueous torch.

3. CAMG

This is the protocol used for the analysis of Ca and Mg. The procedure for sample and standard preparation is given on the protocol sheet at the end of the method. This protocol used the Hildebrand nebulizer and the aqueous torch.

4. HYDGENER

This is the protocol used for the analysis of As, Sb and Se. The procedure for sample and standard preparation is given on the protocol sheet at the end of the METHOD. As and Sb are analyzed together and Se is analyzed alone. This protocol requires the use of the hydride generation tubing kit and the organics torch. Before positioning the plasma, the sodium borohydride solution must also be introduced. This is done using an extra pump tube on the hydride generation tubing kit. Introduce the borohydride solution only after the flow of acid has been well established or the plasma may be extinguished.

5. SILICON

This is the protocol used for the analysis of silicon. The procedure for sample and standard preparation is given on the protocol sheet at the end of the method. This protocol uses the Hildebrand nebulizer and the aqueous torch.

QUALITY ASSURANCE

Low and high standards as well as blanks, replicates, spikes and reference waters should be run routinely. The acceptance criteria are as follows:
Low standards recoveries should be +/- 20%.
High standards recoveries should be +/- 10 %.
Spikes recoveries should be +/- 20%.
Reference water should fall within limits stated on analysis certificate.
Blanks should be no more than 3 times the detection limit.
Calibration curves should have an RRF of 0.95 or greater.
Check standards should also be run and should be +/- 15%.

PRECISION AND ACCURACY

Precision

Ross Res

	Al	Ba	Fe	Zn	Mn	Cr
Average	0.03	0.054	<0.003	0.006	0.0008	<0.001
Std dev	0.01	0.008	0	0.002	0.0004	0
Range	0.02-0.05	0.037-0.069	<0.003	<0.0005-0.0009	<0.0005-0.0017	<0.001
n	12	12	12	12	12	12

	As	Sb	Se	K	Na	Ca
Average	<0.002	<0.003	<0.003	0.9	10.2	43.0
Std dev	0	0	0	0.3	3.6	4.0
Range	<0.002	<0.003	<0.003	0.7-1.6	6.2-17.3	37.3-51.3
n	12	12	12	12	12	12

Recovery

Ross Res Spike

	Al	Ba	Fe	Zn	Mn	Cr
Average % Recovery	106	101	106	102	108	97
Std dev	7	7	9	13	10	10
Range % Recovery	91-114	91-106	93-115	82-120	92-120	82-108
n	7	7	7	7	7	7

	As	Sb	Se	K	Na	Ca
Average % Recovery	94	90	97	101	98	102
Std dev	6	7	6	4	7	5
Range % Recovery	86-101	83-99	89-106	94-107	91-110	93-106
n	7	7	7	7	7	7

Accuracy

Certified Reference Materials

	TMDA-51.2 Al	TMDA-51.2 Ba	TMDA-51.2 Fe	TMDA-51.2 Zn	TMDA-51.2 Mn	TMDA-51.2 Cr
Ave	0.1013	0.0758	0.1158	0.1075	0.0841	0.0631
True Value	0.096	0.0733	0.111	0.106	0.082	0.0625
Std dev	0.0029	0.0046	0.0073	0.0063	0.0053	0.0045

Range	0.097-0.106	0.068-0.081	0.105-0.129	0.097-0.117	0.0749-0.0911	0.054-0.070
n	9	9	9	9	10	10
Ave % Recovery	106	103	104	101	103	101

	TMDA-51.2 As	TMDA-51.2 Sb	TMDA-51.2 Se	ION-20 K	ION-20 Na	ION-92 Ca
Ave	0.0137	0.0130	0.0121	1.30	13.99	43.15
True Value	0.0153	0.0125	0.012	1.21	13.5	42.8
Std dev	0.0008	0.0016	0.0020	0.0753	0.7769	2.1
Range	0.0128-0.015	0.010-0.014	0.099-0.0138	1.152-1.422	13-15.69	40.38-45.75
n	11	11	11	10	10	7
Ave % Recovery	90	104	101	107	104	101

WASTE DISPOSAL

Dispose of samples that are preserved with concentrated HNO_3 (0.5% v/v) into the neutralization tank through the drain with excess tap water.
Any waste solution that contains more than 100 mg/L of toxic metals (eg. 1000 mg/L lead standard) should be put into separate metal waste containers (located inside the fumehood in metal room) for special disposal.
All other waste disposal must be made in accordance with local, provincial and federal regulations.

REFERENCE

A. Method references

1. Standard Methods for the Examination of Water and Wastewater,1998.
2. Leeman Labs ICP Manual and ICP Training Course.

B. SOP references

1. Nitric wash SOP#01.02.
2. Sample Preservation SOP#02.11.
3. Mechanical Dishwasher SOP#01.06
4. Results entry LIMS SOP#11.06
5. Laboratory MSDS SOP#01.21

Revision #	Date Revised	By Who	Approved
1.0	Sept 5, 2000	NB	LG
2.0	Sept 23, 2002	NB	NB
2.1	Nov. 26, 2002	NB	LG
2.2	Apr. 04, 2003	NB	NB

Revision 1.0: Reference added, protocol updated.

Revision 2.0: Added Silicon procedure.

Revision 2.1: Added procedure for new software, referenced SOPs related to this method.
Revision 2.2: Added precision and accuracy.

Corrina Kennedy

From: Clayed CMS Editorial Office : D C Bain <clayed@macaulay.ac.uk>
To: <corrinakennedy@shaw.ca>
Cc: <cms@clays.org>; <mermut@skyway.usask.ca>
Sent: Tuesday, March 16, 2004 4:32 AM
Subject: Re: permission to reproduce a photo in my thesis

Dear Corrina

Permission is granted to reproduce these figures in your thesis, subject to the usual condition that full credit is given to the source.

Best wishes.

Derek Bain

Dr Derek C. Bain
Editor-in-Chief, Clays and Clay Minerals
The Macaulay Institute
Craigiebuckler
Aberdeen AB15 8QH
U.K.

Tel (direct line) +44 (0)1224 498242
Fax from US/Canada 1 240 757 7440
Fax (From Elsewhere) +44 (0) 1224 498207
email: clayed@macaulay.ac.uk

http://www.macaulay.ac.uk
Clay Minerals Society http://cms.lanl.gov

Clays and Clay Minerals online at http://cms.lanl.gov

>>> Corrina Kennedy <corrinakennedy@shaw.ca> 16/03/04 03:57:14 >>>
To the copyright department of Clays and Clay minerals,

I would like to reproduce the photos in your journal in my Masters thesis from the University of Alberta, Edmonton, Alberta Canada. I would like to use Figure 1, 4 and 5 from article "Amorphous aluminum hydroxide fromed at the earliest weathering stages of K-feldspar" Volume 44 no. 5 pges 672-676, 1996.

My masters thesis is on the effects of mixing on aluminum hydroxide precipiation and coagulation with Alum.

Please let me know who I should direct my request to. I need to obtain copyright permission by April 1, 2004.

Sincerely

Corrina Kennedy
7111 81st Street
Edmonton, Alberta
T6C 2T3
(780) 463-8022

3/30/04

Corrina Kennedy

From: Mark Hull <Mark_Hull@materials.org.uk>
To: 'Corrina Kennedy' <corrinakennedy@shaw.ca>
Sent: Tuesday, March 16, 2004 4:21 AM
Subject: RE: obtaining permission to reproduce a British Ceramics TransactionsFigure in a Masters Thesis

Dear Ms Kennedy

I can confirm there is no objection to your using the figures listed for the purpose you describe below, providing full acknowledgement of the original source is given.

Maney administers the copyright on behalf of IoM Communications Ltd. a wholly owned subsidiary of the Institute of Materials, Minerals and Mining.

Regards
Mark Hull

Mark Hull
Managing Editor, Materials Science Journals
Maney Publishing: publisher to The Institute of Materials, Minerals and Mining
1 Carlton House Terrace
London SW1Y 5DB
UK

tel. +44 (0) 20 7451 7312
mobile 0797 6234042
fax +44 (0) 20 7451 7307
email [mailto:mark_hull@materials.org.uk]
Internet http://www.maney.co.uk; http://www.iom3.org

----- Forwarded message from Corrina Kennedy <corrinakennedy@shaw.ca> -----
Date: Mon, 15 Mar 2004 21:26:13 -0700
From: Corrina Kennedy <corrinakennedy@shaw.ca>
Reply-To: Corrina Kennedy <corrinakennedy@shaw.ca>
Subject: obtaining permission to reproduce a British Ceramics Transactions
Figure in a Masters Thesis
To: m.j.edirisinghe@qmul.ac.uk

Dear Dr. M.J. Edirisinghe,

Can you please direct me to your copyright permission department for the British Ceramics Transactions Journal. I have completed my thesis at the Univeristy of Alberta, Edmonton, Canada on the Effects of Mixing of Aluminimum Hydroxide Precipitation and Coagulation with Alum for the Water Treatment Industry and would like to include some figures from your journal.

The figures I would like to include are in the "Synthesis of Aluminum Hydroxide by a Homogeneous precipitation method 1- Effect of Additives on the Morphology of Aluminum Hydroxide" Volume 90 page 44-48, 1991. The figure numbers are Figure 2 on pg 45, Figure 4 and Figure 7.

Thank you for your help.

Corrina Kennedy
7111 81st STreet
Edmonton Alberta
T6C 2T3
(780)463-8022

----- End forwarded message -----

Corrina Kennedy

From: <PhippsBird@aol.com>
To: <corrinakennedy@shaw.ca>
Sent: Tuesday, March 16, 2004 7:02 AM
Attach: PB911 600dpi.jpg
Subject: Re: permission to put G vs Jar paddle RPM diagram in a Master Thesis

You have our permission for the specific purpose stated in your email.
Photograph attached. You already have the graph, correct? Please use the following attribution: "(Photograph) (Graph) courtesy of Phipps & Bird, Inc., Richmond, VA"

Please forward a copy of your thesis for our archives when published.
Thank you!
Wes Skaperdas

Wes Skaperdas,
President
PHIPPS & BIRD, Inc.,
Confast, Inc. & Intelitool
1519 Summit Avenue
Richmond, VA 23230-4511
Tel: 804/254-2737, ext. 201
Tel: 800/955-7621
Fax: 804/254-2955
Email: Wes@phippsbird.com
Websites:
www.phippsbird.com
www.intelitool.com
www.confastinc.com

WebMail - RE: Completion of Static Mixer Project and copyright permission

Delete | File | New | Reply | Reply All | Forward | Previous | Next | Index | Help | Logout

Date Sent: March 16, 2004 2:04 PM

From: "Joe F. Corsaro" <Corsaro@Kenics.Com> Add to Address Book

To: ckennedy

Subject: RE: Completion of Static Mixer Project and copyright permission

Status: ☐ Urgent ☐ New

Hello Corrina:

Yes, please send me a CD of your thesis. You have my permission to use the pictures of the HEV as they relate to your Master Thesis.

Thanks
Joe Corsaro

PS: My mailing address is:

Chemineer, Inc.
125 Flagship Drive
N. Andover, MA 01845

Attn: J. Corsaro

-----Original Message-----
From: ckennedy [ckennedy@ualberta.ca]
Sent: Tuesday, March 16, 2004 12:40 AM
To: Joe F. Corsaro
Cc: Suzanne Kresta
Subject: Completion of Static Mixer Project and copyright permission

Dear Joe Corsaro,

Thank you for the HEV static mixers used in my research project at the University of Alberta for my Master Thesis. My thesis is now complete. If you like I can mail a CD copy to you, as it is too large to send by email. What is your mailing address?

I also need permission to reproduce the pictures of the HEV static mixers that I took off the Chemineer website. Can you please email me back. I do not require a letter of permision: an email is adequate.

Corrina Kennedy

From: Kennedy, Corrina SCAN-- <Corrina.Kennedy@shell.com>
To: <corrinakennedy@shaw.ca>
Sent: Monday, April 05, 2004 8:57 AM
Subject: FW: Sketchs for your Thesis

-----Original Message-----
From: Louis Kennedy [mailto:l.kennedy@sasktel.net]
Sent: April 04, 2004 10:33 AM
To: Corrina Kennedy
Subject: Sketchs for your Thesis

Hi

How is everything ?

I Authorize you to use these sketchs in any way you want. I consider you to be the owner of them as all I did was make sketchs with your information.

Love
Dad

Corrina Kennedy

From: <shook@telusplanet.net>
To: Corrina Kennedy <corrinakennedy@shaw.ca>
Sent: Sunday, April 04, 2004 10:53 AM
Subject: Re: Hi from Corrina

Dear Corrina

Please feel free to use any figure from my class notes in your thesis.

Clifton Shook

Quoting Corrina Kennedy <corrinakennedy@shaw.ca>:

> HI Dr. Shook.
>
> Hope all is well with you. I finally finished off my thesis and I will be
> sending it off to the printers next week. I was wondering if you would like
> to join Jason Schaan and I for little thesis completetion celebration lunch
> or dinner. When would be a good time for you? Also, I need to get
> permission from you to print one of your classnote pictures in my thesis. It
> is the one of particles settling in a jar. All I require is an email with
> your permission.
>
> Thanks
>
> Hope to see you soon.
>
> Corrina
>